Master Thesis in Reservoir Chemistry

Simulation Studies of Hybrid EOR

Emilie Ryen Jomark

Department of Chemistry

University of Bergen

June 2019

Acknowledgement

First, I would like to express my sincere gratitude towards my supervisor, Professor Arne Skauge, for the guidance, support and knowledge throughout the work of this thesis.

I would also like to express gratitude towards Dr. Iselin Salmo for the availability and most valuable discussions.

A special thanks to the research group for providing simulation models and valuable information related to the work of this thesis.

Thank you to my fellow students at the office for the positive working environment, all the laughs and the academic conversations during this process.

Finally, I would like to say thank you to my friends and family for always supporting me. I would especially like to thank my parents, Elisabeth Ryen and Øyvind Jomark, for their everlasting support and encouraging words during stressful times, and for always believing in me.

Emilie Ryen Jomark

Bergen, June 2019

Abstract

Injection of low salinity brine in combination with surfactant and polymer for enhanced oil recovery (EOR) have been proven to substantially increase oil recovery. Large EOR potential exists on the biggest fields on the Norwegian continental shelf, which may provide economically profitable production [1].

This thesis concerns simulation studies of hybrid EOR in three-dimensional reservoir models representing a North Sea oil field. The simulations were conducted by the ECLIPSE Blackoil Simulator, where the applied models assumed a shift in relative permeability due to salinity change. A field model provided by the research group formed a basis from which a generic sector model could be produced for the purpose of sensitivity studies. In addition to the field model, the research group provided an established core model history matched to a composite coreflooding experiment. During simulations, the response of the simulator to injection fluids was evaluated.

The sensitivity of the sector model to change in key reservoir parameters and flow functions was investigated, where final results were applied in the field model. Both models revealed incremental oil recovery caused by an enhanced microscopic sweep by flooding with low salinity water in combination with surfactants. Low salinity water in combination with polymer flooding both accelerated oil recovery and slightly decreased the residual oil saturation through mobility aid, and stabilized flow after high differential pressure was observed when surfactants were injected.

The coreflooding experiment was successfully history matched at lab scale, with approximately equal quantitative results. Predicting model performance based on laboratory results were up-scaled to sector scale and field scale, where simulation results revealed a heterogeneity dependent oil recovery.

ECLIPSE successfully modeled the LSSP processes by interpolating salinity dependent relative permeability and capillary pressure, and interpolating surfactant concentration dependent relative permeability and capillary pressure during surfactant flooding. Polymer-oil relative permeability was treated as water-oil relative permeability.

Table of Contents

Nomenclature

Abbreviations

3D	Three-dimensional
BHP	Bottom-hole pressure
CDC	Capillary desaturation curve
CMC	Critical micelle concentration
COBR	Crude oil/brine/rock
EOR	Enhanced oil recovery
HPAM	Hydrolyzed polyacrylamide
HS	High salinity
HSW	High salinity water
IFT	Interfacial tension
IOR	Improved oil recovery
IPV	Inaccessible pore volume
LS	Low salinity
LSP	Low salinity polymer
LSS	Low salinity surfactant
LSSP	Low salinity surfactant polymer
LSW	Low salinity water
MIE	Multicomponent ion exchange
NCS	Norwegian Continental Shelf
NPD	Norwegian Petroleum Directorate
OOIP	Oil originally in place
PAM	Polyacrylamide
PORV	Pore volume
ppm	Parts per million
PV	Pore volume
RESV	Reservoir fluid volume rate
RRF	Residual resistance factor
WOR	Water-oil ratio

Variables

Symbol	*Parameter*	*Field units (SI)*
A	Area	[m^2]
B	Formation volume factor	[rm^3/sm^3]
C	Concentration	[kg/m^3]
CA	Adsorption isotherm	[kg/kg]
dP	Differential pressure	[mbar]
E_A	Areal sweep efficiency	Dimensionless
E_D	Microscopic displacement efficiency	Dimensionless
E_R	Recovery factor	Dimensionless
E_V	Vertical sweep efficiency	Dimensionless
E_{vol}	Volumetric displacement efficiency	Dimensionless
F_1	Weighting function	Dimensionless
F_2	Weighting function	Dimensionless
F_3	Weighting function	Dimensionless
F_{kr}	Interpolation parameter	Dimensionless
G	Gibbs free energy	[J]
K	Absolute permeability	[mD] ($1\ D = 0.98692 \cdot 10^{-12} m^2$)
K_{eff}	Effective permeability	[mD]
k_r	Relative permeability	Dimensionless
k_r^0	Endpoint relative permeability	Dimensionless
L	Length	[m]
M	Mass	[kg]
M	Mass flux	[$kg/s \cdot m^2$]
M	Mobility ratio	Dimensionless
MD	Mass density	[kg/rm^3]
N	Amount of oil	[m^3]
N_c	Capillary number	Dimensionless
N_o	Corey correlation for oil	Dimensionless
N_{vc}	Capillary number	Dimensionless
$OOIP$	Oil originally in place	[m^3]

P	Phase potential	Dimensionless
P	Pressure	[bar]
$PORV$	Pore volume	[m^3]
PV	Pore volume	[m^3]
q	Flow rate	[m^3/s]
Q	Flow rate	[m^3/s]
r	Radius	[m]
R	Resistance/reduction factor	Dimensionless
RRF	Residual resistance factor	Dimensionless
S	Saturation	Dimensionless
S_{or}	Residual oil saturation	Dimensionless
S_w^*	Normalized water saturation	Dimensionless
S_{wi}	Initial water saturation	Dimensionless
T	Transmissibility	[m^2/day]
u	Darcy velocity	[cm/s]
v	Velocity	[m/s]
V	Volume	[m^3]
z	Height in z-direction	[m]
θ	Contact angle	[º]
ρ	Density	[kg/m^3]
σ	Interfacial tension	[N/m]
λ	Mobility	[mD/cP]
ϕ	Porosity	Dimensionless
τ	Shear stress	[Pa]
ω	Todd-Longstaff mixing parameter	Dimensionless
μ	Viscosity	[cP]
β	Volume factor	[rm^3/sm^3]

Subscripts

A	Areal
$AdsSurf$	Adsorbed surfactant
b	Bulk
c	Capillary
D	Displacement
e	Effective
eff	Effective
g	Gas
i	Initial
i	Specified fluid (water, oil or gas)
k	Relative permeability
m	Mixed
o	Oil
p	Phase
p	Polymer
p	Pore
P	Produced
R	Recovery
r	Relative
r	Residual
ref	Reference
res	Residual
s	Solid
s	Surfactant
$surf$	Surfactant
tot	Total
V	Vertical
vol	Volumetric
w	Water

Superscripts

a	Adsorbed
h	High
HS	High salinity
i	Interpolated
imm	Immiscible
l	Low
LS	Low salinity
max	Maximum
mis	Miscible

List of Figures

List of Tables

1. Introduction

The global demand for energy is expected to increase by a quarter within the year of 2040, with natural oil and gas meeting a major share of the demand [2]. The Norwegian Petroleum Directorate (NPD) estimate that 47% of the remaining petroleum resources of 8.3 billion sm^3 on the Norwegian continental shelf (NCS) have not yet been proven, where the total proven and unproven petroleum resources are estimated to be 15.6 billion sm^3 [3]. With oil and gas reserves on a decline while the energy demand is continuing to grow leaves a significant importance of improving oil recovery.

Oil recovery by water and gas injection is mostly used on the NCS to improve recovery by maintaining pressure and sweep the reservoirs. The current plans and technology leaves large resources of oil behind, leading to a requirement for new technology and recovery methods to be implemented on the NCS. There exists a technical potential for enhanced oil recovery on many fields, where the overall technical potential for 27 of the largest fields on the NCS is estimated by the NPD to be 16-43%, yielding a profitable production [1].

EOR techniques are unconventional recovery techniques implemented to recover oil where conventional methods such as pressure depletion and injection of water and gas are incapable. EOR is only a subpart of increased oil recovery (IOR), which is defined in a broad manner by all economic measures aimed at improving the oil recovery factor or accelerate oil reserves [4]. Relatively recent laboratory studies have shown a substantial increase in oil recovery by injecting low salinity water [5]. Further studies have been performed to investigate the effect of low salinity water in combination with EOR chemicals such as surfactants and polymers on oil recovery. Results have been promising with observed incremental oil production by applying hybrid EOR processes [6].

This thesis concerns simulation studies of hybrid EOR on three scales, where the ECLIPSE Blackoil Simulator have been the tool for conducting the simulations. The initial sections cover insight to theoretical aspects in order to analyze simulation results. Final results from sensitivity studies were up-scaled from sector scale to field scale, while predicting performance based on laboratory results were up-scaled from core scale to sector scale and field scale. The main objective of this thesis is to evaluate the performance of low salinity surfactant/polymer (LSSP) flooding by numerical simulation.

2. Basic Concepts in Reservoir Engineering

In order to evaluate the production potential of a reservoir, petrophysical properties as well as reservoir fluid properties and their interactions with the rock must be known. In the following sections, fundamental concepts regarding reservoir and fluid characteristics are presented for understanding the content of this thesis.

2.1 Petrophysical Properties

2.1 1 Porosity

Void parts between mineral grains in sedimentary rocks constitute the rock's porosity. This void can occur after deposition and cementation of sediments of different shapes and sizes, where the sediments are not completely compacted together. These voids are often filled with water or hydrocarbons, and porosity is therefore a measure of the rock's fluid storage capacity. It is described as the pore volume divided by the total volume, with the latter also known as the bulk volume [7]:

$$\phi = \frac{V_p}{V_b} \tag{2.1}$$

Where V_p and V_b represent pore volume and bulk volume, respectively.

While total porosity refers to all pores that are present in the rock, the interconnected pores are of more interest since these pores can maintain a continuous fluid flow. This porosity is referred to as effective porosity, and the total porosity is the sum of both effective porosity, ϕ_{eff}, and residual porosity, ϕ_{res} [7]:

$$\phi_{tot} = \phi_{eff} + \phi_{res} \tag{2.2}$$

2.1.2 Absolute Permeability

Permeability of a porous medium is the medium's capability to transmit fluids through its network of interconnected pores. Although permeability is directly related to porosity, a high porosity does not necessarily indicate a high permeability. Interconnected pores are required, or else the porous medium will be impermeable [8].

Permeability can be regarded as a constant property of a porous medium only if there is a single incompressible fluid flowing and the porous medium is 100% saturated with this fluid. This absolute permeability is independent of the fluid type, and can be estimated by performing single-phase flow measurements on a core sample. The measured data are then applied to the one-dimensional Darcy's law [8]:

$$K = \frac{Q\mu L}{A\Delta P} \tag{2.3}$$

Where:

- K is absolute permeability [Darcy]
- Q is volumetric fluid flow rate $[cm^3/s]$
- μ is fluid viscosity [cP]
- L is length of core sample [cm]
- A is cross-sectional area $[cm^2]$
- ΔP is pressure difference across core sample [atm]

Figure 2.1 illustrates the different parameters, which constitute Dracys's law:

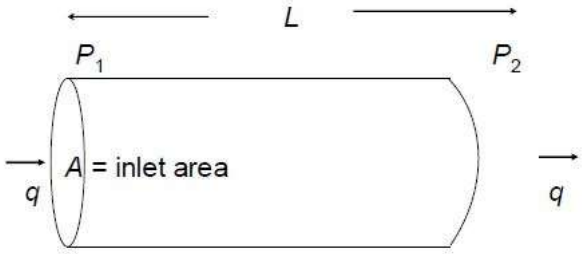

Figure 2.1: Illustration of one-dimensional fluid flow in porous media [4].

Darcy's law is an empirical law, and is valid if certain assumptions are met. As mentioned, the core sample must be 100% saturated with a single, incompressible fluid. There must be no chemical reactions between the fluid and the medium, and the flow must be a laminar, stationary and horizontal flow, where the latter is required so that gravity can be neglected [8].

In this study, three-dimensional fluid flow is assumed during simulations, where flow is governed by Darcy's law in three dimensions:

$$u = -\frac{K}{\mu}\nabla\Phi \tag{2.4}$$

Where u is Darcy velocity. The flow potential Φ is defined by:

$$\Phi = P + \rho g z \tag{2.5}$$

Where z is flow directed upwards. The vector gradient operator in a Cartesian coordinate system is defined as:

$$\nabla = \vec{\imath}\frac{\partial}{\partial x} + \vec{\jmath}\frac{\partial}{\partial y} + \vec{k}\frac{\partial}{\partial z} \tag{2.6}$$

2.1.3 Fluid Saturation

Reservoir rocks usually contain several reservoir fluids, such as water, oil and gas. Saturation describes the amount of fluid that is present in the rock, and is a dimensionless parameter defined as the fraction of pore volume occupied by a particular fluid [9]. The total saturation is given by:

$$S_w + S_o + S_g = 1 \tag{2.7}$$

Where the saturation of each fluid is given by:

$$S_i = \frac{V_i}{V_p} \tag{2.8}$$

Here:

- i is specified fluid (water, oil or gas)
- S_i is saturation of fluid i
- V_i is volume of fluid i
- V_p is pore volume

Saturation varies in time during production, and some fluids will remain trapped in the reservoir after production because of capillary forces. The saturations of these fluids are defined as residual saturations, which will vary depending on reservoir quality, recovery method and wettability [8].

2.1.4 Residual Oil Saturation

In a water-wet system, oil entrapment in the pore space occurs during oil production. The saturation of the remaining immobilized oil is defined as the residual oil saturation, and is denoted S_{or}. The pore doublet model and the snap-off model are two common models that describe this phenomenon, as well as bypassed oil [4,10]:

2.1.4.1 The Pore Doublet Model/Bypassed Oil

Because of capillary forces, water will intrude the narrower channel first where a pore throat splits in two, leaving oil trapped in the broader channel by bypassing water. This is illustrated in figure 2.2:

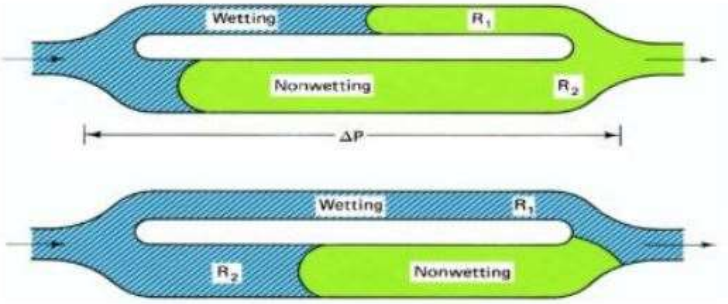

Figure 2.2: Trapping of oil in a pore doublet model [4].

2.1.4.2 The Snap-Off Model

The snap-off model describes the trapping of oil caused by capillary forces and interfacial tension between water and oil. With water being the wetting phase, oil will flow in the center of the pores where a thin water film covers the pore walls. As water saturation increases during a waterflood, the water film will thicken in the narrow pore throats, causing the oil to snap off into immobile globules that are located in the center of the pores. Figure 2.3 illustrates the snap-off model:

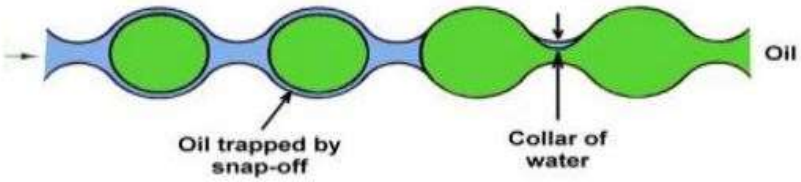

Figure 2.3: Trapping of oil in a snap-off model [4].

2.1.4.3 Combining Trapping Mechanisms

Is has been confirmed by experimental observations that trapping of oil can occur by combining both the snap-off model and the pore doublet model with bypassed oil, depending on local conditions [10]. The two models can be combined in several ways: trapping of oil can occur only by snap-off or only by bypassing, or different combinations of the two, as illustrated in figure 2.4:

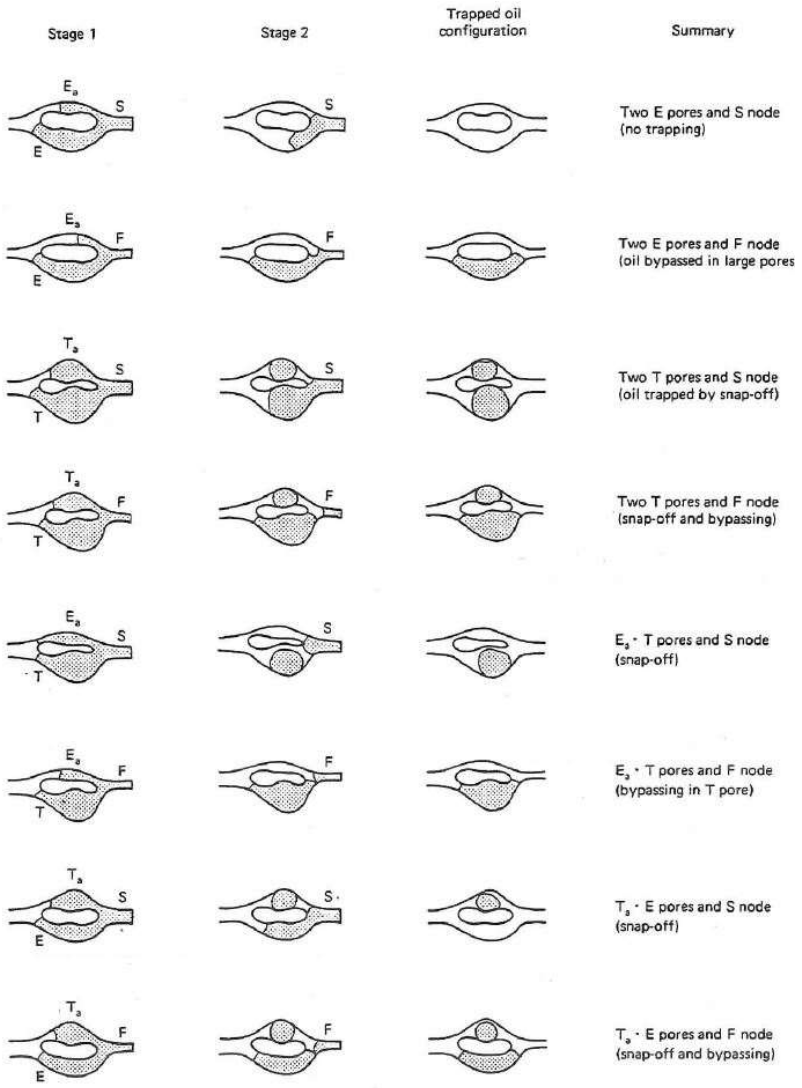

Figure 2.4: Sketches of trapping mechanisms and configuration of residual oil in pore doublets [10]

2.1.5 Effective and Relative Permeability

There are usually two or three non-miscible fluids present in a reservoir, and it can therefore be defined a permeability for each fluid called effective permeability. Effective permeability is strongly dependent on each fluid's relative saturation, and is a measure of the fluid's ability to flow in the presence of other immiscible fluids, as one fluid will hinder the free flow of the other fluids [8]. Effective permeability can be defined as an extension of the one-dimensional Darcy's law expressed in section 2.1.2, and states for each fluid flowing:

$$K_{eff,i} = \frac{Q_i \mu_i L}{A \Delta P_i} \tag{2.9}$$

Where $K_{eff,i}$ is effective permeability of fluid i.

Relative permeability is a dimensionless parameter dependent on fluid saturation, rock properties and wettability. It is defined as the ratio between a rock's effective permeability to a particular fluid and its absolute permeability [8]:

$$k_{r,i} = \frac{K_{eff,i}}{K} \tag{2.10}$$

Where $k_{r,i}$ is the relative permeability of fluid i.

To investigate relative permeability's dependence on saturation and wettability, it is common to plot relative permeability curves. Relative permeability for each phase present is plotted as a function of saturation, usually water saturation [8]. Figure 2.5 illustrates typical water-oil relative permeabilities under strongly water-wet and strongly oil-wet conditions.

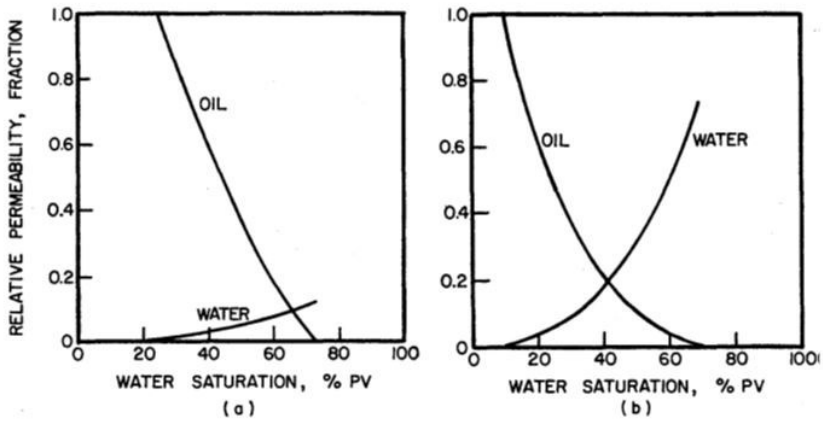

Figure 2.5: Typical relative permeability curves for (a) strongly water-wet system, and (b) strongly oil-wet system [11].

2.1.5.1 Corey Relative Permeability Correlation for Oil

The Corey relative permeability correlation for oil was utilized for a modification of oil relative permeability curves during sensitivity studies. In the Corey correlation, relative permeability is a function of normalized water saturation [12]:

$$S_w^* = \frac{S_w - S_{wi}}{1 - S_{or} - S_{wi}} \tag{2.11}$$

$$k_{ro} = k_{ro}^0 (1 - S_w^*)^{N_o} \tag{2.12}$$

The curvature is given by the parameter N_o for oil relative permeability. k_{ro}^0 is endpoint relative permeability for oil, and S_w^* is normalized water saturation. Figure 2.6 illustrates how the Corey parameter N_o affects the behavior of k_{ro}.

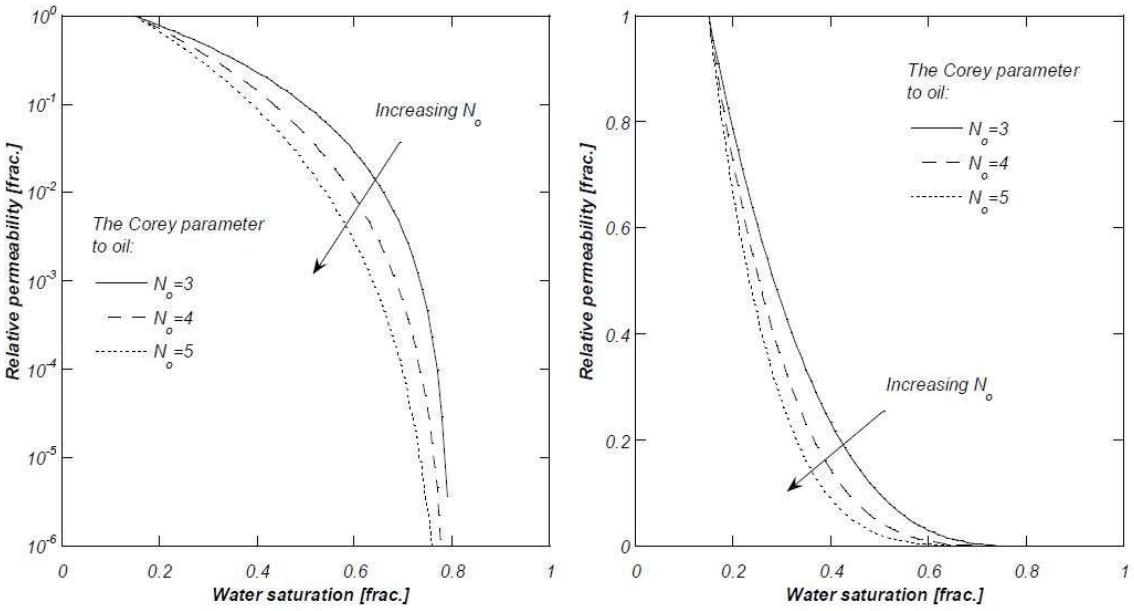

Figure 2.6: Behavior of k_{ro} by varying the Corey correlation [12]. The illustration to the left displays a logarithmic scale for relative permeability, while the illustration to the right displays a linear scale for relative permeability.

2.2 Fluid Properties

2.2.1 Interfacial Tension

There are several forces acting on molecules in reservoir fluids, where the combined effect of these phenomena controls the saturation distribution and fluid contacts. There exists attractive electrostatic forces between the molecules within a fluid, as well as between molecules in adjoining fluids. This type of force is referred to as cohesion. If the intramolecular attraction is greater than the intermolecular attraction, the fluids are said to be immiscible and will not mix. Otherwise, the fluids mix and are called miscible. The molecules of each fluid can also be attracted to an adjoining solid by an electrostatic force referred to as adhesion [8].

Two immiscible fluids in contact with each other give rise to a basic property known as interfacial tension (IFT). At the boundary between two immiscible fluids, there exists a membrane-like surface separating the phases. The cohesive force is stronger on the denser fluid's side, which causes a sharp change in pressure across the boundary. This state of tangential tension at the boundary is called interfacial tension, and the magnitude of the IFT represents the work, or energy, required to keep the fluids from mixing [8]:

$$\sigma = \left(\frac{\partial G}{\partial A}\right)_{T,P,m_{1,2}} \tag{2.13}$$

Where:

- σ is IFT
- G is Gibbs free energy
- A is interface area
- T is temperature
- P is pressure
- m is mass

If the IFT is positive ($\sigma > 0$) the fluids are immiscible and their contact surface is minimized. A negative IFT ($\sigma < 0$) indicates that the fluids are miscible, a miscibility known as dissolution, which leads to a stable new fluid. A neutral IFT ($\sigma \approx 0$) yields "truly" miscible fluids, and their slow diffusion will lead to complete mixing [8].

2.2.2 Capillary pressure

Capillary pressure is defined as the molecular pressure difference across the interface of two immiscible fluids. It results from both the internal and external electrostatic forces acting upon the two fluids, and can be defined by the Laplace equation, which for a water-wet system is [8]:

$$P_c = p_{non-wetting} - p_{wetting} = p_o - p_w \tag{2.14}$$

Where:

- P_c is capillary pressure
- p_o is internal oil pressure
- p_w is internal water pressure

When two immiscible fluids are placed in a pore channel, the stronger adhesive force of the wetting fluid causes the interface to curve [8]. When this happens, the pressure will abruptly increase across the interface to balance the interfacial tension forces. This pressure jump is the capillary pressure, and Laplace equation can then be extended to Young-Laplace equation, expressed in terms of the pore radius and the interfacial tension forces [13]:

$$P_c = \frac{2\sigma_{ow}cos\theta}{r} \tag{2.15}$$

Where:

- σ_{ow} is interfacial tension between oil and water
- θ is contact angle
- r is pore radius

It becomes apparent from equation 2.15 that capillary pressure is a function of interfacial tension, wettability and pore size distribution [8].

2.2.3 Viscosity

Molecules in a flowing fluid experience a force resisting the flow because of frictional interaction [4]. This internal resistance to flow is defined as viscosity:

$$\mu = \frac{\tau}{dv/dy} \tag{2.16}$$

Where μ is viscosity, τ is shear stress and dv/dy is shear rate.

Dependent on their viscosity behavior, fluids can be classified as either Newtonian or non-Newtonian fluids. The viscosity of Newtonian fluids, such as water, is independent of shear stress and shear rate, and these fluids therefore obey a linear relationship between shear stress and shear rate. The viscosities are considered constant in this case. The viscosities of non-Newtonian fluids, however, are shear dependent, and are not considered constant. Polymer solutions possess this non-Newtonian behavior [4].

2.2.4 Mobility

A factor that is of importance for the recovery of hydrocarbons is the mobility of the individual reservoir fluids [14]. The mobility of a fluid is defined as the ratio between the endpoint relative permeability and the viscosity of the fluid:

$$\lambda_i = \frac{k_{ri}^0}{\mu_i} K \tag{2.17}$$

Where:

- λ_i is the mobility of fluid i
- k_{ri}^0 is endpoint relative permeability of fluid i
- μ_i is viscosity of fluid i
- K is absolute permeability

The mobility ratio between two fluids is crucial when determining to what extent one fluid will displace the other, as it can predict production behavior. It is defined as the ratio between the displacing fluid and the displaced fluid [14]. For water displacing oil:

$$M_{wo} = \frac{\lambda_w}{\lambda_o} = \frac{k_{rw,or}}{k_{ro,iw}} \frac{\mu_o}{\mu_w} \tag{2.18}$$

The most ideal mobility ratio for oil recovery is $M_{wo} \leq 1$ [14]. At this mobility ratio, oil flows as fast or faster as the injected water, leading to a good recovery as the injection water pushes the oil ahead. This leaves less oil isolated in the formation, and the amount of residual oil saturation is reduced. At $M_{wo} > 1$, water is more mobile than oil, which can lead to an early water breakthrough and unfavorable low amounts of recovered oil.

2.3 Basic Concepts in Oil Recovery

2.3.1 Wettability

The wettability of a solid can be defined as the tendency of one fluid to spread on the surface of a solid in the presence of other immiscible fluids. If two or more fluids coexist in the pore space of a reservoir, the most adhesive one sticks preferentially to the rock surface and is called the wetting fluid. The spatial configuration of fluids in the rock is dependent on the wettability of the rock, as wettability controls the location, flow and distribution of fluids in the porous medium [11]. It has been shown experimentally that rock wettability affects oil displacement [8].

One way to estimate the wettability of a rock is to measure the contact angle between the liquid-liquid's interface and the solid's surface quantitatively. This contact angle is also known as the wetting angle, and is defined by the Young-Dupré equation, which for a water/oil/rock system is [8]:

$$cos\theta_{ow} = \frac{\sigma_{os} - \sigma_{ws}}{\sigma_{ow}} \tag{2.19}$$

Where θ is wetting angle and σ is the surface or interfacial tension between the different phases.

By convention, the wetting angle is measured through the denser fluid's side of the interface [8]. This is illustrated in figure 2.7, which also illustrates the wetting angle for different wettabilities in a water/oil/rock system.

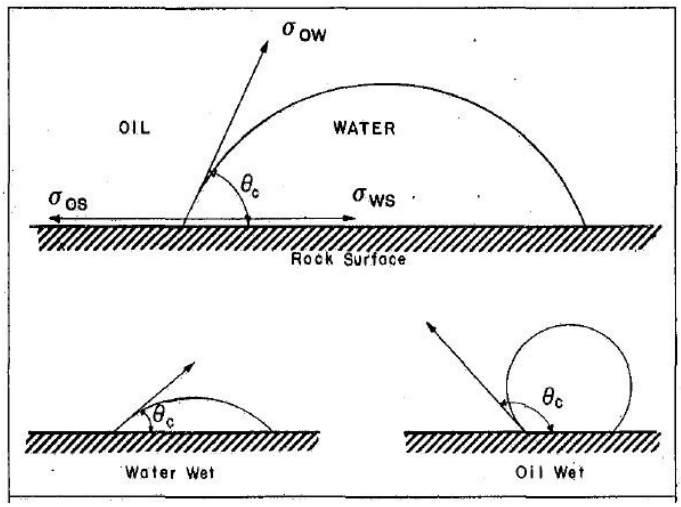

Figure 2.7: Wetting angles for different wettabilities in a water/oil/rock system [15].

Table 2.1 lists different wettability preferences and the corresponding values for the wettability angles.

Table 2.1: Wettability classes for a water-oil system [8]

Wetting angle [°]	Wettability preference
0-30	Strongly water wet
30-90	Preferentially water-wet
90	Neutral wettability
90-150	Preferentially oil-wet
150-180	Strongly oil-wet

2.3.1.1 Wettability and Its Effect on Waterflooding

Waterfloods in water-wet and oil-wet systems are known to behave very differently, as the wettability of a system will strongly affect its waterflood behavior – it is a major factor in controlling the flow, location and spatial distribution of fluids present in a porous medium. For uniformly wetted system, it is discovered that waterfloods in water-wet systems are more efficient than in oil-wet systems [16].

In a water-wet system, water will occupy the small pores as a thin film covering the pore walls at irreducible water saturation. During waterflooding, water moves through the medium as a uniform front, causing a displacement of oil into the large pores as the water imbibes into the smaller pores. After the waterfront has passed, almost all the remaining oil is trapped as globules at the center of the pores, leaving the oil immobile. After breakthrough, there is little or no additional production of oil [16].

The location of the fluids is reversed in an oil-wet system, and oil is found as a thin film covering the pore walls at low oil saturations. At the start of the waterflood, water will form continuous channels through the center of the large pores, displacing oil in front of it. As waterflooding continues, the water-oil ratio (WOR) of the produced fluids gradually increase as water forms additional continuous channels through the smaller pores. When the flow of the water is nearly unrestricted through the continuous channels, the oil flow falls to a very low level, causing a small oil recovery before water breakthrough [16]. To recover a given

amount of oil, water must be injected for a longer period of time in an oil-wet system, causing longer tail productions for oil-wet systems [16].

2.3.2 Drainage and Imbibition

Drainage is a displacement process where the wetting phase is displaced by the non-wetting phase, and the saturation of the wetting phase decreases. During drainage, the non-wetting phase will enter the largest pores first as the capillary pressure is lowest in these pores. This can be seen from the Young-Laplace equation 2.15, which indicates that capillary pressure is inverse proportional to the pore radii, hence the lowest capillary pressures are found in the largest pores. As the threshold capillary pressure is reached and exceeded, the saturation of the non-wetting phase increases. So does the capillary pressure until the remaining wetting phase is disconnected and the irreducible wetting phase saturation is reached at a high positive capillary pressure [13].

The opposite process where the non-wetting phase is displaced by the wetting phase is called imbibition, which is distinguished between spontaneous and forced imbibition. During spontaneous imbibition, the wetting phase will enter the smallest pores first, reducing the capillary pressure to zero as the wetting phase saturation increases. At zero capillary pressure, the pressure in the wetting phase must exceed the pressure in the non-wetting phase in order for the wetting phase to imbibe further, resulting in a negative capillary pressure [13].

Figure 2.8 illustrates a capillary pressure curve for a water-wet system:

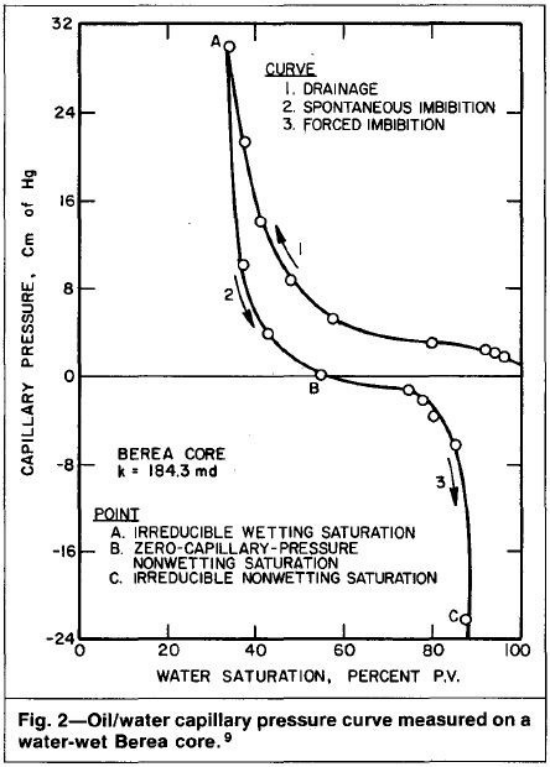

Fig. 2—Oil/water capillary pressure curve measured on a water-wet Berea core.[9]

Figure 2.8: Capillary pressure curve for a water-wet system [13].

2.3.3 Capillary Number

The capillary number is a dimensionless number, which expresses the ratio between viscous forces and capillary forces. Defined by the use of Darcy's law, the capillary number is written as [4]:

$$N_{vc} = \frac{u_w \cdot \mu_w}{\sigma_{ow}} \tag{2.20}$$

Where:

- N_{vc} is capillary number
- u_w is Darcy velocity of injected water
- μ_w is water viscosity
- σ_{ow} is interfacial tension between oil and water

According to experimental results, there is a relationship between the capillary number and residual oil saturation, which is illustrated by a capillary desaturation curve (CDC) in figure 2.9. In order to mobilize residual oil, the capillary number must be increased by several orders

of magnitude [4]. Adding EOR chemicals to injection water can either reduce capillary forces at the oil/water interface or increase water viscosity, depending on the chemical, leading to an increase in capillary number and a decrease in residual oil saturation [8].

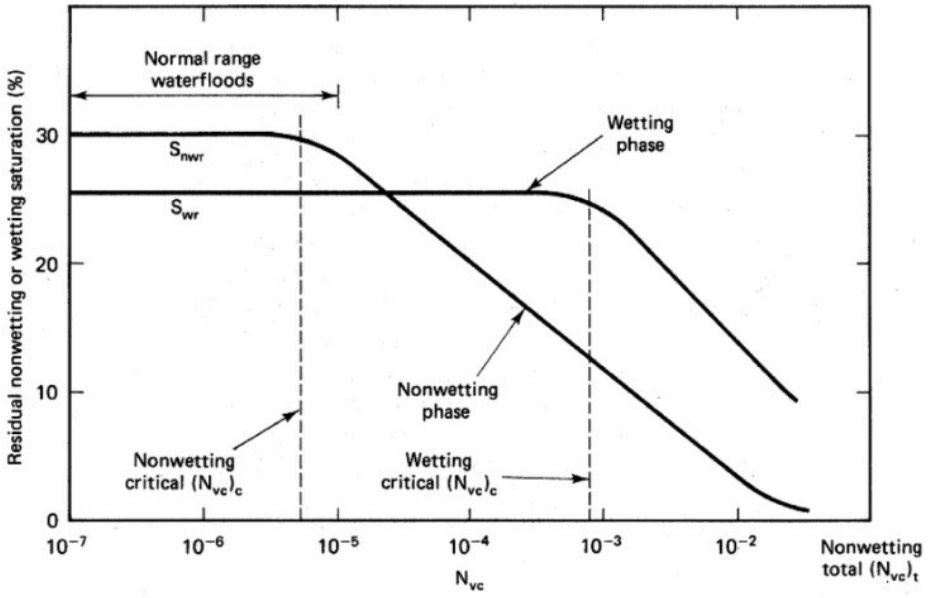

Figure 2.9: Capillary desaturation curves for wetting and non-wetting phase [10].

The residual saturation for both the wetting and non-wetting phase remains roughly constant at plateau values when capillary numbers are low. By increasing N_{vc} to a critical value, a knee in the curve occurs as residual saturation starts to decrease. This critical value is higher for the wetting phase than the non-wetting phase, as displayed in figure 2.9. The plateau of the wetting phase is less than for the wetting phase [10].

3. Enhanced Oil Recovery

The need for energy in the world is continuing to increase, where exploring new and exploiting already existing oil and gas reserves has become a necessity, as oil and gas are one of the most requested energy sources. By developing both new and improving already existing technology and methods, improvement of recovery efficiencies can be achieved [17].

Hydrocarbons can be produced by either primary, secondary or tertiary recovery methods. Primary and secondary methods are referred to as conventional methods, unlike tertiary methods that are referred to as unconventional methods. Hydrocarbon recovery by utilizing the natural reservoir pressure is called pressure depletion, which is primary recovery. Secondary recovery involves injecting water and gas for pressure support, as well as displacing oil. Tertiary recovery involves injection of materials that are not normally present in the reservoir, and is known as enhanced oil recovery [14].

3.1 Recovery Factor and Displacement Efficiencies

The recovery factor of a hydrocarbon reservoir determines the amount of hydrocarbons that can be produced and whether field development will be profitable or not, and is defined as:

$$E_R = \frac{N_P}{N} = \frac{Oil\ produced}{Oil\ originally\ in\ place\ (OOIP)} \tag{3.1}$$

The recovery factor is dependent on different factors, and can also be written as:

$$E_R = E_D \cdot E_{vol} = \frac{Volume\ of\ oil\ displaced}{Volume\ of\ oil\ contacted} \cdot \frac{Volume\ of\ oil\ contacted}{Volume\ of\ oil\ in\ place} \tag{3.2}$$

Where E_D and E_{vol} are microscopic displacement efficiency and volumetric displacement efficiency, respectively.

E_{vol} can further be divided into:

$$E_{vol} = E_A \cdot E_V = \frac{Area\ contacted\ by\ water}{Total\ area} \cdot \frac{Cross\text{-}sectio\quad area\ contacted\ by\ water}{Total\ cross\text{-}section\quad area} \tag{3.3}$$

Where E_A and E_V are areal sweep efficiency and vertical sweep efficiency, respectively [4].

The main purpose of EOR is to increase the recovery factor by increasing the microscopic and volumetric displacement efficiencies. By adding surfactants to injection water, capillary trapped oil can be mobilized by reducing the interfacial tension between oil and water. This

results in a larger recovery of the contacted oil and an enhanced microscopic displacement efficiency. Enhancing the volumetric displacement efficiency can be achieved by adding polymers to injection water, causing a more favorable mobility ratio by increasing the viscosity of the aqueous solution. This allows the injected solution to sweep a larger part of the reservoir, and more oil is contacted [4].

3.2 Low Salinity Waterflooding

Low salinity water (LSW) flooding is one of the emerging oil recovery techniques, which has gained its popularity in the past decades [18]. It has now become the most widely adopted improved oil recovery technique, after waterflooding first was practiced for pressure maintenance in earlier years [19].

Several studies indicate that a reduction in salinity of the injection water results in an increased oil recovery. However, the mechanisms behind low salinity water injection responsible for improving oil recovery are still uncertain, and the oil industry is continuing to discover the leading effects [20]. Different theories have been suggested on the mechanisms behind low salinity waterflooding, and previous laboratory and field studies on the subject will be presented in the following sections, as well as modeling of low salinity waterflooding.

3.2.1 Laboratory Studies

Early studies on the use of fresh water flooding was done by Martin in 1959 [21]. He observed an increased recovery of heavy oil by injection of fresh water, where he suggested that the increase was caused by swelling and migration of clays.

Further studies on the subject was later performed by Bernard in 1967 [22], which confirmed the beneficial effects of fresh water on oil recovery. Bernard studied the effect of different flooding water salinities in cores containing hydratable clays, where the results showed higher oil recoveries by fresh water injection. At salinities between 1-15 wt% NaCl, little or no additional oil was recovered, as well as the differential pressure being unaffected. However, at salinities between 0,1-1 wt% NaCl, oil recovery was increased, accompanied by a relatively high pressure drop. Bernard suggested that this pressure drop was caused by fines blocking pore channels, which led to mobilizing of residual oil and an increase in oil recovery.

Since the 1990's, activity around this technique has increased, as oil recovery by low salinity water injection has become of more and more interest [23]. The 1990's publications on wettability effects on oil recovery by Norman Morrow with co-workers advanced the research on low salinity brine injection [24]. This recovery technique would in the following years be further laboratory tested to investigate the brine salinity effect on oil production.

Tang and Morrow [25] suggested that a mechanism behind low salinity waterflooding is a wettability change towards a water-wet system, which leads to an additional recovery of crude oil by spontaneous imbibition. Three different crude oils were used in the experiment, and brine salinity was varied by factors of 0.01, 0.1 and 2 of salt concentration. The results showed an increase in oil recovery by reduction of injected brine salinity, where more water-wet conditions gave the highest oil recoveries [25].

Tang and Morrow [26] also studied how brine composition and fines migration influence crude oil/brine/rock (COBR) interactions and oil recovery. They suggested potentially mobile fine particles play a key role in the sensitivity of oil recovery to salinity, as recovery of crude oil was essentially independent of salinity after fines had been stabilized by firing and acidizing. This independency was also reported when a refined oil was used instead of crude oil. Furthermore, results from their studies revealed another necessary condition, in addition to mobile fines and crude oil, which was also required in order to increase oil recovery by a decrease in salinity – an initial water saturation [26].

Although the majority of published papers show an increase in oil recovery by injection of low salinity brine, Sharma and Filoco [27] performed centrifuge experiments to discover that oil recovery was found to be independent of the salinity of the brine injected, and primarily governed by the salinity of the connate water. Higher oil recoveries were achieved for lower salinity connate water.

3.2.2 Field Study Observations

Various studies on this topic have been conducted mainly at laboratory scale. Promising results from laboratory tests on increasing oil recovery by low salinity water injection have led to several experiments on field trials [20].

Webb et al [28] performed a log-inject-log field test to investigate if effects of low salinity injection water could be observed within the near wellbore region of a reservoir, and how low salinity water injection compared to seawater injection would affect oil recovery. Multiple log passes were conducted for each brine injected to compare waterflooding with varying brine. The results showed 25-50% reduction in residual oil saturation after flooding with low salinity brine.

Skrettingland et al [29] also performed a study on the subject where coreflooding experiments and a single-well chemical tracer-test were performed to compare residual oil saturation after low salinity waterflooding and after seawater flooding. The results showed little response to low salinity waterflooding, as the wetting conditions of the field was close to optimal. The authors concluded that wetting condition is a crucial property for determining the effect of low salinity injection.

3.2.3 Suggested Mechanisms behind Low Salinity Flooding

There are several proposed underlying mechanisms behind improving oil recovery by low salinity waterflooding, where the leading mechanisms are not yet fully understood [20]. Proposed mechanisms are presented in the following sections.

3.2.3.1 Fines Migration and Electrical Double Layer Expansion

During their investigations on salinity sensitivity in sandstones, Tang and Morrow [26] discovered that mobile fines is an important mechanism behind low salinity waterflooding and the resulting oil recovery. Cores with higher clay content was observed to yield an incremental oil production.

The balance between mechanical (capillary and viscous) forces and DLVO forces for colloidal systems explain the theory behind fines migration [26]. DLVO theory accounts for the balance between attractive van der Waals forces and the repulsive electrostatic forces caused by an overlap of electrical double layers. A double layer consists of ions of opposite charge to the surface that adsorb directly onto the surface, while a diffuse second layer of free ions exists with ions attracted to the surface charge, which in combination constitutes the electrical double layer [30].

The polar components in oil adhere to the potentially mobile fines at the pore walls. The injection of low salinity brine causes stripping of these mixed-wet fines as the electrical double layer between fine particles is increased, causing the migrated fines to locate at the oil-water interface. This, in combination with stripped fines with adhered oil drops can cause an increase in oil production. Tang and Morrow also observed a reduction in permeability, which could be caused by blocking of pore channels, leading to an increase in macroscopic sweep and incremental oil recovery. This pore channel blocking was followed by an observed increase in pressure drop [26].

3.2.3.2 Wettability Alterations

Many authors agree that a change in wettability is one of the primary causes for increasing oil recovery by low salinity water injection [31]. Lager et al [24] proposed several mechanisms causing this increase in oil recovery, where wettability alterations were one of them. While clay particles remain undisturbed when in contact with high salinity water, low salinity water causes clay particles to detach from the surface and migrate with the fluid flowing. During fines migration, exposure of the underlying surfaces increase water-wetness of the system, with weakly water-wet system yielding the highest oil recoveries [24]. Low salinity water also causes a destabilization of the bonding between the clay surface and polar oil components, causing a shift towards a more water-wet system [32].

3.2.3.3 Multicomponent Ion Exchange

Multicomponent ion exchange (MIE) describes the phenomenon where ions are adsorbed onto rock surface as a result from low salinity waterflooding, which also causes a desorption of directly adsorbed organic compounds formed with multivalent ions from the surface. This ion exchange takes place at the clay surface and promotes water-wet systems, resulting in an increase in oil recovery [31].

3.2.3.4 Effect of pH

At reservoir conditions, a chemical equilibrium is established with regards to pH and other factors, and both basic and acidic organic materials in addition to inorganic Ca^{2+} from formation water adsorb onto clay. Low salinity injection water consist of a much lower ion

concentration than formation water, causing a disturbance in the chemical equilibrium. This results in desorption of Ca^{2+}, leading to a substitution by protons, H^{+}, from surrounding water, which adsorb onto the clay. A local increase in pH close to the clay surface causes a reaction between the adsorbed basic and acidic materials, which partly desorb from the surface and cause a shift towards more water-wet conditions [20].

3.2.4 Modeling Low Salinity Waterflooding

As low salinity waterflooding is still an emerging EOR technique, models of low salinity waterflooding have been created in recent years for evaluating projects with varying scales by the use of simulations [18].

Jerauld et al [18] presented a model on low salinity waterflooding based on established modeling approaches for chemical EOR. The model represents both corefloods, single-well tests and field-scale simulations. The low salinity flooding is based on salinity-dependent oil/water relative permeability functions and a capillary pressure function resulting from wettability change, where high and low salinity relative permeability are inputs, and shapes are linearly interpolated between. Residual oil saturation, viscosity and density of the aqueous phase are also modeled as salinity-dependent, and development of connate water- and oil banking are accounted for in the model [18].

The results showed that the model with salinity-dependent wettability curves well describes the benefits of low salinity waterflooding, where the model is also capable of describing the physical phenomenon occurring during tertiary flooding [18]. The salinity-dependent relative permeabilities and capillary pressure are defined as:

$$k_{rw} = \theta k_{rw}^{HS}(S^*) + (1-\theta)k_{rw}^{LS}(S^*) \tag{3.4}$$

$$k_{row} = \theta k_{row}^{HS}(S^*) + (1-\theta)k_{row}^{LS}(S^*) \tag{3.5}$$

$$P_{cow} = \theta P_{cow}^{HS}(S^*) + (1-\theta)P_{cow}^{LS}(S^*) \tag{3.6}$$

$$\theta = (S_{orw} - S_{orw}^{LS})/(S_{orw}^{Hs} - S_{orw}^{LS}) \tag{3.7}$$

$$S^* = (S_o - S_{orw})/(1 - S_{wr} - S_{orw}) \tag{3.8}$$

Where the superscripts HS and LS denote high and low salinity, respectively [18].

Kuznetsov et al [31] published a simulation study of the low-salinity effect in a sandstone reservoir, where they developed two mechanistic chemical reaction models that describe multicomponent ion exchange and double layer expansion effects occurring during low salinity flooding. The chemical reaction sets are incorporated with "wettability weighting coefficients that reflect the contribution of different adsorbed ions to the wettability of the rock". Relative permeability curves and capillary pressure are interpolated between high and low salinity sets to account for wettability change. Two different single-tracer models were also developed. The four models in total are successful in describing the low salinity waterflooding effects, where the two detailed mechanistic models are useful when analyzing laboratory studies, while the simpler single-tracer models are advantageous for field-scale simulations as they run faster [31].

3.3 Surfactants

Oil becomes trapped in pores after waterflooding because of capillary forces, leading to a residual oil saturation. In order to recover this capillary-trapped residual oil, surfactants are added to injection water to lower the interfacial tension between water and oil, and to reduce residual oil saturation in water swept zones. As there is an experimentally proven relationship between the capillary number and residual oil saturation, as illustrated in figure 2.9, the capillary number must be increased by several orders of magnitude to mobilize residual oil. This can be achieved by injecting surfactants to lower the interfacial tension between water and oil, which leads to a more efficient microscopic displacement and an enhanced oil recovery [4].

3.3.1 Surfactant Properties

Surfactants are amphiphilic compounds that possess both hydrophilic and hydrophobic properties. They consist of a polar head group that prefers contact with water and a non-polar tail that prefers to avoid water [30]. The structure of a surfactant is illustrated in figure 3.1. Due to its dual nature, the surfactants tend to accumulate at the water-air and oil-water interfaces, hence the term surfactant, which is a widely used contraction for *surface active agents* [33].

Figure 3.1: Schematic structure of a surfactant [34].

Surfactants are classified according to the charge of the polar head group. They are divided into four main classes: anionic, cationic, nonionic and amphoteric. Anionic surfactants are the most used in oil recovery because of their beneficial properties and effect on lowering IFT, as well as being stable and not expensive [8].

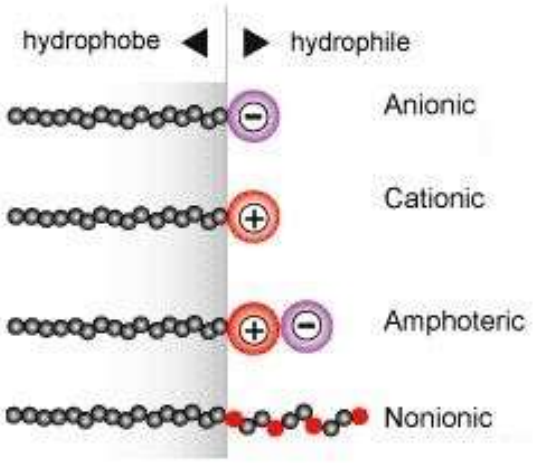

Figure 3.2: Surfactants classified according to charge [35].

Increasing surfactant concentration in an aqueous phase in contact with an oleic phase will lead to a reduction in IFT. When a certain concentration is reached, the surfactant monomers can no longer accumulate at the already fully saturated interface, and will rather start aggregating themselves into micelles; with hydrophobic parts oriented inwards and hydrophilic parts oriented outwards. This point in concentration is known as the critical micelle concentration (CMC), and a further addition of surfactants will have no impact on the IFT [4].

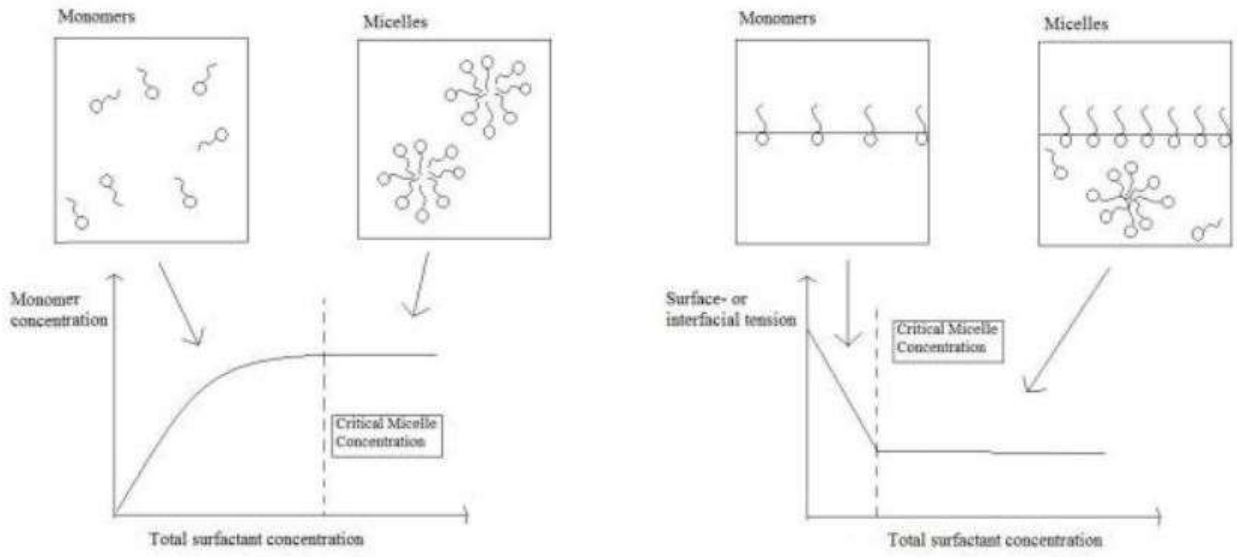

Figure 3.3: Surfactant monomer concentration curve and illustration of CMC [8].

3.3.2 Phase Behavior

Surfactant behavior is dependent on salinity as the brine salinity can alter how surfactants are solubilized in the bulk oleic and aqueous phases, which in turn can affect the interfacial tension. Depending on salinity, three different types of phase systems can occur [8]. Figure 3.4 illustrates the different types of phase systems.

At low salinity, it has been proven that typical surfactants usually exhibit good solubility in the aqueous phase and poor solubility in the oleic phase. This causes an overall composition splitting into two phases: an excess oil phase and a microemulsion phase containing brine, surfactants and some solubilized oil existing inside the micelles. This type of phase system is known as Type II(-) system, or Winsor type I system. No more than two phases can exist in this type [10].

At high salinities, the solubility of the surfactants in the aqueous phase is drastically reduced because of electrostatic forces of the brine. This also causes an overall composition of two phases, except the excess phase is here brine, and the microemulsion phase contains oil, surfactants and solubilized brine inside the micelles. This type of system is called type II(+), or Winsor type II system [10].

The two types of systems just described are extremes and roughly mirror images. There also exists a third system type at intermediate salinity. This is the type III system, or Winsor type III. Unlike the other two types, the type III system causes an overall of three phases: an excess

brine phase, excess oil phase, and a microemulsion phase. At intermediate salinities, there exists two IFTs; one between the oil and microemulsion, and one between the brine and microemulsion [10].

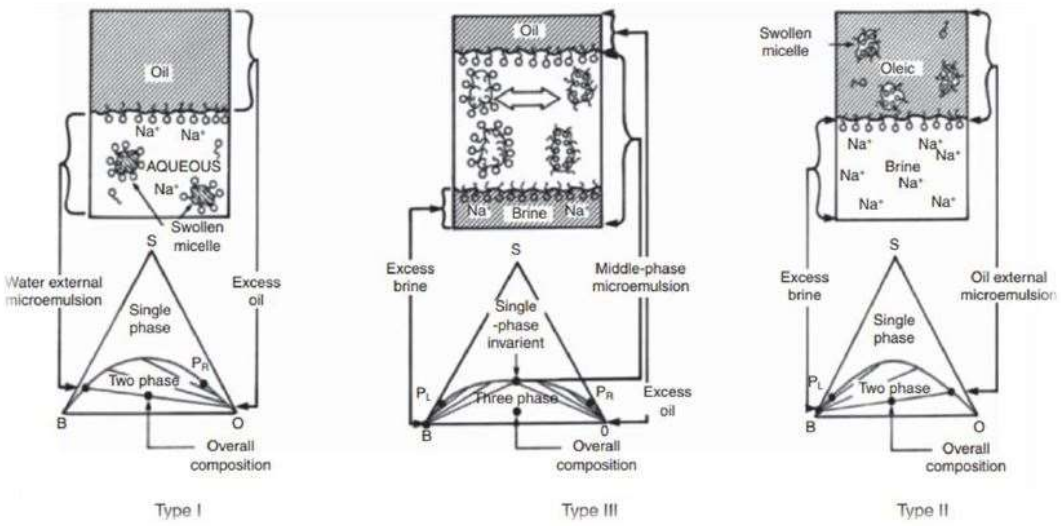

Figure 3.4: Illustration of the surfactant-oil-brine environment at different Winsor types [10].

Observations from laboratory experiments confirm that the Winsor type III system yields the lowest IFTs, and is therefore the most optimal salinity for oil recovery during surfactant injection [8]. In contradiction to this, Spildo et al [36] proposed that Winsor type I systems provide the most optimal phase environment during surfactant flooding. The authors performed a systematic study of surfactant solubility, phase behavior, interfacial tension and retention as a function of salinity. Their experiments revealed high retention values and a turbid aqueous solution at ultralow IFT in the Winsor type III system. A region in the Winsor type I area was observed where IFT was low, retention 10 times lower than at optimal salinity and the aqueous solution was clear, resulting in a conclusion that Winsor type I phase environment is the most optimal during surfactant flooding [36].

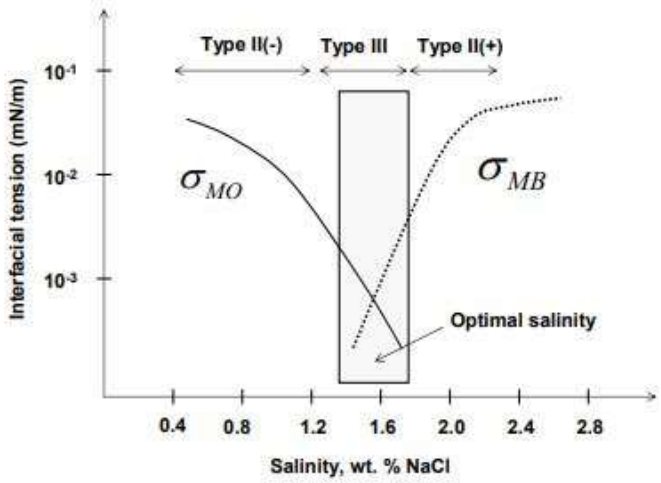

Figure 3.5: Interfacial tension at different salinities [4].

In both the simulation runs and coreflood experiment studied in this thesis, the salinities of the waters in combination with surfactants correspond to a Winsor type I behavior of the solutions. It is therefore reasonable to assume that swollen micelles containing solubilized oil have formed in the surfactant solutions. The salinities of low salinity water during simulation runs and the coreflood experiment are 4000 ppm and 3600 ppm, respectively.

3.3.3 Surfactant Retention

Retention can cause a drastic reduction in the surfactant concentration, and is therefore a problem to field application of surfactant flooding [4]. The four types of retention that can lead to surfactant retention are:

- Adsorption
- Precipitation
- Ion exchange
- Phase trapping

In this thesis, the only type of retention that was taken under consideration during modeling of surfactant flooding was adsorption. Surfactant monomers can adsorb by bonding with cationic surface sites.

3.3.4 Laboratory Studies on Low Salinity Surfactant (LSS) Flooding

The effect of combining low salinity brine injection with surfactant flooding has long been considered a promising supplement to enhanced oil recovery methods. Among the advantages of using surfactants at low salinity conditions is improved surfactant solubility and reduced retention [32].

Alagic and Skauge [32] presented a study on coreflood experiments performed by combining low salinity water injection in secondary mode and surfactant flooding in tertiary mode to investigate the beneficial effects. Mixed wet sandstone core samples were pre-flooded with either high salinity brine or low salinity brine. An increase in oil recovery of 6 saturation units was observed at changes from high salinity waterflooding to low salinity waterflooding, which was caused by a change towards water-wet behavior observed for cores flooded with low salinity brine. Low salinity brine can destabilize the bonding between the clay surface and polar oil components, causing a shift towards a more water-wet system.

Results showed a high oil recovery of 30-33% of OOIP after surfactant flooding in pre-established low salinity environment, while only 20% of OOIP was produced after flooding in pre-established high salinity environment. The presence of Mg^{2+} and Ca^{2+} (divalent ions) in high salinity water made the surfactant flooding less efficient in reducing interfacial tension, as high salinity environment caused an unfavorable Winsor type II system [32].

Effluent ion analyses of the low salinity waterfloods showed a continuous production of Ca^{2+}. As the connate water bank ahead of the injection water was displaced, a likely conclusion is dissolution of minerals containing calcium being the major contributor of the produced Ca^{2+}, where dissolution was caused by low salinity water. Effluent ion analyses also showed that Mg^{2+} was strongly retained in the core [32].

3.3.5 Modeling Low Salinity Surfactant Flooding

A simulation study of combined low salinity brine and surfactant flooding was performed by Skauge et al [5], where results from two coreflooding experiments were modeled in UTCHEM and ECLIPSE. Both coreflooding experiments gave incremental oil production by low salinity flooding followed by surfactant injection.

The UTCHEM simulator used a salinity based wettability alteration model. This required two sets of relative permeability, capillary pressure and CDCs corresponding to each wetting

phase in order to alter the wettability. ECLIPSE modeled brine tracking and the low salinity option, where given two sets of saturation functions, one for low salinity and one for high salinity, relative permeabilities and capillary pressure were interpolated [5].

Results showed that both simulation approaches were able to match oil recovery and differential pressure, where a shift in relative permeability due to wettability alterations is assumed to be the main mechanism. It was concluded that "the ECLIPSE version has a more flexible interpolation scheme for history matching, while the UTCHEM model is a more predictive approach that can be more easily up-scaled" [5].

3.4 Polymers

Polymers are added to injection water in order to increase water viscosity. The result of a higher water viscosity is a more favorable mobility ratio between water and oil, and a stable front, which prevents viscous fingering and early water breakthrough. This results in an improved volumetric sweep and an increase in the recovery efficiency. However, polymer flooding is most favorable in reservoirs containing heavy oil, or in heterogeneous reservoirs [4].

The effect of polymer additives on the reduction of water viscosity is not sufficient enough to increase the capillary number in equation 2.20 by the required number of magnitude in order to reduce the residual oil saturation significantly. The polymers are therefore added to injection water in order to accelerate recovery rather than to enhance it [4].

Polymers may also be used as gels, which are useful for near-well treatment by blocking high permeability zones, leading water to unswept low permeability zones. This leads to a more favorable water cut development [4].

3.4.1 Polymer Types and Chemistry

Polymers are molecules of long chains with repeating units linked by covalent bonds. There are two types of polymers extensively used in enhancing oil recovery, where the difference is whether they are naturally occurring (biopolymers) or synthetically produced. Synthetic

polymers are mostly used in field operations, as they are less expensive to produce and can be produced in large amounts [8].

Polyacrylamide (PAM), or hydrolyzed polyacrylamide (HPAM), is a synthetic polymer, where the structure of a HPAM molecule is illustrated in figure 3.6. The viscosifying effect of HPAM is good as the molecules are large. In low salinity water, the electrostatic repulsion between the negatively charged groups causes a rod-like stiff molecule, which provides a strong viscosifying effect. At higher salinities, however, the repulsive forces are reduced in particular because of divalent ions such as Mg^{2+} and Ca^{2+}. As a result, the molecules assume a rather coiled shape, which decreases the viscosifying effect. HPAM is mostly used in field operations as is less sensitive to shear rate, which can cause degradation, and less sensitive to salinity compared to PAM [8].

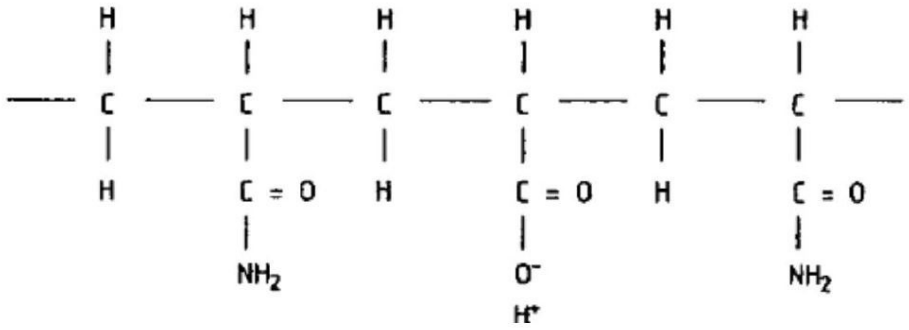

Figure 3.6: Structure of a partially hydrolyzed PAM molecule [4].

Xanthan polymers are biopolymers used for EOR purposes. The helical and rod-like molecule structure, illustrated in figure 3.7, yields a high viscosifying effect, and the polymer is almost insensitive to salinity. However, biopolymers are susceptible to biological degradation such as bacterial attacks, and they are expensive to produce [8].

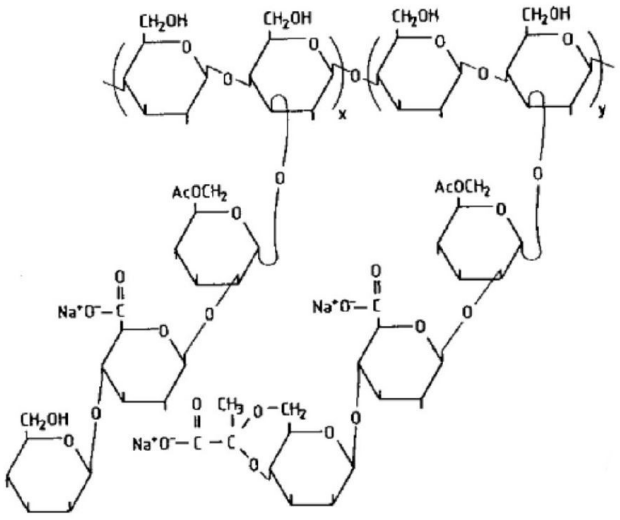

Figure 3.7: Structure of a Xanthan molecule [4].

3.4.2 Rheology

Polymer solutions behave like non-Newtonian fluids, with Newtonian regimes at low and very high shear rates. Their behavior is described as pseudo-plastic, which indicates a viscosity decrease with increasing shear rate. The Carreau model in figure 3.8 best describes the behavior of polymer solution viscosity. At low and high rates, the viscosity remains constant and displays a Newtonian behavior. At increasing rates, the shear-thinning non-Newtonian behavior becomes apparent as a gradual decrease in viscosity, where the molecules start to deform and orient themselves in the flow direction [8].

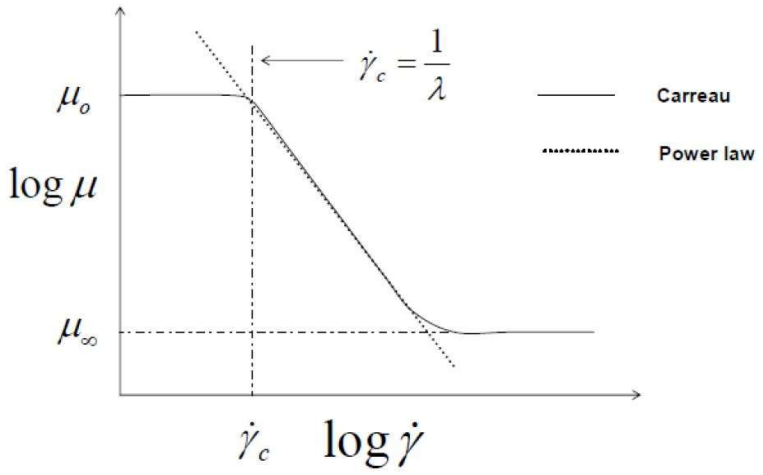

Figure 3.8: The Carreau model for describing polymer solution viscosity at different shear rates [4].

3.4.3 Polymer Retention and Inaccessible Pore Volume

As a polymer bank propagates through the reservoir, the loss of polymers from the leading front edge is inevitable, and is caused by retention. This term covers the mechanisms causing a reduction in polymer solution viscosity [8].

Adsorption of polymers onto surface rock have been repeatedly observed for polymer floods. Mechanical trapping and precipitation also cause a dilution of the polymer solution, leading to a decrease in viscosity and a possible drastically reduction in the mobility control effect. However, reduction in rock permeability where polymers are retained can have a positive effect on flooding, as the mobility of both polymer solution and chase water is reduced, leading to a more favorable mobility ratio [8].

Narrow pore throats hindering the flow of large polymer molecules cause inaccessible pore volume (IPV) of the porous rock. An undesired result of IPV is a smaller range of the macroscopic sweep, which can cause a higher residual oil saturation as oil trapped in smaller pores is not reached by the displacing solution [4].

3.4.4 Laboratory Studies on Low Salinity Polymer (LSP) Flooding

The application of low salinity water in combination with polymer flooding is of great interest, where the combined processes involve altering frontal stability and sweep in order to reduce residual oil saturation. Shiran and Skauge [37] presented a study on the topic where low salinity waterflooding in both secondary mode (at initial water saturation) and tertiary mode (after seawater residual oil saturation) on sandstone cores was performed, followed by flooding with polymers to investigate the beneficial effects.

Injection of polymers after a low salinity environment was established gave higher recoveries, where the highest recoveries were found for polymer injection in low salinity environment established at S_{wi} rather than at S_{or}. The reason for incremental oil recovery by LSP flooding is a more efficient oil banking caused by a more favorable mobility ratio, and an inaccessibility to pores containing connate water, which hinders a highly mobile connate water bank and results in a better sweep efficiency and increased oil recovery [37].

3.4.5 Modeling Low Salinity Polymer Flooding

Mechanistic modeling of low salinity water in combination with polymers have not been quantified until recent years. Mohammadi and Jerauld [38] presented in 2012 a study on mechanistic modeling of these two processes where emphasis was placed on the beneficial effects of adding polymers to low salinity injection water. In their study, the VIP reservoir simulator was used to model the combined processes and to conduct one-dimensional simulation runs. The low salinity model was based on the salinity-dependent relative permeabilities and capillary pressure, among other key features, first described by Jerauld [18]. The polymer model was based on early versions of the UTCHEM model, where polymer solution viscosity was a function of polymer concentration, shear rate and water salinity, and retention was considered [38].

The reservoir simulator STARS was additionally used to run a three-dimensional simulation to study the combination of low salinity water and polymer. Although STARS did not account for salinity-dependent polymer concentrations or viscosities, the simulator adequately modeled these processes by interpolating basic relative permeability and capillary pressure data as a function of water salinity, and viscosity was modeled through shear thinning and thickening power law relations [38].

The results from the study revealed an incremental oil production by the combined EOR technique in both secondary and tertiary mode, where flooding in secondary mode gave better timing of oil recovery [38].

3.5 Low Salinity Waterflooding Combined with Surfactants and Polymers

The term hybrid EOR processes denotes the combination of two or more injection processes in order to maximize oil recovery. The combination of low salinity water and surfactant flooding have in particular been investigated during coreflood studies, as the experiments have shown a large increase in oil recovery. Similarly, combined low salinity water and polymer flooding have shown an increase in oil recovery, and more interest is given to the combination of low salinity water with surfactant and polymer flooding, which is a topic requiring more research [6]. Many experiments of these hybrid processes have shown that the composite effect of several fluids injected in tertiary mode have resulted in higher recoveries than the individual fluid contributions [39].

3.5.1 Modeling Composite Low Salinity Surfactant/Polymer (LSSP) Flooding

Skauge [6] performed a simulation study where modeling change from high to low salinity injection water as well as combining the HS-LS process with surfactant and polymer flooding was conducted by the reservoir simulator STARS. The applied models were both governed by the main assumptions of a shift in relative permeability due to salinity change and increase in capillary number. History matching experimental coreflood results was also performed.

The complex EOR processes were successfully simulated by the use of multiple interpolation schemes in STARS, which enabled the relative permeability dependence on salinity and surfactant concentration. The simulations were able to history match total oil recovery and differential pressure for the complex process [6].

Pettersen and Skauge [39] addressed the challenges of extending the laboratory scale results of complex hybrid EOR processes to field scale, as the former have in particular been investigated and validated through history matching, and if simulated results can reproduce the observed results. The paper presents a study of how two simulators perform when the simulation models are extended from lab to field scale. The simulators used in the study were an enhanced black oil simulator based on modifying the standard black oil equations, and a general component model in STARS, which computes concentration factors by combining all present components. The component simulator defines two relative permeability sets, as double interpolation as a function of two tertiary fluids is allowed, with a limitation that a third polymer relative permeability set is not yet possible to define.

The simulation computational order was a typical injection scheme for hybrid EOR processes: seawater injection followed by establishing a low salinity environment. Low salinity surfactant flooding follows to enhance the macroscopic sweep, then a low salinity polymer flooding to ensure a stable displacement and preventing viscous fingering. Lastly, a low salinity chase water slug was injected [39].

Results showed satisfactory result for the component model simulator when extension and upscaling was performed. The enhanced black oil model simulator was sensitive to relative permeability curves, and resulted in computational problems. However, the black oil model can successfully be used for qualitatively screening studies [39].

4. Reservoir Simulation

Simulation of the performance of a petroleum reservoir refers to the construction of a model whose behavior assumes the appearance of an actual reservoir [40]. The purpose of a reservoir simulator is to simulate field exploitation and estimate field performance of a real reservoir without the costs of real life trial and error, which therefore makes simulators important tools in petroleum engineering [40,41].

Once a reservoir simulation model is constructed, it may be adjusted so that it reasonable models the historical behavior of an existing reservoir and wells. This adjustment process is known as history matching. Forecasts can then be made under a variety of operating conditions. These results combined together with economic models can enable the engineer to make decisions concerning the operation of the reservoir [40].

The ECLIPSE Blackoil Simulator was applied for reservoir modeling in this study. By numerical modeling, reservoir simulation is used to quantify and interpret physical phenomena, which can be further extended to project future performance. The reservoir is divided into several discrete cell units in three dimensions, namely (x, y, z), or dimensions (I, J, K) used in this thesis. The progression of reservoir and fluid properties are further modeled through time and space in a series of discrete steps [42].

4.1 ECLIPSE Black Oil Simulator – Reservoir Simulation Tool

The ECLIPSE Blackoil Simulator treats gas and oil phases as representatives of one component through time. The model assumes that there are no compositional changes of gas and oil components, as they are treated as constants relative to pressure and temperature [42]. The model utilizes PVT tables to define variation of physical properties, as well as data that relates the surface and reservoir volumes of the oil and gas components [43].

4.1.1 Set of Equations

A mathematical simulation model is based on a set of equations that describe the physical processes active in the reservoir [40]. Darcy's law in three dimensions, as first described in

section 2.1.2, describes fluid flow in the reservoir. The material balance equation assures the mass flow into a cell is equal to the mass flow out of the cell and into the neighboring cell, and is defined as:

$$-\nabla \cdot M = \frac{\partial}{\partial t}(\phi\rho) + Q \tag{4.1}$$

Where M is the mass flux, ϕ is porosity, ρ is density and Q is cumulative flow [42].

The simulator flow equation solved for each cell and timestep in ECLIPSE is a combination of Darcy's law and the material balance equation:

$$\nabla \cdot \left[\left(\frac{k_r}{\mu\beta}\right)(\nabla P - \gamma\nabla z)\right] = \frac{\partial}{\partial t}\left(\frac{\phi}{\beta}\right) + \frac{Q}{\rho} \tag{4.2}$$

Where k_r is relative permeability and β is volume factor. The term $\left(\frac{k_r}{\mu\beta}\right)(\nabla P - \gamma\nabla z)$ represents the mobility of a fluid phase.

For reservoir simulation, it is also required a well model, or flow equation, which provides a detailed description of fluid flow in the well bore:

$$q_{p,j} = T_{wj}M_{p,j}(P_j - P_w - H_{wj}) \tag{4.3}$$

Where:

- $q_{p,j}$ is flow of phase p in connection j
- T is transmissibility
- M is mobility
- P_j is nodal pressure
- P_w is bottom-hole pressure (BHP)
- H_{wj} is head pressure

4.1.2 Computational Order of Input Data

In order to run a simulation, ECLIPSE requires a single input data file created by the engineer, which contains a complete description of the model. The parameters described concerns reservoir, fluid and rock property descriptions, as well as a planned recovery schedule. The input data for ECLIPSE is prepared in free format using a keyword system [42]. The simulation data files that are read by ECLIPSE comprises the following structure of sections:

1. RUNSPEC section
2. GRID section
3. EDIT section (Optional. Not included in the data files in this thesis)
4. PROPS section
5. REGIONS section
6. SOLUTION section
7. SUMMARY section
8. SCHEDULE section

ECLIPSE reads the data files section by section, and outputs various information about the simulation results defined by the engineer. After a completed run, the outputs can be analyzed and visualized in postprocessors such as FloViz and Office, which were applied during the work of this thesis.

Figure 4.1 illustrates which sections contribute to the different terms in the flow equation 4.3.

Figure 4.1: Illustration of each individual section's contribution to the flow equation [42].

4.2 EOR Simulation in ECLIPSE

As a simulation tool, Eclipse enables the engineer to model chemical enhanced oil recovery techniques to improve tertiary recovery within the simulation workflows [44]. The aim for using EOR techniques is to improve the recovery efficiency by altering fluid properties. The three main types of EOR are miscible, chemical and thermal [43]. Chemical EOR is emphasized in this thesis.

4.2.1 Low Salinity Waterflood Modeling in ECLIPSE

The low salinity option can be selected by specifying the LOWSALT keyword in the RUNSPEC section. Along with the BRINE keyword, this initializes the modeling of the low salinity effects.

LOWSALT enables modeling the salinity dependence of the oil and water relative permeabilities and the water-oil capillary pressure as functions of salt concentration, while gas relative permeability and gas-oil capillary pressure are assumed to be independent of salt concentration and are looked up directly in the high salinity gas saturation table. The SATNUM and LWSLTNUM keywords are further used to define the immiscible high and low salinity saturation regions, respectively [43].

In systems where water and oil are defined as active phases, The SWOF keyword is used to input tables of water relative permeability, oil-in-water relative permeability and water-oil capillary pressure as functions of water saturation. For a three-phase system where gas is an additional active phase, the SGOF keyword is also specified, which tabulates the gas/oil saturation functions [43]. See appendix A or B for application example of the low salinity option.

The coreflood experiment described in this thesis, from which production results and differential pressures would be history matched by the research group, was performed by constant rate imbibition governed by an unsteady-state flow regime. Unsteady-state flow gives uncertain estimates to capillary pressure, and capillary pressure was not measured separately. The capillary pressure was therefore defined to be zero in the core model and sector model simulation runs applied with results from history matching.

4.2.1.1 Relative Permeability and Capillary Pressure Interpolation

The *Schlumberger Technical Description* provides a detailed description of the salinity dependence of relative permeabilities and capillary pressure, which is modeled as a two-stage process. Summarized, the saturation function table lookups are performed using scaled saturation end-points. The following description of the relative permeabilities and capillary pressure interpolations are directly collected from the *Schlumberger Technical Description*, and holds for three-phase modeling [43]:

The relative permeabilities and capillary pressure are interpolated according to:

$$k_{rw}^{i} = F_1 k_{rw}^{l} + (1 - F_1) k_{rw}^{h} \tag{4.4}$$

$$k_{row}^{i} = F_1 k_{row}^{l} + (1 - F_1) k_{row}^{h} \tag{4.5}$$

$$k_{rog}^{i} = F_1 k_{rog}^{l} + (1 - F_1) k_{rog}^{h} \tag{4.6}$$

$$P_{cow}^{i} = F_2 P_{cow}^{l} + (1 - F_2) P_{cow}^{h} \tag{4.7}$$

Where:

- F_1 and F_2 are weighting functions tabulated in the LSALTFNC keyword in the PROPS section.
- Superscripts h, l, i denote the high, low and interpolated table saturation end-points, respectively.

The low salinity model applied in ECLIPSE is based on the salinity-dependent relative permeabilities and capillary pressure proposed by Jerauld et al [18], equation 3.4-3.8, where this default LOWSALT option gives a linear interpolation of the relative permeabilities and capillary pressure.

In a two-phase water-oil system, only the water relative permeability, two-phase oil relative permeability to water and the water-oil capillary pressure are employed. These relative permeabilities and capillary pressure are modeled in a similar manner to the description above [43].

4.2.2 Surfactant Flood Modeling in ECLIPSE

The surfactant option can be enabled by specifying the SURFACT keyword in the RUNSPEC section. The ECLIPSE surfactant model does not aim to model detailed chemistry of a surfactant flooding process. It rather models the important features of surfactant floods on a full field basis [43]. See appendix A or B for application example of the surfactant option.

4.2.2.1 Surfactant Option, Relative Permeability and Capillary Pressure Interpolation

Specifying the SURFACT keyword in combination with the LOWSALT keyword in the RUNSPEC section, the high and low salinity immiscible saturation functions are combined in a similar manner to the description in section 4.2.1.1, and are further combined with the miscible saturation functions. The miscible saturation region is specified by the SURFNUM keyword in the REGIONS section, combined with the immiscible saturation regions SATNUM and LWSLTNUM [43].

The following description of the relative permeabilities and capillary pressure interpolations are directly collected from the *Schlumberger Technical Description* [43]:

The oil-water capillary term is taken from the interpolated immiscible term in equation 4.7. The miscible and immiscible water and oil relative permeability are interpolated according to:

$$k_{rw}^{i} = F_3 k_{rw}^{mis} + (1 - F_3) k_{rw}^{imm} \tag{4.8}$$

$$k_{row}^{i} = F_3 k_{row}^{mis} + (1 - F_3) k_{row}^{imm} \tag{4.9}$$

Where:

- F_3 is a weighting function, function of the capillary number, and tabulated in the SURFCAPD keyword in the PROPS section:

$$F_3 = F_{kr}(logN_c) \tag{4.10}$$

- F_{kr} is an interpolation parameter
- Subscripts mis, imm denote the miscible and immiscible table saturation end-points, respectively.

For the default three-phase oil relative permeability model, the oil relative to gas is interpolated between the miscible and the immiscible values:

$$k_{rog}^{i} = F_3 k_{rog}^{mis} + (1 - F_3) k_{rog}^{imm} \tag{4.11}$$

The capillary number is defined in the *Schlumberger Technical Description* as:

$$N_c = C_N \frac{\|K \cdot \nabla P_o\|}{\sigma_{ow}} \tag{4.12}$$

Where:

- C_N is a conversion factor depending on the units used
- K is permeability
- P_o is the potential
- σ_{ow} is the IFT

4.2.2.2 Surfactant and Surface Tension

By specifying surfactants in the models, the SURFST keyword is required in the PROPS section to control the surfactant relative permeability and capillary pressure model. Adding surfactants to injection water causes the surface tension between water and oil to decrease. This will further lead to a reduced capillary pressure, giving rise to reduction in residual oil saturation as previously capillary trapped oil is mobilized. The surface tension also affects the water and oil relative permeabilities through the capillary number. The SURFST keyword tabulates the water-oil surface tension as a function of surfactant concentration [43].

4.2.2.3 Surfactant Solution Viscosity

The viscosity of the pure salted water is defined in the PVTW keyword in the PROPS section. In order to investigate how an addition of surfactants modifies the viscosity of the water, the SURFVISC keyword is specified in the PROPS section to define surfactant viscosity as a function of surfactant concentration [43]. Water-surfactant solution viscosity is then calculated as follows:

$$\mu_{ws}(C_{surf}, P) = \mu_w(P) \frac{\mu_S(C_{surf})}{\mu_w(P_{ref})} \tag{4.13}$$

Where:

- μ_{ws} is viscosity of water-surfactant solution
- C_{surf} is present surfactant concentration
- P is pressure
- μ_w is water viscosity defined in the PVTW keyword
- μ_S is the viscosity from the SURFVISC keyword
- P_{ref} is reference pressure defined in the PVTW keyword

4.2.2.4 Surfactant Adsorption

The amount of surfactant adsorbed by the rock formation is a function of the surrounding surfactant concentration, defined in the SURFADS keyword in the PROPS section [43]. The quantity of adsorbed surfactant is calculated as follows:

$$M_{AdsSurf} = PORV \cdot \frac{1-\phi}{\phi} \cdot MD \cdot CA(C_{surf}) \tag{4.14}$$

Where:

- $M_{AdsSurf}$ is mass of adsorbed surfactant
- $PORV$ is pore volume of the cell
- ϕ is porosity
- MD is mass density of the rock defined in the SURFROCK keyword
- $CA(C_{surf})$ is adsorption isotherm as a function of local surfactant concentration

4.2.3 Polymer Flood Modeling in ECLIPSE

The enabling of modeling polymer floods is activated by specifying the keyword POLYMER in the RUNSPEC section. The desirable decrease in water mobility as a result of adding polymer to injection water can be caused by two effects: A higher solution viscosity, and reduction of rock permeability as polymers adsorb onto the rock surface or become trapped [43]. The polymer-oil relative permeability is the same as the water-oil relative permeability. See appendix A or B for application example of the polymer option.

4.2.3.1 Polymer Solution Viscosity

When considering the effect of polymer on viscosity of the aqueous phase, both effects of physical dispersion at the leading edge of the polymer slug and viscous fingering at the rear edge of the slug must be incorporated by allocating effective viscosity values to the fluid components. These viscosity values are calculated using the Todd-Longstaff technique, where a mixing parameter is applied to the viscosity terms in the fluid flow equations [43].

The effective polymer viscosity is:

$$\mu_{p,eff} = (\mu_m(C_p))^{\omega} \cdot \mu_p^{1-\omega} \tag{4.15}$$

Where:

- $\mu_m(C_p)$ is viscosity of a fully mixed polymer solution as a function of increasing polymer concentration
- μ_p is viscosity of the solution at maximum polymer concentration
- ω is the Todd-Longstaff mixing parameter

The mixing parameter is provided using the obligatory PLMIXPAR keyword in the PROPS section, which defines the degree of segregation between water and polymer. If $\omega = 0$, the water is completely segregated from the polymer solution, while $\omega = 1$ yields a fully mixed solution. The PLYMAX keyword specifies the maximum salt and polymer concentrations to be used in calculating the effective viscosities [43].

The partially mixed water viscosity is calculated in an analogous manner:

$$\mu_{w,e} = (\mu_m(C_p))^{\omega} \cdot \mu_w^{1-\omega} \tag{4.16}$$

Where μ_w is pure water viscosity.

The PLYVISCS keyword is defined in the PROPS section where the viscosity of a fully mixed polymer solution is a function of polymer solution concentration. The SALTNODE keyword is also specified if the brine option is activated, where the number of entries corresponds to the number of polymer solution viscosities entered in the PLYVISCS keyword [43]. Non-Newtonian rheological behavior for polymer solutions is not included in this study, as the reservoir bulk rates are approximately constant.

4.2.3.2 Polymer Adsorption

The amount of polymer adsorbed is entered as a function of polymer solution concentration, defined in the PLYADS keyword in the PROPS section, indicating there is no salinity dependence of the adsorption. Adsorption is treated as an instantaneous effect, where a stripped water bank is created at the leading edge of the polymer slug [43].

As polymer is adsorbed, a reduction in permeability of the rock to the passage of the aqueous phase follows. This reduction is directly related to the adsorbed polymer concentration, and requires a specification of the residual resistance factor (RRF) for each rock type in order to compute the reduction in permeability. This is defined in the PLYROCK keyword in the PROPS section [43]. The actual resistance factor, or relative permeability reduction factor, is calculated:

$$R_k = 1.0 + (RRF - 1.0)\frac{C_p^a}{C_p^{a\,max}} \tag{4.17}$$

Where:

- C_p^a is concentration of adsorbed polymer
- $C_p^{a\,max}$ is maximum adsorbed polymer concentration

The dead pore volume for each rock type must also be specified in the PLYROCK keyword, which represents the inaccessible pore volume to the polymer solution in each grid cell [43].

5. Simulation Models

Tertiary recovery methods were modeled and simulated on different scales in this study to evaluate the applicability of EOR methods on a North Sea oil field, and to evaluate how key reservoir conditions and properties of the injected tertiary fluids affected field performance and recovery. In combination with history matching performed on core scale as an analytical function for adapting the models, optimized field-development plans could be selected and field prognosis could be acquired from the results.

The three following simulation models form the basis of the simulations evaluated in this study:

- Core model
- Sector model
- Field model

Each model represents a section at distinctive scales from the North Sea oil field. The most evident differences between the models are volume and grid dimensions, which will be defined for each model later in this chapter. Otherwise, they resemble each other according to fluid properties and to some extent petrophysical properties. These properties were further altered in order to evaluate the EOR methods and their effect on oil recovery.

The data files containing the field model was provided by the research group, which is a detailed description of the North Sea oil field investigated in this thesis. By producing a generic sector model with properties collected from the PROPS section of the field model for timesaving purposes, sensitivity studies could be conducted on this model with a smaller scale, as the number and size of the cells in the model is directly linked to the time required to solve a timestep [42]. The alterations done on the conditions and properties during the sensitivity studies were evaluated. If the results were satisfying, these alterations could further be applied in the field model simulations.

The data file containing the core model was provided by the research group, with properties collected from a coreflood experiment conducted on a core from the North Sea oil field. By history matching the production results and the measured differential pressure from the coreflood experiment, relative permeability curves were estimated. These estimated relative

permeability curves along with measured core properties were further applied in the sector model and field model to provide insight and useful knowledge about the flooding performance of the North Sea oil field.

The ECLIPSE Blackoil Simulator has been the main tool for the simulation runs in this study, as well as history matching results from the composite coreflood experiment performed by the research group. The simulation models will be defined in the following sections, with results from simulation runs, sensitivity studies and history matching presented in later chapters.

5.1 Initial Conditions and Properties – an Overview of the Models

In the following sections, an overview of the governing conditions and properties of the initial models will be presented.

The initial data files of the models used for simulations are presented in appendix A and B, with exception of the data file and numerous include files for the field model, as these data are too voluminous to include in the appendix section.

5.1.1 Core Model

The core model follows block centered geometry; a basic grid indexing system with dimensions 102, 1 and 1 grid blocks in I, J and K directions, respectively. This is defined in the RUNSPEC section. The lengths of grid blocks 2-101 in I direction are 0.182 cm, while the outermost grid blocks, namely 1 and 102, are both at 0.01 cm. As the core model is representing core flooding, the two outermost blocks will therefore deviate from the other blocks concerning properties; injection and production during experiments will happen at the inlet and outlet of the core, respectively, and not through drilled wells, explaining the shorter lengths of these outermost blocks. The grid blocks in J and K directions are 3.28 cm, defined in the GRID section. Figure 5.1 visualizes the three-dimensional (3D) core model at initial conditions, where the illustrated scale represent oil saturation within the reservoir.

The core model consists of two wells. The properties of the wells are defined in the SCHEDULE section, where the injection well named INJ is located to the left in grid blocks (1, 1, 1), while the production well named PROD is located to the right in grid blocks (102, 1, 1). The injection well is controlled by surface flow rate set to a target of 5.79 ml/h, defined in the WCONINJE keyword in the SCHEDULE section. This is different from the production

well controlled by bottom-hole pressure set to a lower limit of 1 atm, defined in the WCONPROD keyword.

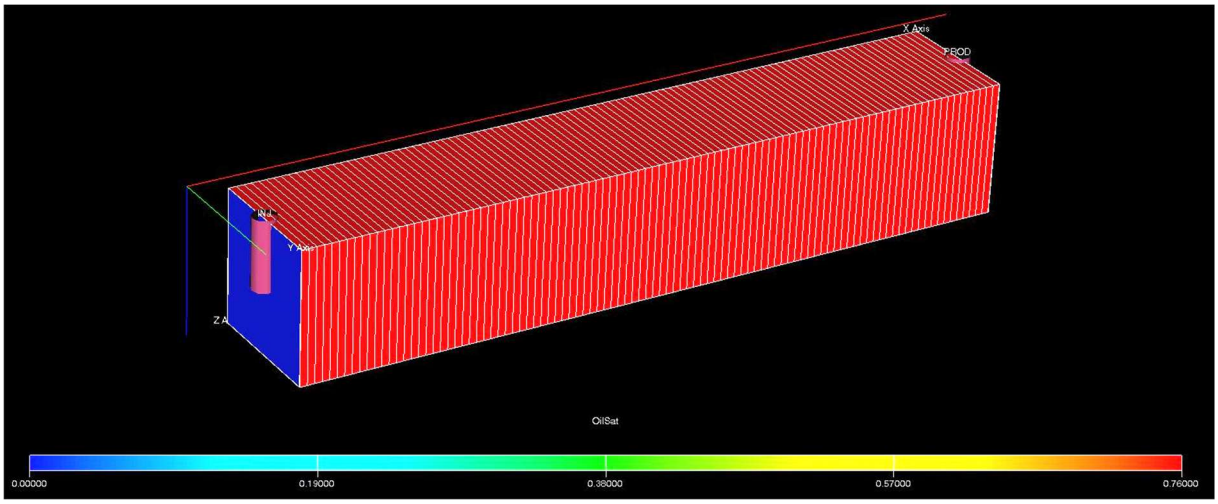

Figure 5.1: Three-dimensional illustration of the core model grid at initial distribution of reservoir oil, visualized in the postprocessor option FloViz. The illustrated scale represent oil saturation within the reservoir. The injector (INJ) and producer (PROD) are marked.

The porosity and permeability of the core model was experimentally measured to be 28.4% and 862 mD, respectively. These values are both set as constant values for blocks 2-101, indicating a homogeneous model. However, these values do not apply to the two outermost grid blocks in I direction, as they differ from the other grid blocks, as mentioned. The porosity and permeability is here 99.9% and 10 000 mD, respectively, to ensure free flow of the fluids in the injection and production wells representing inlet and outlet, respectively.

The pore volume is 55.6 cm^3 and the volume of the oil originally in place is 42.5 cm^3. The initial water saturation is 0.24 and equal for grid blocks 2-101. The initial water saturation for the outermost blocks is 1.

5.1.2 Sector model

As for the core model, the sector model follows block centered geometry with dimensions 10, 100 and 10 grid blocks in I, J and K directions, respectively. The length of each grid block in I and J directions are 5 m, while the grid blocks in K direction are only 1 m. Figure 5.2 visualizes the three-dimensional sector model at initial conditions.

The sector model consists of two wells, similar to the field model. The injection well named INJ is located to the left in grid blocks (5, 7, 2-9), and the production well named PROD is located to the right in grid blocks (5, 93, 2-9). The scale illustrated in figure 5.2 represents oil saturation within the reservoir. Both the injection rate and production rate is controlled by reservoir fluid volume rate set to a target of 34 rm^3/day, which corresponds to 1 pore volume (PV) of water injected per 5 years. Reservoir volumetric rate as a control mode is different from the initial field model. This will be elaborated later in this thesis.

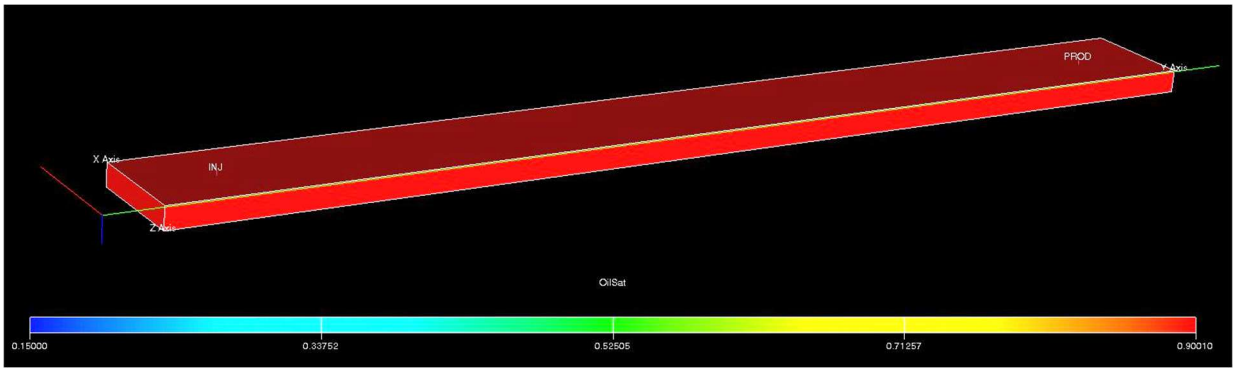

Figure 5.2: Three-dimensional illustration of the sector model grid at initial distribution of reservoir oil, visualized in the postprocessor option FloViz. The illustrated scale represent oil saturation within the reservoir. The injector (INJ) and producer (PROD) are marked.

The porosity of the sector model is defined to be 25% for each cell, while the horizontal permeability is set to 200 mD in both I and J directions, indicating a homogeneous model. Vertical permeability in K direction is also set to 200 mD, allowing for cross-flow between layers and gravitational effects on fluid distribution throughout the simulations.

The pore volume of the sector model is 62 500 m^3, where the total volume of the oil originally in place is 44 734 m^3.

It becomes apparent from figure 5.2 that the initial water saturation is equal for each grid block in the model. This has been defined using the keyword SWATINIT in the PROPS section, where the initial water saturation is set to 0.10 for each cell in the model.

5.1.3 Field Model

In the GRID section, dimensions of the field model are listed as 11, 25 and 90 grid blocks in I, J and K directions, respectively. Include files containing values defined in the keywords COORD and ZCORN specifies corner point geometry, meaning that the locations of all eight corners are provided independently, and not all angles are necessarily right angles [45]. Figure 5.3 visualizes the three-dimensional field model at initial conditions. The illustrated scales represent oil saturation within the reservoir.

The model consist of two wells, where the injection well named A-7 is located to the left in grid blocks (2, 2, 29-90), and the production well named A-8 is located to the right in grid blocks (10, 24, 2-17), as can be seen in figure 5.3. The injection well is controlled by surface flow rate, which is set to a target of 718 sm^3/day. This is different from the production well, which is controlled by liquid rate set to a target of 675 sm^3/day.

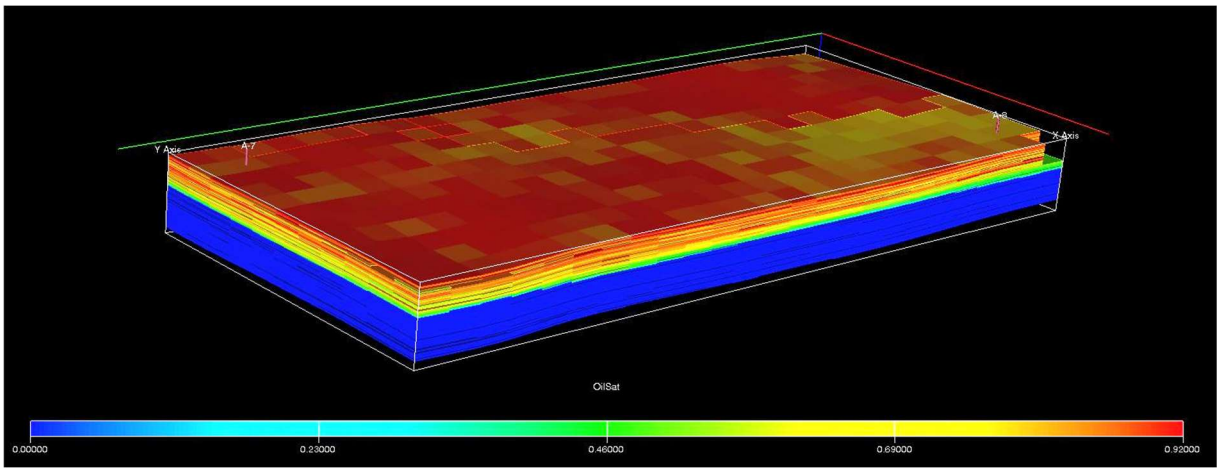

Figure 5.3: Three-dimensional illustration of the field model grid at initial distribution of reservoir oil, visualized in the postprocessor option FloViz. The illustrated scale represent oil saturation within the reservoir. The injector (A-7) and producer (A-8) are marked.

Permeability and porosity are defined at an average weighted by either pore volumes or bulk volumes. The horizontal permeability in I and J directions weighted by pore volumes is 3816.75 mD, while the vertical permeability in K direction is 444.66 mD. This is different from the permeabilities weighted by bulk volumes, where the horizontal permeability is 3338.92 mD and the vertical permeability is 398.28 mD. As for the permeability, porosity differs between the weighted values. Defined by weighting pore volumes, the overall porosity

is 25.29%, while the overall porosity is 24.58% weighted by bulk volumes. These indifferences indicate that the reservoir is heterogeneous, which can cause a decrease in sweep efficiency as heterogeneity affects the distribution of reservoir fluids [4].

The pore volume of the field model is $14.39 \cdot 10^6$ m^3, where the total volume of the oil originally in place is $35.62 \cdot 10^5$ m^3. The initial water saturation in all grid blocks from layer 44-90 in K-direction is 1, with all initial oil existing in the upper half of the model, where S_{wi} is 0.38. The model therefore contains a total average initial water saturation at 0.70.

5.2 Properties of Phases Initially in Place

The active phases initially present in the models and their properties are mostly common for all three models for the purpose of phase similarity between the models. As the initial sector model is a generic model with properties collected from the field model, naturally these two models have several more properties in common than with the core model, which is produced based on empirical results achieved by the research group.

The common phases initially present are high salinity formation water and oil. In addition to water and oil, gas and dissolved gas are also defined as initial phases in the sector model and field model.

The connate water initially in place has a salinity of 40 kg/m^3. This holds for both the sector model and the field model, which also have the following properties in common. The water has a viscosity of 0.3162 cP and a density of 1037 kg/m^3. Since the oil contains dissolved gas, oil viscosity is listed in the PVTO keyword in the PROPS section as it varies with field pressure. This varying viscosity also holds for the gas, which is listed in the PVDG keyword. The oil and gas densities are set to be 835.14 kg/m^3 and 1.33 kg/m^3, respectively.

In the core model, the connate water has a salinity of 0.036 g/cm^3. The water viscosity at 0.5 cP is slightly higher than in the sector and field model, as is the water density at 1.1 g/cm^3. No gas is defined as an initial phase in the core model, resulting in a dead oil with constant viscosity of 2.6 cP, and a density of 0.87 g/cm^3.

The phase properties described in section 5.2 remained unaltered through all simulation runs in chapter 6, while the properties from history matching were applied in the sector model and field model in chapter 7.

5.3 Low Salinity Water, Surfactant and Polymer Modeling

5.3.1 Injection Fluids

As for the phases initially present in the models, the injection fluids and their properties utilized in the simulations were mostly similar for all three models. For sensitivity study results from one model to be applicable in another model, the conditions and injection fluid properties in the models bust be similar.

The properties of the injection fluids are defined in the PROPS section, while the concentrations are defined in the SCHEDULE section – the WPOLYMER keyword is used to define the salt and polymer concentrations in the injection stream of each well, and the WSURFACT is used to specify the surfactant concentration in the injection stream of each well [45]. Table 5.1 lists the initial concentrations of the different injection fluids utilized in each model, where the concentrations for injected high and low salinity water remained unaltered in each model through all simulations conducted in this study, with exception of the sector and field model runs in chapter 7 where results from history matching were applied.

Table 5.1: Initial concentration of injection fluids for each model

	Sector and Field Model	***Core Model***
Injection Fluid	**Concentration [kg/m^3]**	**Concentration [g/cm^3]**
High Salinity Water	40	0.036
Low Salinity Water	4	0.0036
Surfactant	5	0.01
Polymer	0.5	0.001

The solution viscosity and adsorption of the individual chemical is a function of the added chemical's concentration. As sensitivity of the models to changes in surfactant viscosity, adsorption and surface tension will not be investigated in this thesis; these properties remained unaltered through all simulations in chapter 6. Otherwise, both polymer viscosity and adsorption were modified in the sector model as a sensitivity study.

5.3.1.1 Initial Surfactant Viscosity, Adsorption and Surface Tension

The following initial surfactant viscosities, adsorptions and surface tensions of the different models are collected from the corresponding initial data files, listed in the appendix section. These values are equal for the sector model and field model. Surfactant viscosity, adsorption and surface tension are defined in the SURFVISC, SURFADS and SURFST keywords, respectively.

Core model:

```
SURFVISC                SURFADS                 SURFST
-- S-conc Visc          -- S-conc   Ads         -- S-conc   ST
-- g/cm3    cP          -- g/cm3    g/g         -- g/cm3    dynes/cm
0.0         0.5         0.0         0.0         0.0         16
0.01        7.0         0.001       0.000001    0.001       0.01
                        0.002       0.00001     0.01        0.005
                        0.01        0.00002
```

Sector model and field model:

```
SURFVISC                SURFADS                 SURFST
-- S-conc Visc          -- S-conc   Ads         -- S-conc   ST
-- kg/m3   cP           -- kg/m3   kg/kg        -- kg/m3    N/m
 0.0        0.3162      0.0         0.0         0.0         0.016
 1.0        0.437       1.0         0.00001     1.0         0.00001
 5.0        2.08        2.0         0.0001      5.0         0.000005
                        10.0        0.0002
```

5.3.1.2 Initial Polymer Viscosity and Adsorption

The following initial polymer viscosities and adsorptions of the different models are collected from the corresponding initial data files, listed in the appendix section. These values are equal for the sector model and field model. Polymer viscosity and adsorption are defined in the PLYVISCS and PLYADS keywords, respectively.

Core model:

```
PLYVISCS                        PLYADS
-- PolConc  WaterVisc           -- LocPolConc SatConcPolAds
-- g/cm3    cP                  -- g/cm3          g/g
0.0         1                   0.0               0.000
            1                   0.001             0.00003
            1
0.001       8.0
            8.0
            8.0
```

Sector model and field model:

```
PLYVISCS                        PLYADS
-- PolConc  WaterVisc           -- LocPolConc SatConcPolAds
-- kg/m3    cP                  -- kg/m3          kg/kg
0.0         1.0                 0.0               0.000
            1.02                0.4               0.0015
            1.039 /             0.8               0.0025
0.7         10.0
            10.2
            10.39
```

5.4 Initial Relative Permeability Curves

Properties such as relative permeabilities and capillary pressures depend on the phase saturations, and are described by saturation functions. In this study, the core model is treated as a two-phase system where these properties are one-dimensional functions dependent on water saturation. Data for these functions are entered as tables in the SWOF keyword in the PROPS section. Unlike the core model, the sector model and field model are treated as three-phase systems where water and gas relative permeabilities are treated as one-dimensional functions, while oil relative permeability is treated as a two-dimensional function by interpolating the oil-water and oil-gas relative permeabilities. Data for these functions are entered as tables in the SWOF and SGOF keywords in the PROPS section [43].

The initial relative permeability curves are presented in this section, as the curves presented in section 5.4.2 will later be altered during sensitivity studies.

5.4.1 Core Model – Initial Relative Permeability Curves

The initial relative permeability curves for the core model are illustrated in figure 5.4-5.5. The curves are estimated by performing a history match in ECLIPSE, and are provided by the research group.

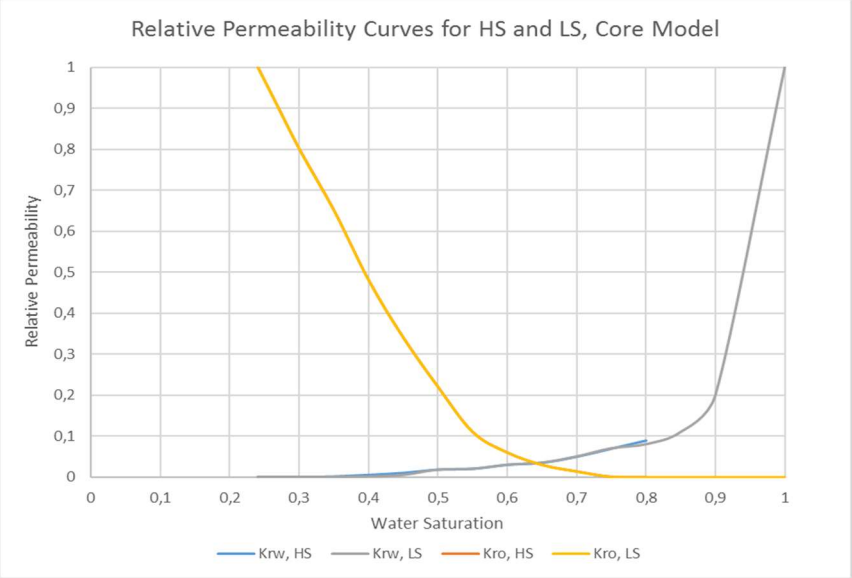

Figure 5.4: Initial relative permeability curves in core model for high salinity and low salinity water. Provided by the research group.

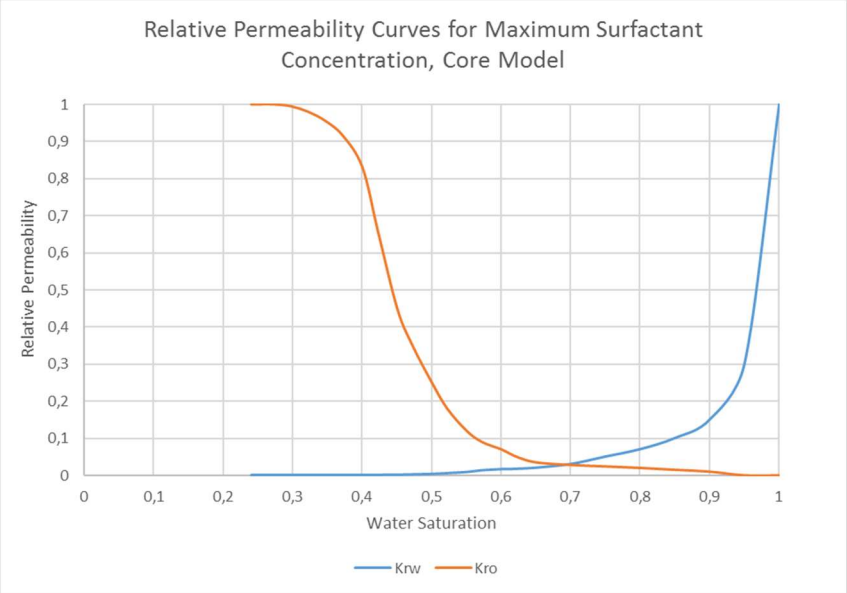

Figure 5.5: Initial relative permeability curves in core model for maximum surfactant concentration. Provided by the research group.

5.4.2 Sector Model and Field Model – Initial Relative Permeability Curves

Figure 5.6-5.7 illustrate the initial relative permeability curves modeled in the sector and field model. The curves are provided by the research group.

The relative permeability curves modeled during low salinity waterflooding in combination with surfactant is based on an assumption of an extreme process where there exists a linear relationship between the relative permeabilities and water saturation, indicating an approximately miscible displacement. This relationship is displayed in figure 5.7, where the residual oil saturation, S_{or}, is assumed to be 0.

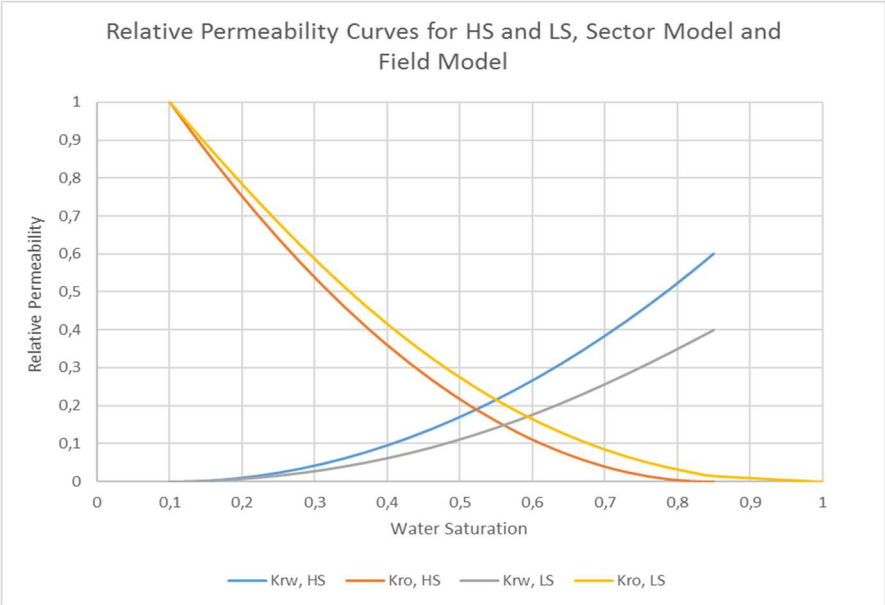

Figure 5.6: Initial relative permeability curves in sector model and field model for high salinity and low salinity water. Provided by the research group.

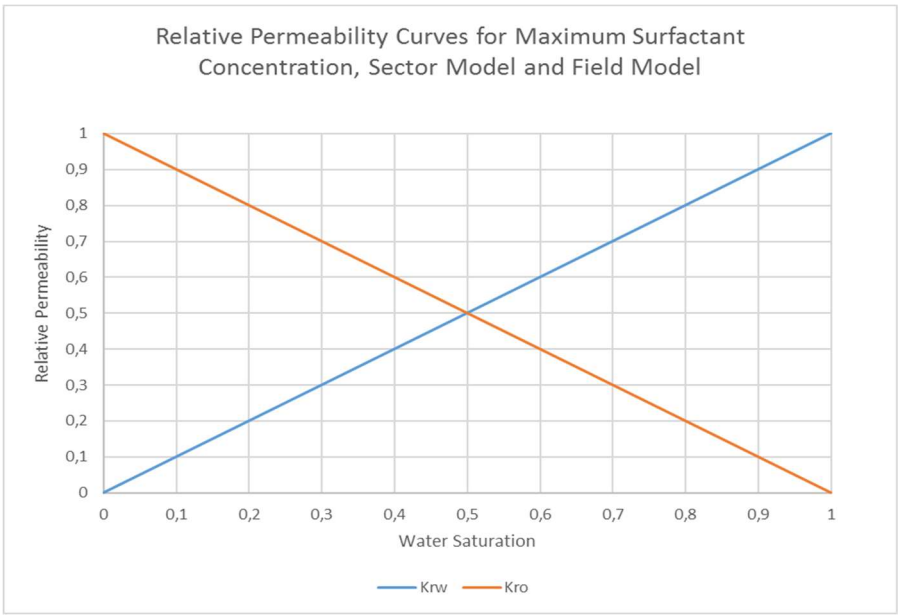

Figure 5.7: Initial relative permeability curves in sector model and field model for maximum surfactant concentration. Provided by the research group.

6. Sensitivity Studies and Simulation Results

The initial models defined in chapter 5 provide base case simulations. According to Fanchi [46], such base case simulations establish a basis from which to compare changes in field performance resulting from changes in existing operating conditions. Sensitivity studies provide useful insight on the sensitivity of a model to changes in input parameters, and to further determine the likelihood that a set of parameters will be realized [46].

The current chapter presents an investigation on the effect of altering different key reservoir properties in the sector and field model, as well as alternative flooding strategies, in order to optimize the field performance.

6.1 Adjustment of the Field Model

The initial field model was run to evaluate the potential of the model and input parameters that needed to be adjusted in order to optimize the model. Little attention was given to sensitivity studies of EOR chemicals on the initial field model as this would be investigated later in the sector model. The results from the runs conducted in this section are presented in appendix C. The parameters evaluated in the field model are as listed:

- Location of injection well perforation
- Governing injection and production control modes

The initial production results indicated that the field model had not yet reached its full potential, and more oil could be produced. Increasing the flooding time span could result in an increase in recovery. Another option, which was investigated, was to elevate the location of the injection well perforation and decreasing the perforation area. This allowed for a larger macroscopic sweep of the reservoir by the injected fluids caused by gravitational effects, which resulted in an incremental oil recovery.

An important finding was the great change in bottom-hole pressure during production, which is illustrated in appendix figures C.2 and C.6. Injection and production rates were governed by surface flow rate, causing a deviation from material balance and a resulting unstable pressure over time. As approximately constant pressure during flooding is desirable, reservoir fluid

volume rate (RESV) was defined to be the governing control mode for both the injector and producer. This resulted in a more stable pressure and voidage replacement was achieved.

The desirable effect of changing control modes to RESV on pressure was further applied in the sector model, where sensitivity studies on flow functions and EOR chemicals were conducted, presented in section 6.2.

6.2 Sensitivity Study on Sector Model

Sensitivity studies were performed on the sector model in ECLIPSE to investigate how altering different parameters affect the simulation results. The satisfactory results from the sensitivity studies would later be applied in the field model. The parameters evaluated in the sector model are as listed:

- Flow functions
- Chemical adsorption
- Chemical concentration
- Chemical viscosity
- Analytical flow functions
- Timing of slugs

6.2.1 Distribution of Residual Oil

The initial flooding sequence was a high salinity waterflooding over a time span of 5 years (1 PV) followed by a low salinity chase water injected for 10 years (2 PV). The high and low salinity salt concentrations were 40 kg/m^3 and 4 kg/m^3, respectively. Production results from the initial simulation run are listed in table 6.1, with oil recovery, corresponding recovery factor, water cut and bottom-hole pressure. Figure 6.1-6.2 displays development of oil recovery, water cut and BHP during flooding.

Table 6.1: Production results at the last production date from the initial HS-LS flooding

Case study	Oil Recovery [%OOIP]	Oil Produced [m^3]	Water Cut [%]	BHP [bar]
HS-LS	86.92	38 883.11	95.61	249.52

The high salinity waterflooding resulted in an oil recovery of 68.76% of OOIP, with additional 18.16% resulting from low salinity waterflooding. This gave a low S_{or} of 0.12. Water breakthrough occurred after 2.5 years, with a steady incline of oil recovery until end of flooding, displayed in figure 6.1. No visual effect of LS on oil recovery indicates that the LS flooding is an extension of the too effective HS flooding, which is contradictory to expected results discussed in section 3.2. The LS injection only results in a slight decrease in water cut after 7.8 years of flooding.

A slight BHP increase caused by initiating LS flooding was observed as a response to additional oil mobilized by the LSW. The steady BHP decline throughout the entire flooding may be caused by an increase in water relative permeability leading to less resistance to water flow as a result of a declining oil saturation.

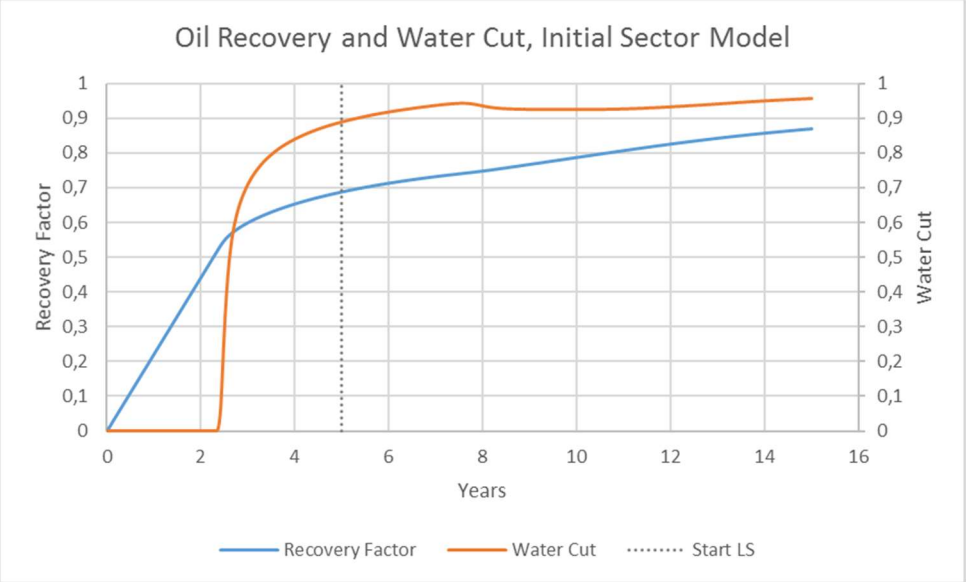

Figure 6.1: Oil recovery and water cut for the initial run of the sector model.

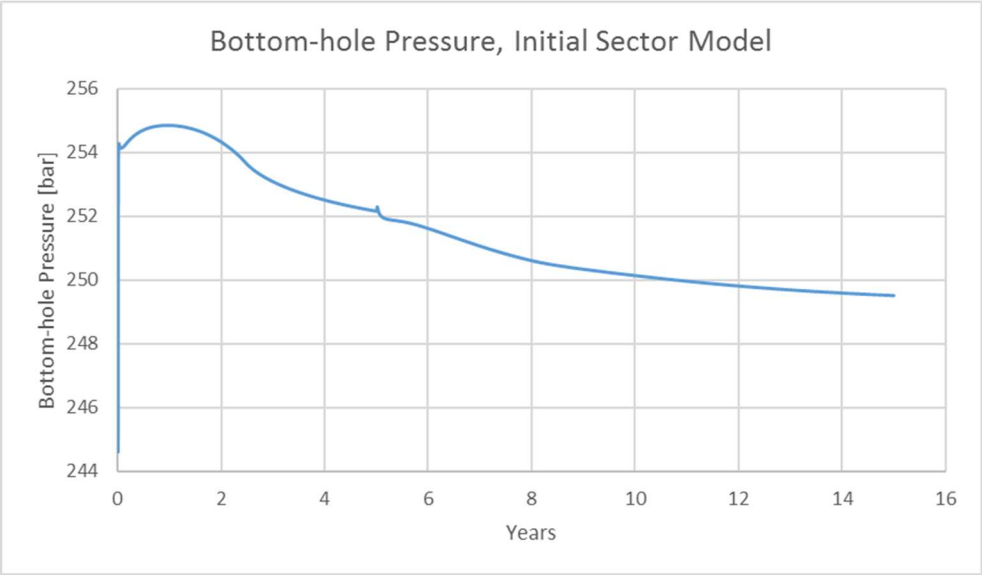

Figure 6.2: Injection well bottom-hole pressure for the initial run of the sector model, altered x-axis.

The 3D illustration of the initial sector model at the end of production in figure 6.3 supports the statement that the simulated process was too effective. A large part of the reservoir was sweeped, where the majority of the residual oil only existed in the upper layers of the reservoir.

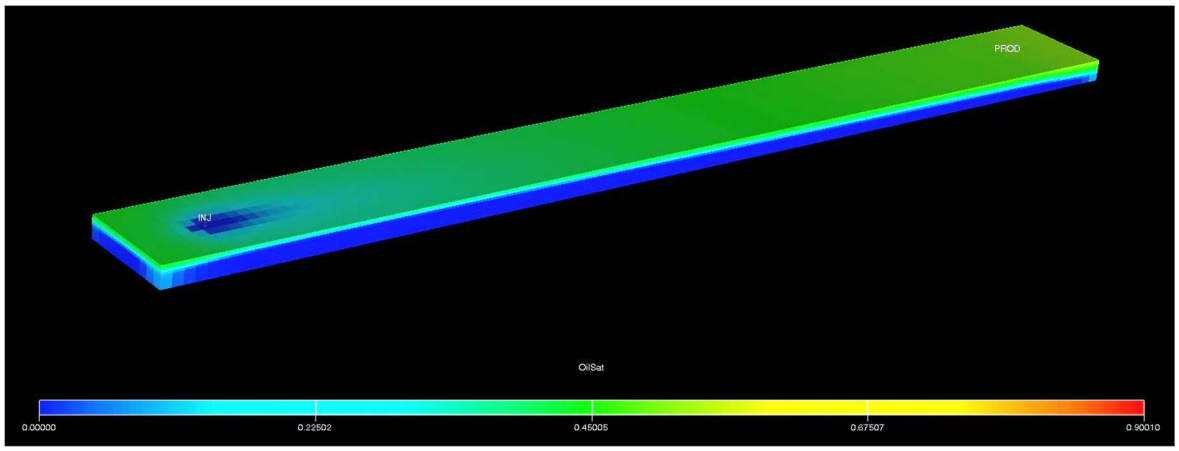

Figure 6.3: 3D illustration of the initial sector model at the end of production, illustrated with oil saturation scale.

6.2.2 Impact of Flow Functions on Oil Recovery

It becomes evident that oil flowed over a wide range of water saturation when the initial relative permeability curves displayed in figure 5.6-5.7 were applied. The residual oil saturation changed from 0.15 to 0 for the transition from high salinity to low salinity in regards to oil relative permeability. After the initial HS-LS flooding, the potential for EOR chemicals was low. A manual modification of k_{ro} is displayed in figure 6.4-6.5, where a reduction in k_{ro} would affect the fluid flow in the formation by reducing the water saturation range over which oil flows. To further impact the fluid flow, S_{or} was increased from 0.15 to 0.3 for HS, and from 0 to 0.15 for LS. These modifications would lead to a more unfavorable mobility ratio and less efficient sweep of the high salinity injection water, as primarily $k_{ro}(HS)$ was reduced.

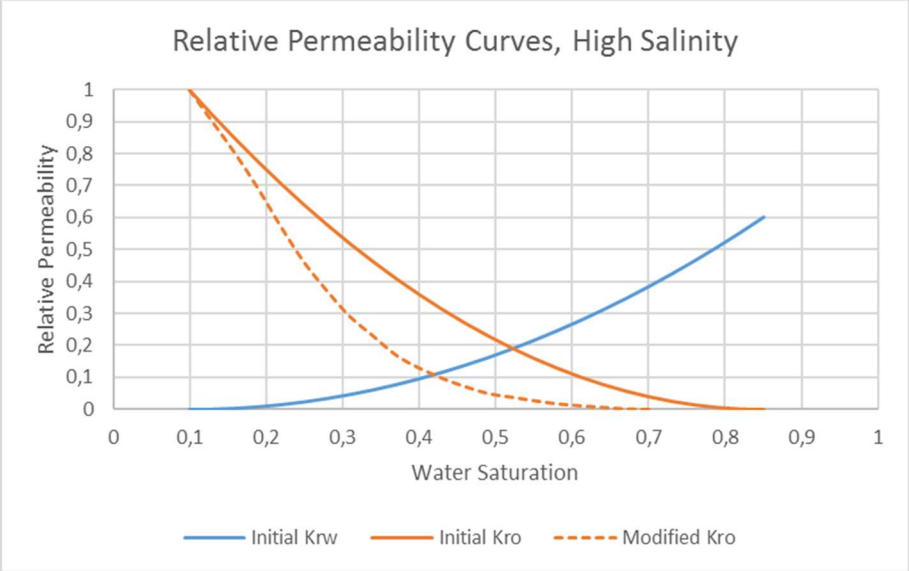

Figure 6.4: Illustration of oil relative permeability alterations compared with initial oil relative permeability and initial water relative permeability, high salinity.

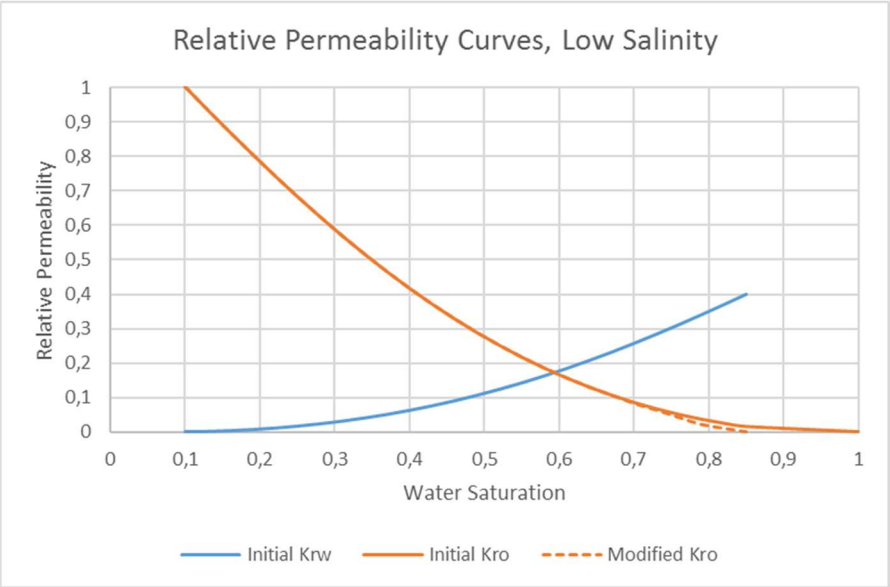

Figure 6.5: Illustration of oil relative permeability alterations compared with initial oil relative permeability and initial water relative permeability, low salinity.

Production results achieved after altering the flow functions are tabulated in table 6.2. The total recovery potential after HS-LS flooding was enhanced by a reduction in recovery factor of 6.01% of OOIP.

Table 6.2: Production results at the last production date from the initial HS-LS flooding and HS-LS flooding with modified k_{ro}

Case study	Oil Recovery [%OOIP]	Oil Produced [m^3]	Water Cut [%]	BHP [bar]
Initial HS-LS	86.92	38 883.11	95.61	249.52
Modified k_{ro}	80.91	36 192.90	98.31	253.83

The oil recovery after 5 years of HS flooding resulted in 54.88% of OOIP, which is 13.88% lower than the initial 5 years HS flooding, revealing a great impact of altering $k_{ro}(HS)$. This caused a significant increase in oil recovery of 26.03% by 10 years of LS flooding. An earlier

water breakthrough after 1.9 years is observed in figure 6.6, with a more distinct effect of LS on oil recovery.

A more unfavorable mobility ratio and an earlier water breakthrough resulted in an earlier increase in water cut, displayed in figure 6.7. The large increase in oil recovery by LS flooding becomes apparent as a drop in water cut to a local minimum of 64.89%, indicating additional mobilized and recovered oil by LSW injection.

A higher restriction to oil flowing as oil relative permeability was decreased resulted in an elevated BHP. The LS effect was revealed as a larger BHP buildup, displayed in figure 6.8.

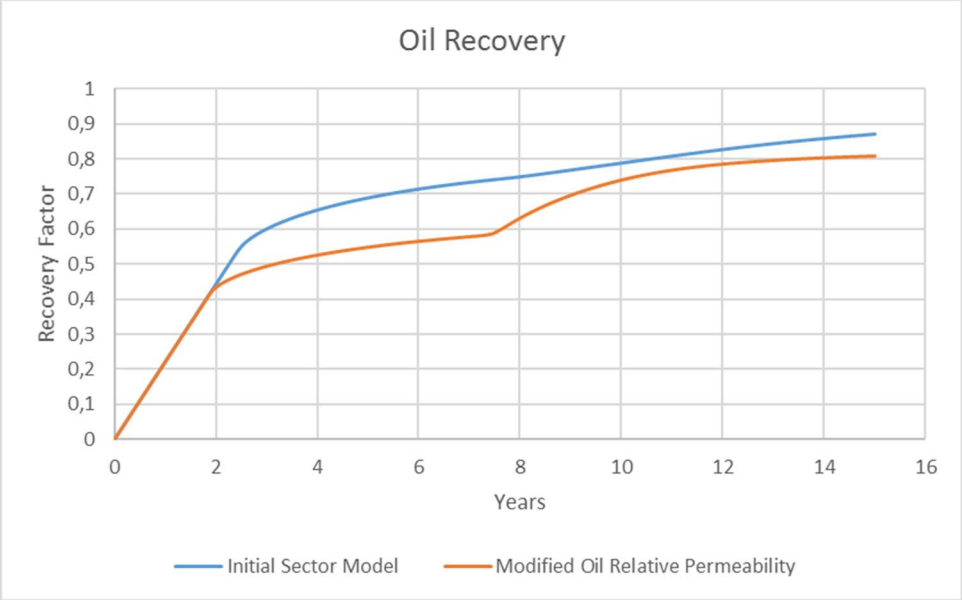

Figure 6.6: Oil recovery for initial HS-LS flooding and HS-LS flooding with modified oil relative permeability.

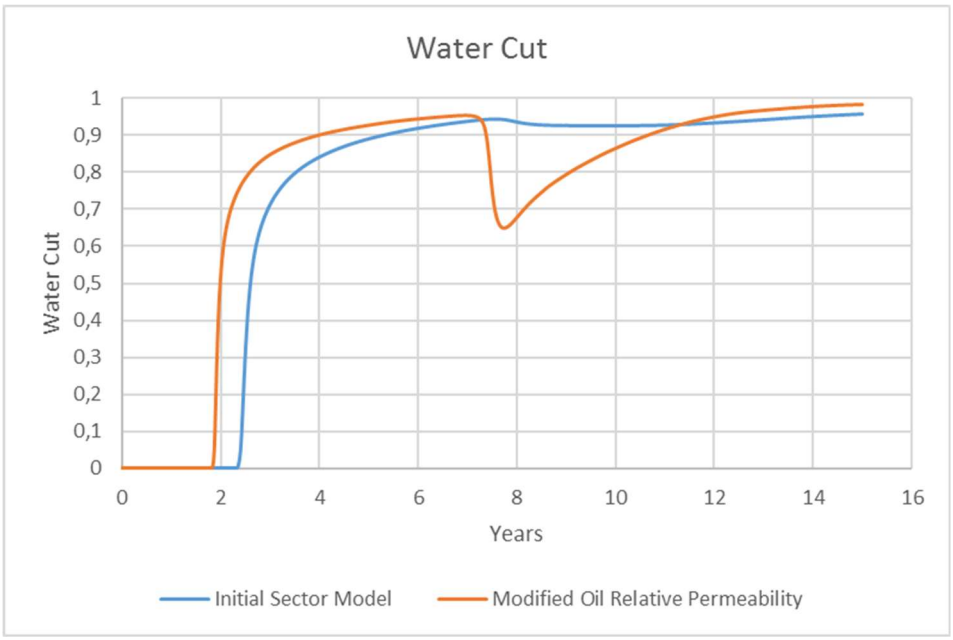

Figure 6.7: Water cut for initial HS-LS flooding and HS-LS flooding with modified oil relative permeability.

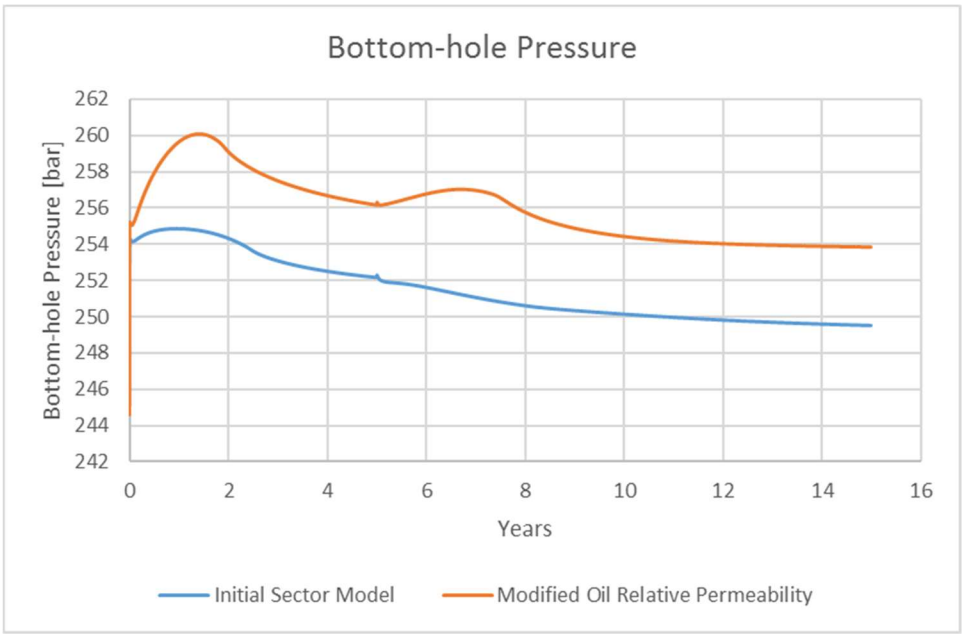

Figure 6.8: Bottom-hole pressure in injection well for initial HS-LS flooding and HS-LS flooding with modified oil relative permeability, altered x-axis.

Residual Oil

The S_{or} was increased from 0.12 to 0.17 by applying a higher restriction to oil flowing. Figure 6.9-6.10 visualizes the compared processes before and after modification at the last production date, with illustrated oil saturation scales. Figure 6.10 reveals a slightly higher residual oil saturation throughout the entire reservoir and corners of the reservoir, with exception of the upper layers.

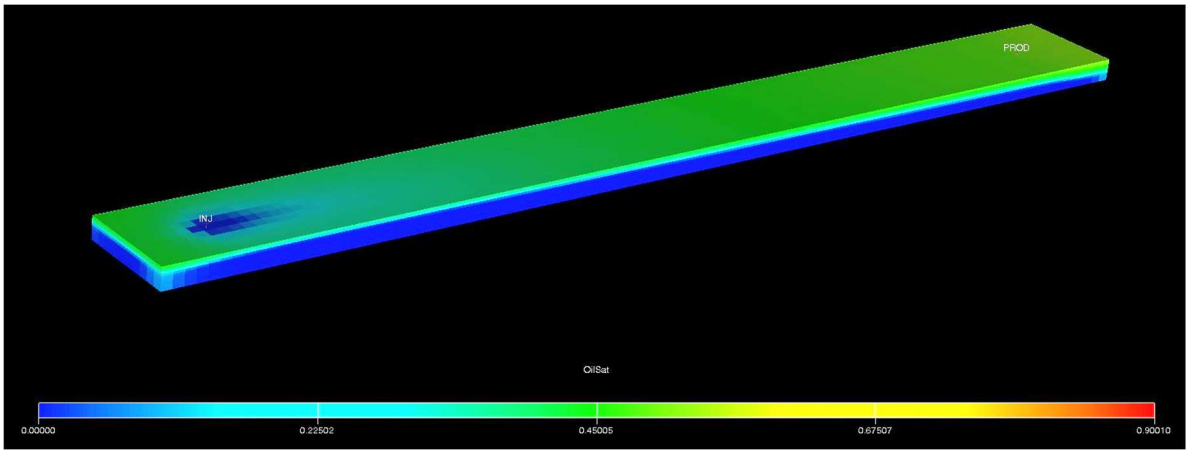

Figure 6.9: 3D illustration of the initial sector model at the end of production, illustrated with oil saturation scale. Figure collected from section 6.2.1.

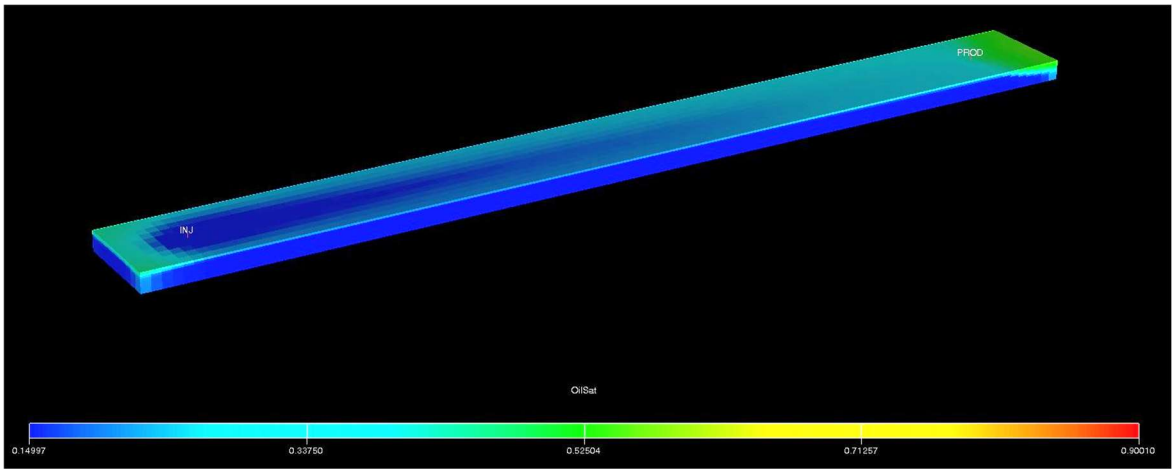

Figure 6.10: 3D illustration of the sector model with modified oil relative permeability at the end of production, illustrated with oil saturation scale.

6.2.3 Effect of EOR Chemicals in the Sector Model

Chemical EOR methods are applied in fields for the purpose of incremental oil recovery. By adding chemicals such as surfactants and polymers to low salinity injection water to decrease surface tension and for mobility aid, it is expected a positive response in recovery. In order to investigate how EOR chemicals affect the simulation results, sensitivity studies on chemical properties were performed on the sector model.

Three hybrid EOR processes with alternative flooding sequences were modeled, initialized with the HS-LS flooding described in section 6.2.2. Following was chemical flooding in tertiary mode, completed with a LS chase water slug. The surfactant concentration and polymer concentration were 5 kg/m^3 and 0.5 kg/m^3, respectively, diluted in low salinity water with a salt concentration of 4 kg/m^3.

The flooding schedules are listed in table 6.3, while the results of flooding with different EOR strategies are listed in table 6.4.

Table 6.3: Flooding sequence of the LSS, LSP and LSSP processes

Case Study	HS [years]	LS [years]	Surfactant [years]	Polymer [years]	LS [years]
LSS	5	10	5	-	10
LSP	5	10	-	5	10
LSSP	5	10	5	5	10

Table 6.4: Production results at the last production date from the initial LSS, LSP and LSSP processes

Case Study	Oil Recovery [%OOIP]	Oil Produced [m^3]	Water Cut [%]	BHP [bar]
Initial LSS	86.69	38 781.51	99.97	251.64
Initial LSP	83.07	37 162.08	99.84	255.57
Initial LSSP	86.72	38 795.50	99.99	253.05

Figure 6.11 displays an increase in oil recovery as a result of surfactants injected after 15 years for the LSS and LSSP processes. The high recoveries were due to the combination of mobilized oil by LSW and surfactants reducing the capillary pressure, securing that the mobilized oil was not re-trapped. Injecting surfactants resulted in an increase of 6-7% of OOIP compared to HS-LS flooding. Contradictory to expected results, the LSP and LSSP processes display a continuous plateau of oil recovery after polymer injection in tertiary mode, and no visual effect of polymers injected. No incremental oil production was achieved by flooding with polymers in a LS established environment, causing the LSS and LSSP recoveries to terminate close in value.

Figure 6.12 displays polymer adsorption, polymer injection rate and total polymer production. These values also holds for the LSSP process, with exception of time (years) where the injection of polymers happened after 20 years of flooding. The polymer adsorption steeply increased at the start of polymers injected at a rate of 16.39 kg/day, where the process terminated with a total polymer adsorption of $29.93 \cdot 10^3$ kg. This corresponds to an absolute adsorption of polymers, explaining why there was a lack of incremental oil production by injecting polymers. A sensitivity study on polymer adsorption will be presented in the next section.

The lack of additional oil recovery by the injection of polymers also becomes apparent in figure 6.13, which illustrates water cut for the processes investigated. The LSS and LSSP processes were approximately equal until production end, where effect of surfactants injected is visible as a drop in water cut after 18.5 years of flooding. The water cut for both the LSP and LSSP processes show no effect of the polymers injected.

Response in BHP by EOR chemicals showed expected results, with polymer injection yielding the most rapid BHP increase caused by a higher viscosity of the polymer solution. The BHP drop with shift to LS chase water stabilized at lower values until flooding termination, as displayed in figure 6.14.

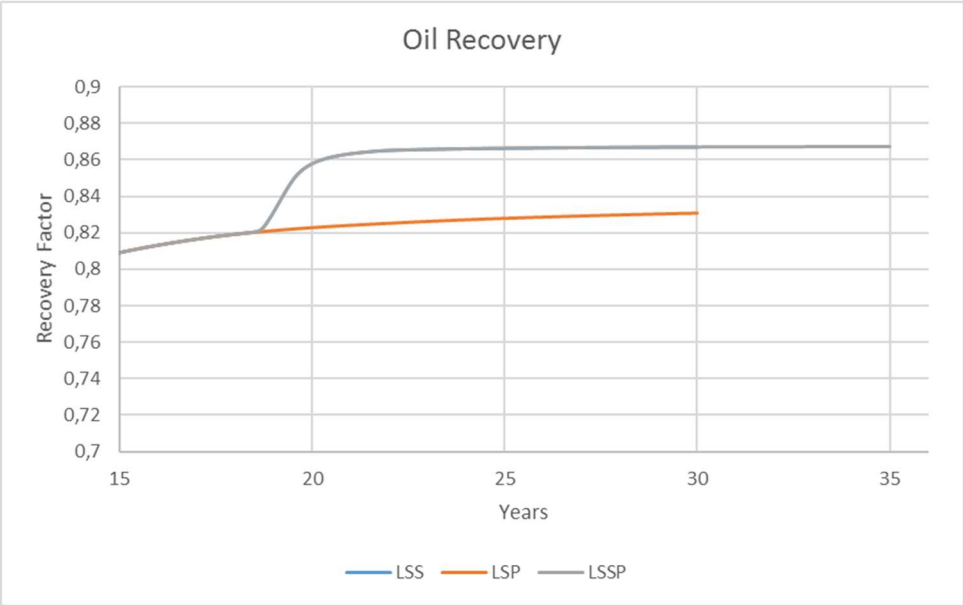

Figure 6.11: Oil recovery for initial LSS, LSP and LSSP processes, altered x-axis and y-axis.

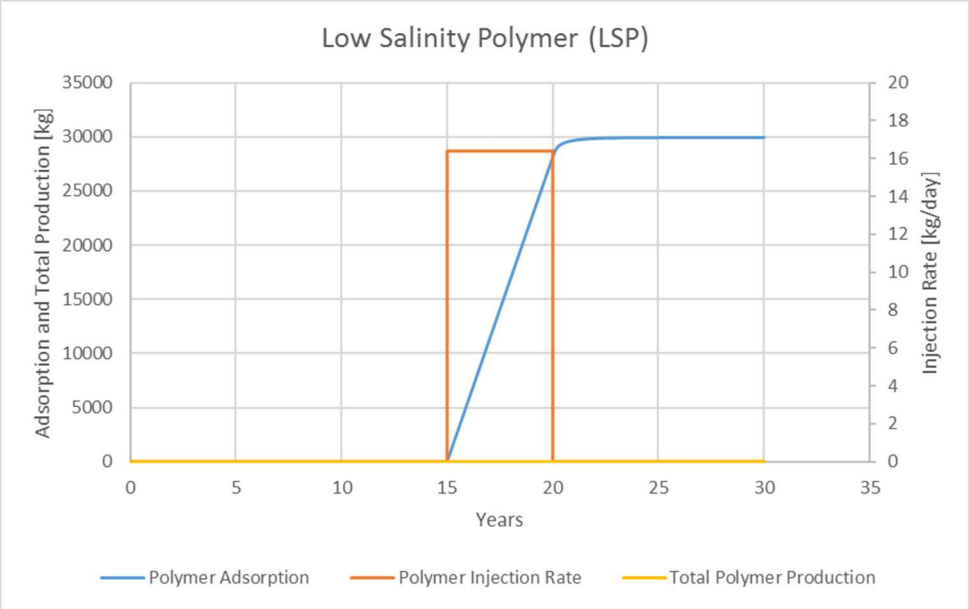

Figure 6.12: Illustration of polymer adsorption, polymer injection rate and total polymer production for the initial LSP process.

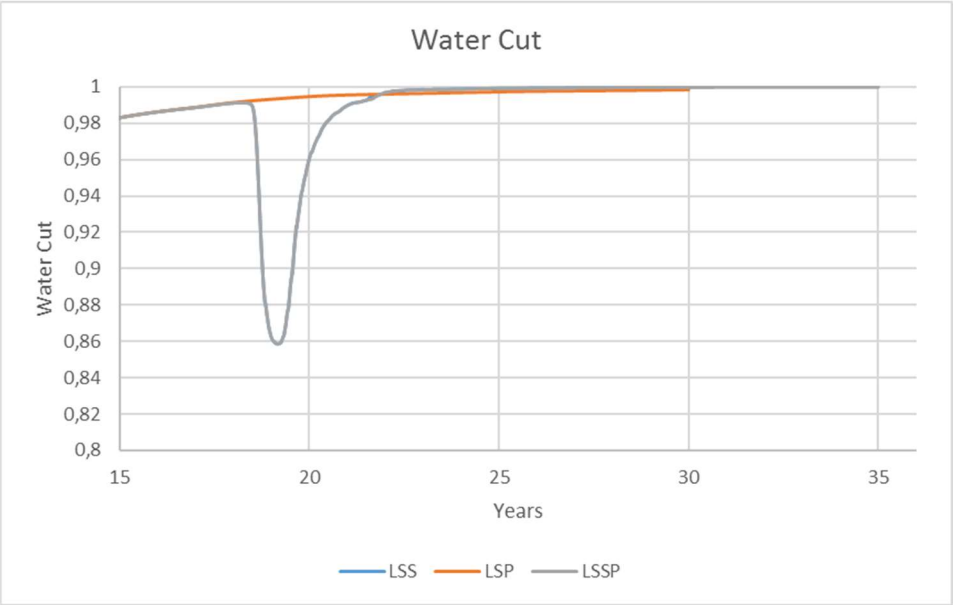

Figure 6.13: Water cut for the initial LSS, LSP and LSSP processes, altered x-axis and y-axis.

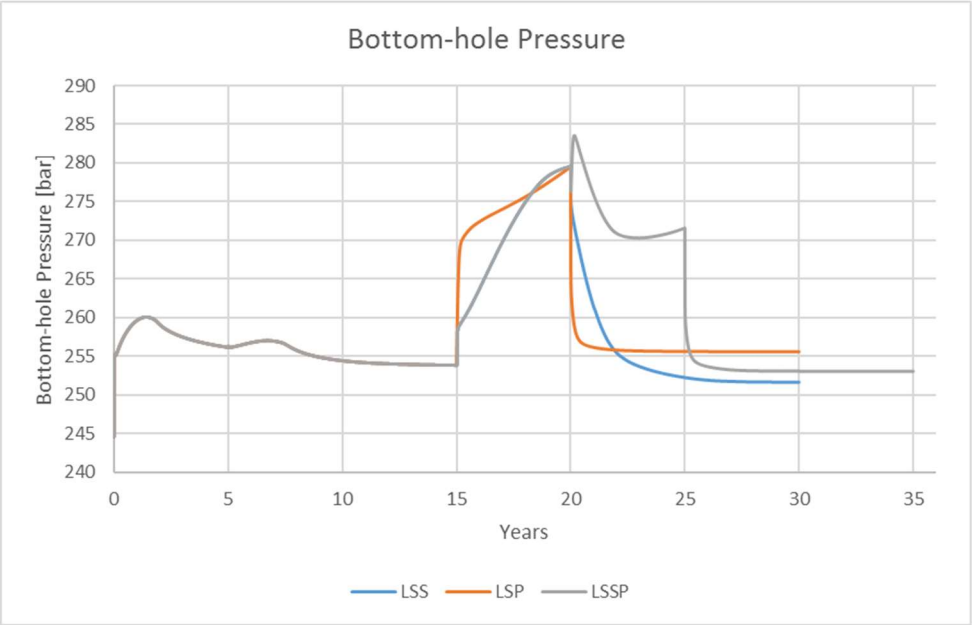

Figure 6.14: Bottom-hole pressure in injection well for the initial LSS, LSP and LSSP processes, altered x-axis.

6.2.4 LSP Sensitivity Study – Modifying Polymer Properties

As adsorption was discovered to be absolute in section 6.2.3, investigations on polymers and their effect on oil recovery in this study could not be conducted while running simulations with the initial adsorption defined in section 5.3.1.2. A sensitivity study on polymer properties was therefore performed in order to gain useful insight in the sensitivity of the sector model to changes in polymer input parameters: 1) polymer concentration was increased to investigate the impact on adsorption, 2) adsorption parameters were altered to identify an optimal adsorption, and 3) an assumption that a further increase in polymer viscosity having no effect on incremental oil production was investigated.

Polymer Concentration

The polymer concentration from the initial LSP process was increased by a number of 10 to 5 kg/m^3, defined in the WPOLYMER keyword in the SCHEDULE section. Table 6.5 lists a comparison of production results from the initial LSP process and the LSP process with modified polymer concentration.

Table 6.5: Production results at the last production date from the initial LSP process and the LSP process with modified polymer concentration

Case Study	Oil Recovery [%OOIP]	Oil Produced [m^3]	BHP [bar]
Initial LSP	83.07	37 162.08	255.57
LSP Modified Polymer Concentration	83.24	37 237.09	267.65

Figure 6.15 reveals only a minimal increase in oil recovery by increasing polymer concentration, with an additional oil recovery of 0.17% of OOIP. The resulting water cut curve by modifying concentration is approximately equal to the LSP water cut displayed in figure 6.13, and is displayed in appendix figure D.1.

Increasing polymer concentration resulted in a total polymer adsorption 10 times higher than the initial LSP process, as well as an injection rate 10 times higher, displayed in figure 6.16.

Absolute polymer adsorption again occurred, as the relative amount of adsorbed polymer was unaffected by the increased polymer concentration.

The only significant difference was the response in BHP, which increased as a result of a higher polymer concentration and a resulting higher viscosity of the polymer solution, as displayed in figure 6.17. In addition, an increase in polymer injection rate contributed to the increase in BHP.

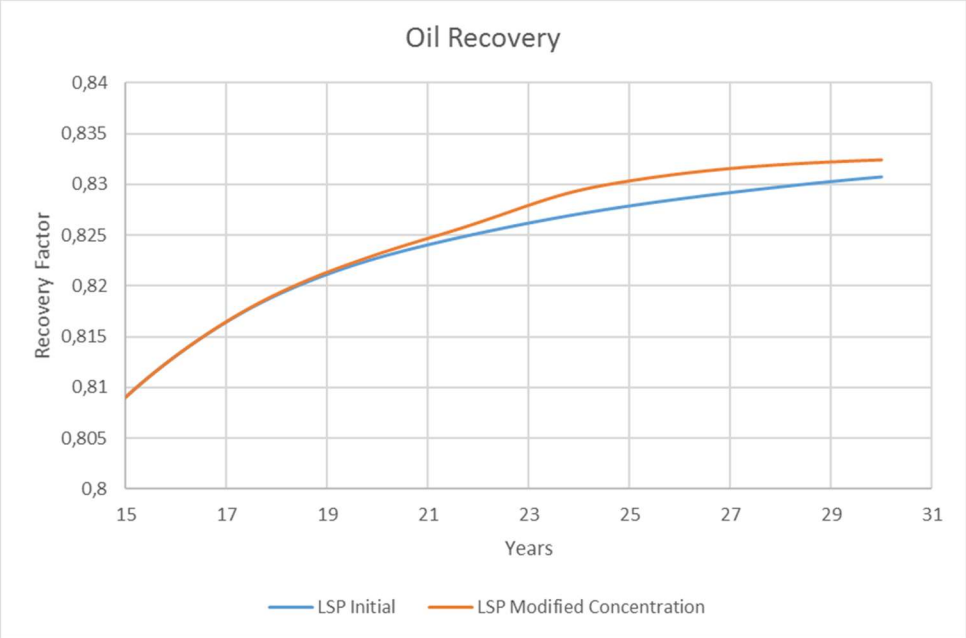

Figure 6.15: Oil recovery for the initial LSP process and LSP with modified concentration, altered x-axis and y-axis.

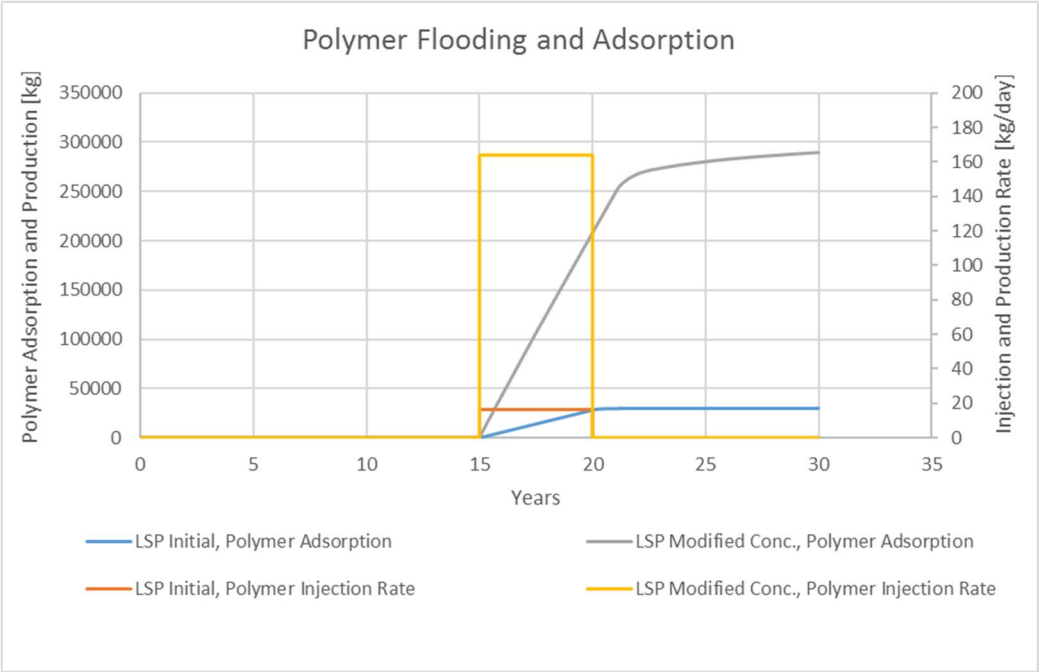

Figure 6.16: Illustration of total polymer adsorption and polymer injection rate for initial LSP process and LSP with modified concentration.

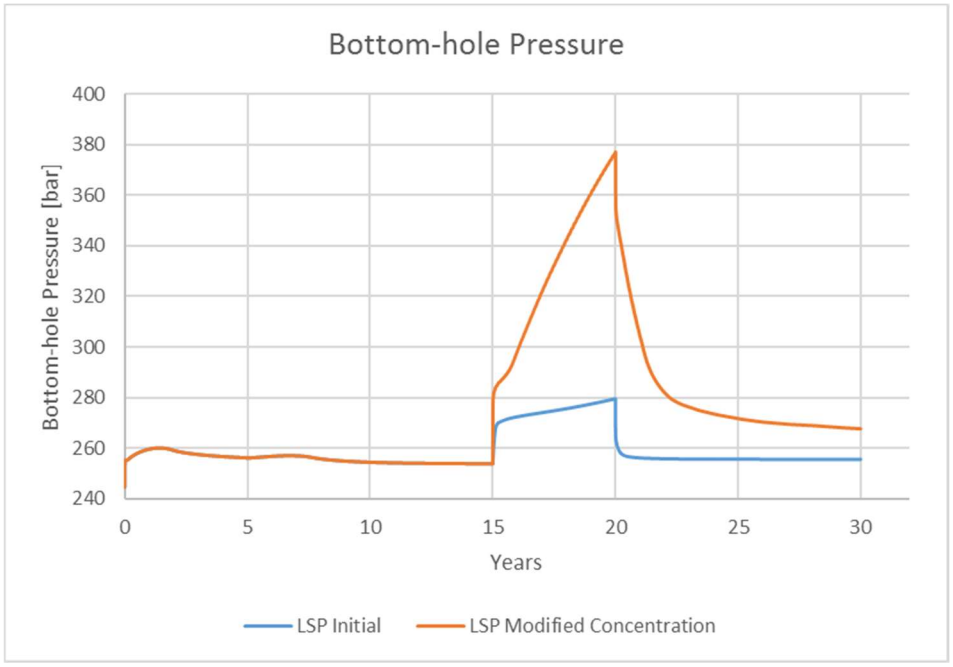

Figure 6.17: Bottom-hole pressure in injection well for the initial LSP process and LSP with modified concentration, altered x-axis.

Polymer Adsorption

Further was the LSP process investigated by applying the extreme assumption of no polymer adsorption onto rock. The results from the simulated process are presented in table 6.6, which compares the production results with results from the initial LSP process.

Table 6.6: Production results at the last production date from the initial LSP process and the LSP process where no polymer adsorption is assumed

Case Study	Oil Recovery [%OOIP]	Oil Produced [m^3]	Water cut [%]	BHP [bar]
Initial LSP	83.07	37 162.08	99.84	255.57
LSP No Adsorption	83.32	37 272.04	99.99	256.73

The lack of polymer adsorption caused an unchanged polymer concentration and polymer viscosity, which resulted in an enhanced microscopic sweep. The polymer effect becomes apparent in figure 6.18 as an acceleration in oil production, with the largest difference after 20 years of flooding. As the oil recovery of the initial process was still increasing at this point, the final oil recovery was only increased by 0.25% of OOIP.

No polymer adsorption resulted in a final polymer production of $27.16 \cdot 10^4$ kg. Figure 6.19 illustrates the total polymer production, and polymer injection and production rate for the process with no polymer adsorption.

The decrease in mobility ratio, which caused a better sweep of the reservoir, is also observed in water cut for the process with no polymer adsorption, displayed in figure 6.20. After approximately one year of polymer flooding, there was a 9% drop in water cut, indicating incremental oil production.

As no polymer was adsorbed onto the porous rock, the concentration of the polymer solution was assumed constant, and so was the viscosity. The BHP response was a larger BHP increase than compared to the initial process, as displayed in figure 6.21, where the polymer viscosity in the initial process decreased as a result of polymer adsorption.

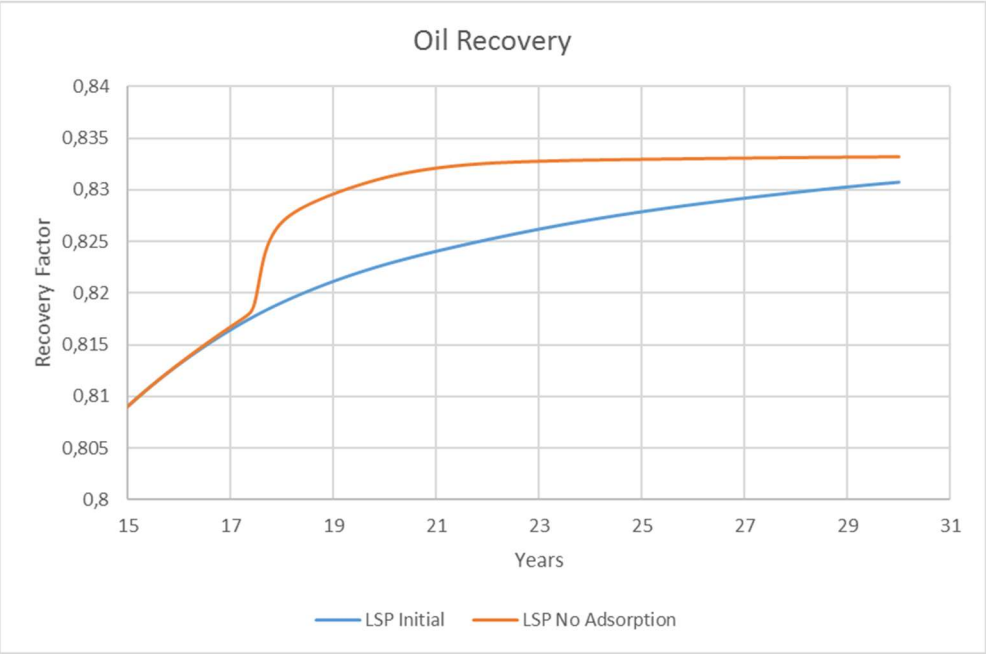

Figure 6.18: Oil recovery for the initial LSP process and LSP with no polymer adsorption, altered x-axis and y-axis.

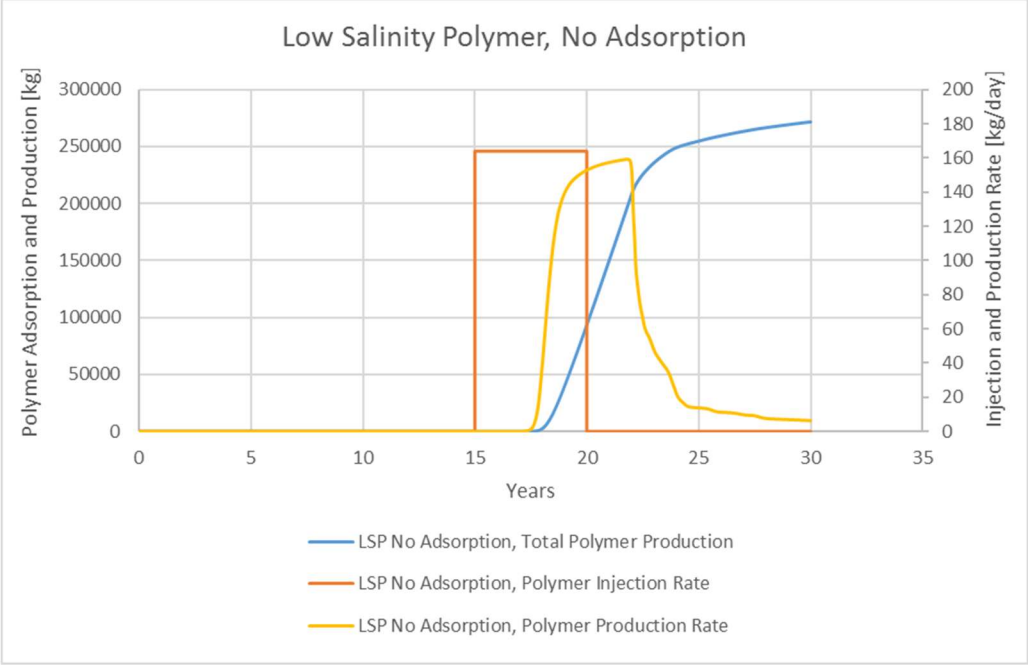

Figure 6.19: Illustration of total polymer production, polymer injection rate and polymer production rate for the LSP process with no polymer adsorption.

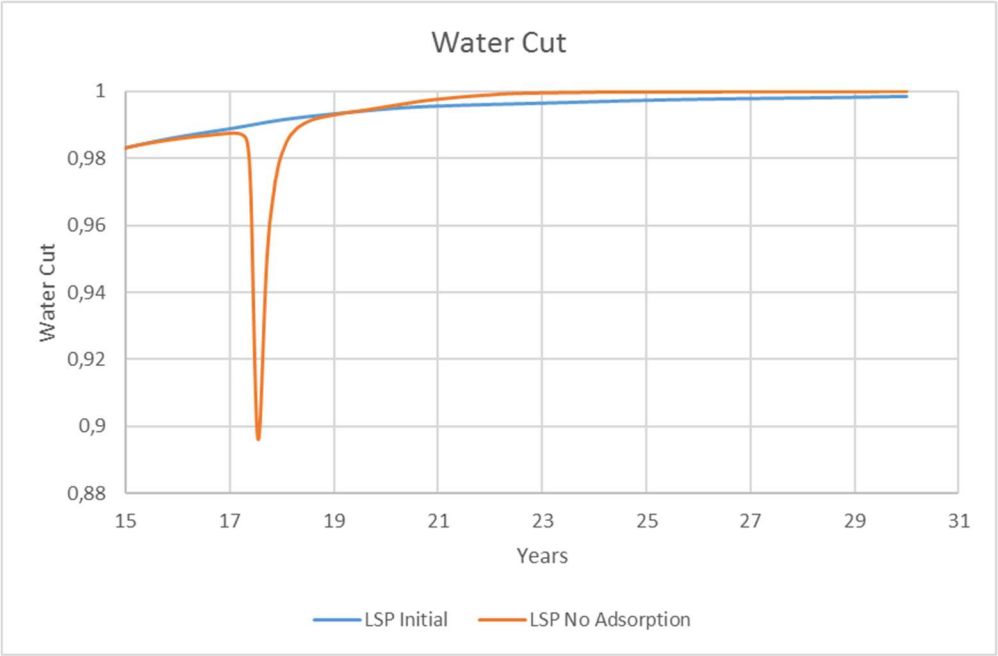

Figure 6.20: Water cut for the initial LSP process and LSP with no polymer adsorption, altered x-axis and y-axis.

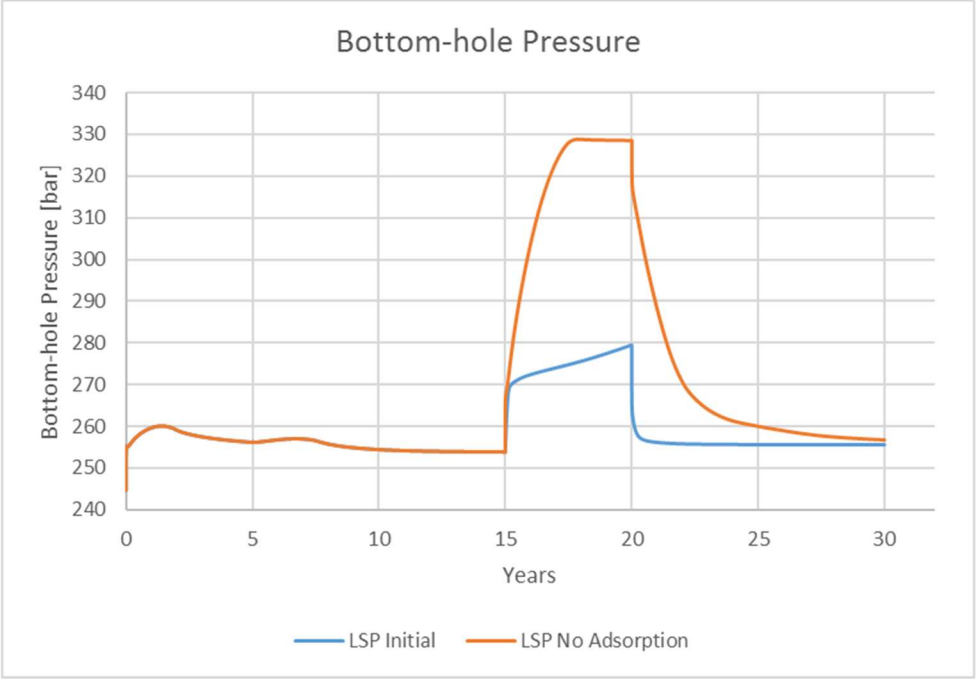

Figure 6.21: Bottom-hole pressure in injection well for initial LSP process and LSP with no polymer adsorption, altered x-axis.

As no polymer adsorption onto reservoir rock was an unrealistic assumption, a new maximum adsorption was defined since the initial polymer adsorption was too effective. $5 \cdot 10^{-5}$ kg/kg was assumed to be a realistic value for maximum adsorption. In combination with the initial polymer concentration of 0.5 kg/m^3 applied, polymer adsorption was then defined in the model as:

```
PLYADS
-- LocPolConc SatConcPolAds
-- kg/m3          kg/kg
      0.0        0.000
      0.4        0.000025
      0.8        0.00005
```

Table 6.7 lists a comparison of the production results at the last production date for the LSP process with no polymer adsorption and the LSP process with modified maximum adsorption.

Table 6.7: Production results at the last production date from the LSP process with no polymer adsorption and the LSP process with modified maximum adsorption

Case Study	Oil Recovery [%OOIP]	Oil Produced [m^3]	Water cut [%]	BHP [bar]
LSP No Adsorption	83.32	37 272.04	99.99	256.73
LSP Modified Maximum Adsorption	83.27	37 250.54	99.98	254.04

The effect of modifying the maximum adsorption was a delayed polymer effect on oil recovery. After 22 years of flooding, the oil recovery curves in figure 6.22 starts leveling out and terminates close in value.

Figure 6.23 illustrates a decrease in both polymer production, injection rate and production rate compared to the corresponding values for the LSP process with no polymer adsorption in figure 6.19. This response was expected as the polymer concentration was decreased.

The water cut curves in figure 6.24 corresponds well with the observed results in oil recovery, where the polymer effect was delayed compared to the process with no polymer adsorption. The decrease in water cut was less than where no adsorption was assumed, as loss of polymers onto rock led to a less efficient sweep by the injected polymer solution.

An increased polymer adsorption caused a smaller BHP increase, as displayed in figure 6.25. This was expected, as adsorbed polymer will result in a lower polymer concentration in solution, and therefore a decrease in viscosity.

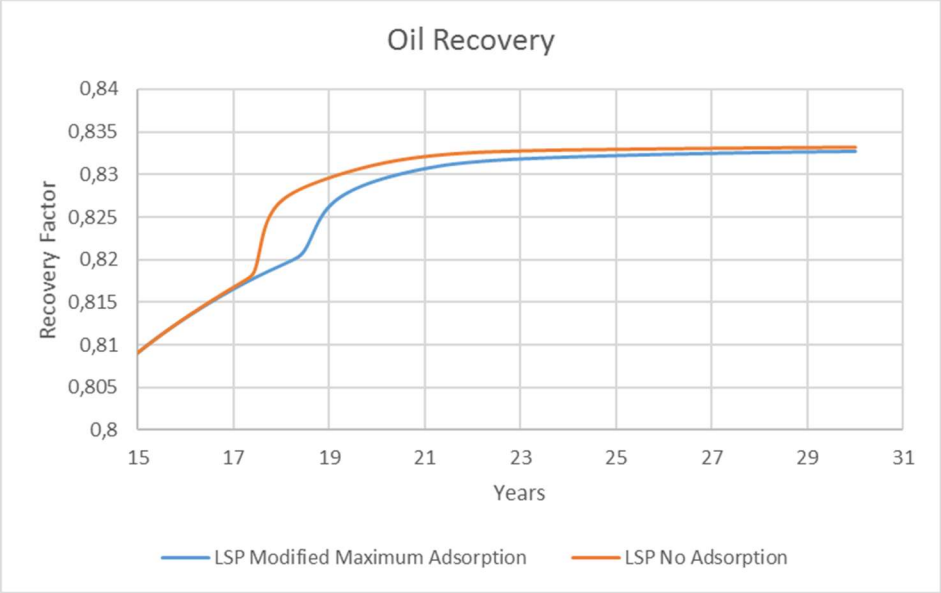

Figure 6.22: Oil recovery for the LSP process with modified maximum polymer adsorption and LSP process where no adsorption is assumed, altered x-axis and y-axis.

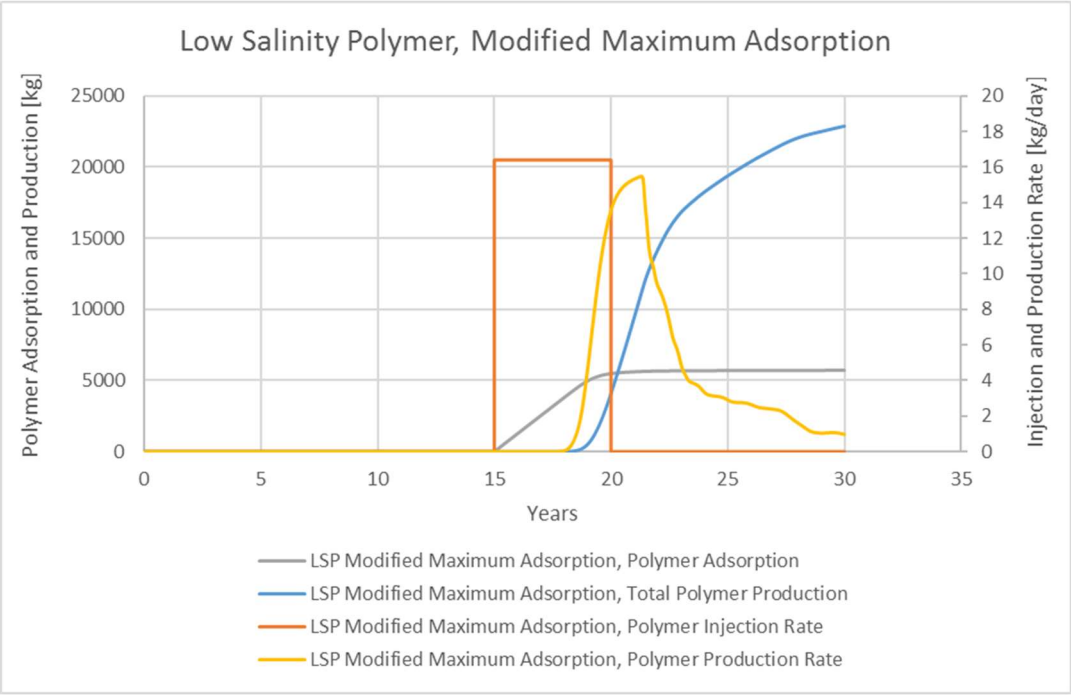

Figure 6.23: Illustration of polymer adsorption, total polymer production, polymer injection rate and polymer production rate for the LSP process with modified maximum polymer adsorption.

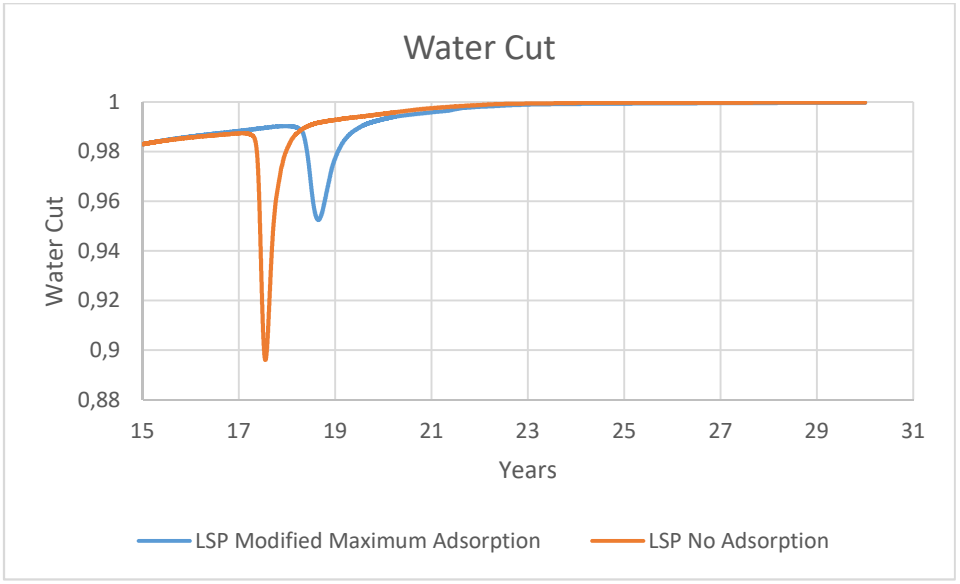

Figure 6.24: Water cut for the LSP process with modified maximum polymer adsorption and LSP process where no adsorption is assumed, altered x-axis and y-axis.

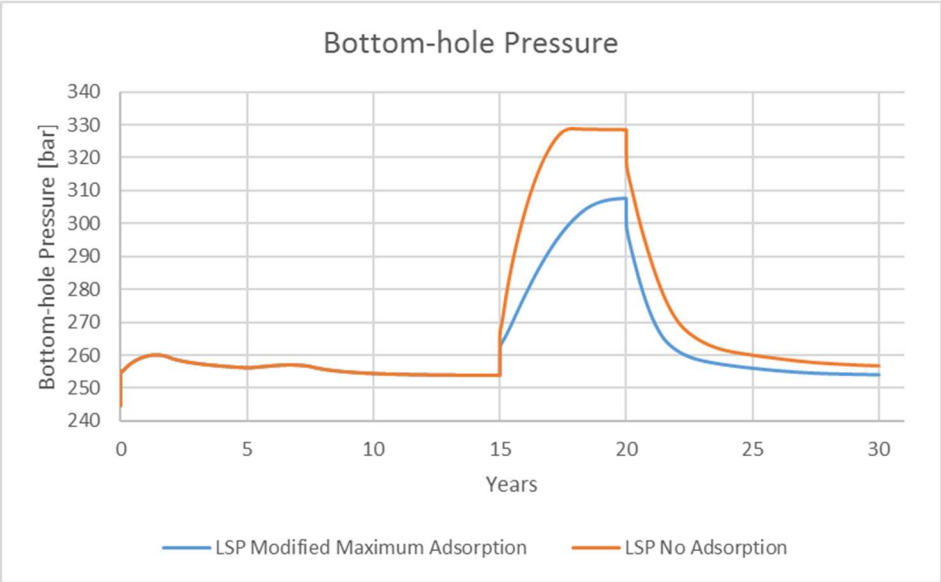

Figure 6.25: Bottom-hole pressure in injection well for LSP with modified maximum polymer adsorption and LSP with no polymer adsorption, altered x-axis.

Polymer Viscosity

The polymer viscosity was increased by a number of ten, along with results from sensitivity studies so far applied in the model. Production results were compared to the previous LSP process where the polymer adsorption was modified, and are listed in table 6.8.

Table 6.8: Production results at the last production date from the LSP process with modified maximum adsorption and the LSP process with modified polymer viscosity

Case Study	Oil Recovery [%OOIP]	Oil Produced [m^3]	Water cut [%]	BHP [bar]
LSP Modified Maximum Adsorption	83.27	37 250.54	99.98	254.04
LSP Modified Polymer Viscosity	83.35	37 285.75	99.96	384.49

The effect of modifying viscosity resulted in an earlier effect of the polymer solution as a slight incremental oil production after 16 years of flooding, followed by a larger increase in

oil recovery after 19.5 years. The compared cumulative oil productions terminated very close in value and varied only with 0.08% of OOIP. The same trends were observed in water cut in figure 6.27.

The large increase in viscosity caused the BHP to reach the target limit of 500 bar, indicating that the injection switched from RESV control to target BHP control, corresponding to figure 6.28. The switch to LS chase water caused the BHP to decrease and terminate at the higher value of 384.49 bar.

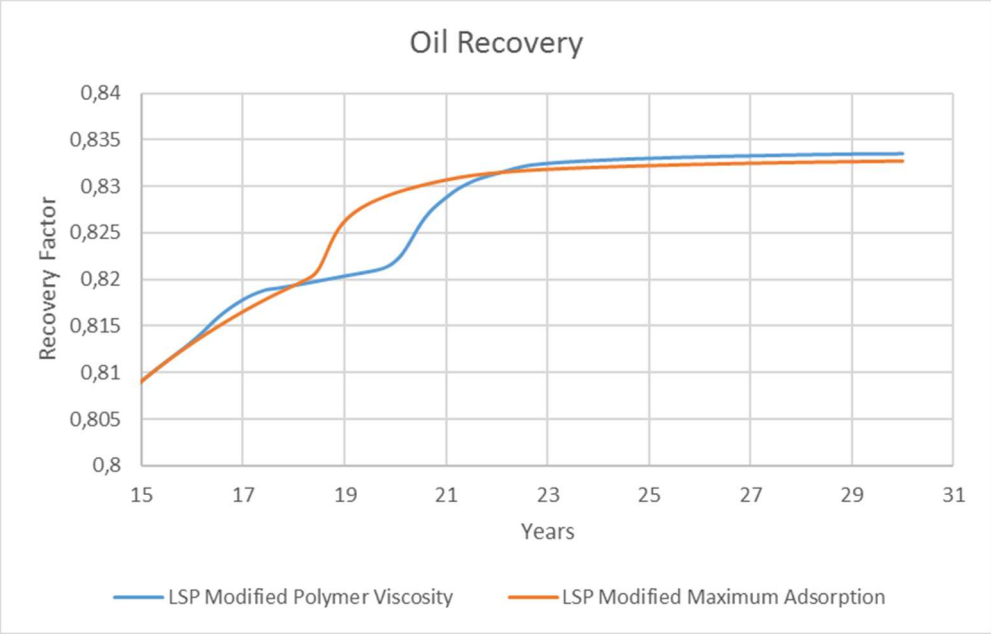

Figure 6.26: Oil recovery for LSP modified maximum adsorption and LSP modified polymer viscosity, altered x-axis and y-axis.

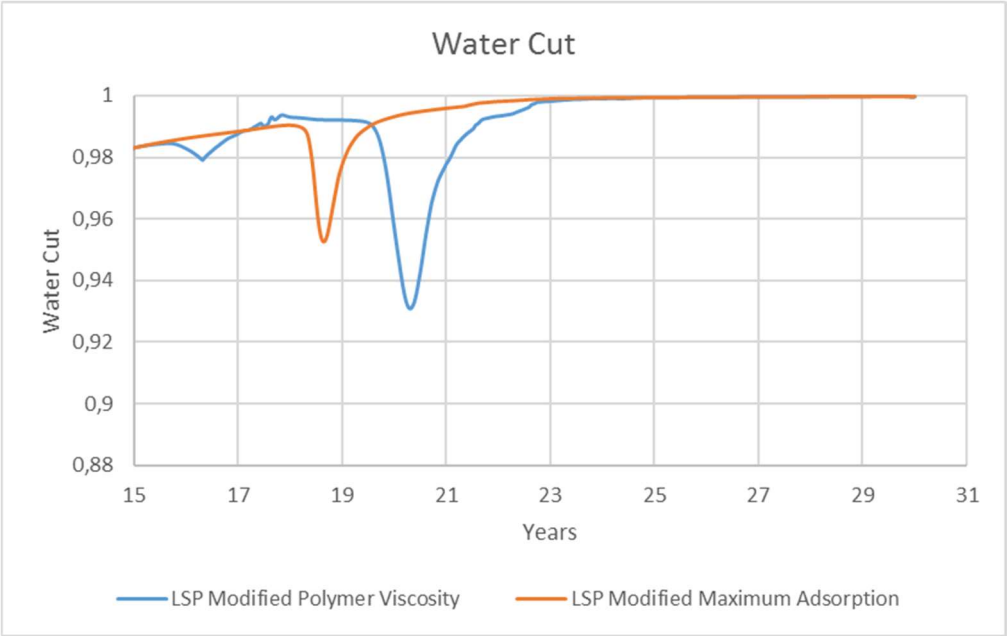

Figure 6.27: Water cut for LSP modified maximum adsorption and LSP modified polymer viscosity, altered x-axis and y-axis.

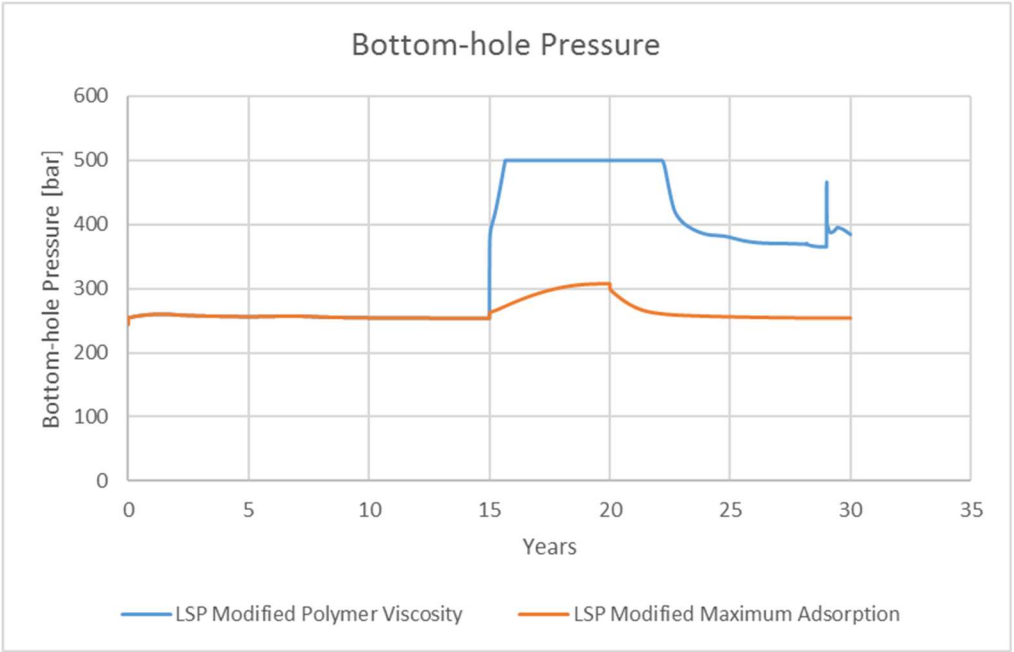

Figure 6.28: Bottom-hole pressure in injection well for LSP modified maximum adsorption and LSP modified polymer viscosity.

6.2.5 LSS Sensitivity Study – Modifying Surfactant Properties

Surfactant concentration of the initial LSS process was increased to investigate the sensitivity of the sector model to changes in the surfactant concentration input parameter. Two processes were compared to the initial LSS process; an LSS process where the surfactant concentration was doubled and an LSS process where surfactant concentration was increased by a number of 10. The production results are listed in table 6.9 in order to compare the processes.

Table 6.9: Production results at the last production date from the initial LSS process and two LSS processes with modified surfactant concentration – 2x and 10x surfactant concentration

Case Study	Oil Recovery [%OOIP]	Oil Produced [m^3]	Water Cut [%]	BHP [bar]
Initial LSS	86.69	38 781.51	99.97	251.64
LSS 2x Concentration	86.82	38 838.88	99.97	251.76
LSS 10x Concentration	86.87	38 859.21	99.98	252.91

The effect of increasing surfactant concentration was an accelerated oil recovery, as displayed in figure 6.29. Otherwise, the final oil recoveries for the processes varied only with 0.18% of OOIP, indicating that increasing surfactant concentration did not yield a considerable amount of incremental oil recovery in the sector model. The water cuts in figure 6.30 corresponds well to the observed results in oil recovery, where the final water cuts are approximately equal.

There was no crucial effect on BHP by increasing surfactant concentration, as can be seen from figure 6.31. The difference in BHP was a more rapid increase where the surfactant concentration was higher. Otherwise, the BHPs all terminated close in value.

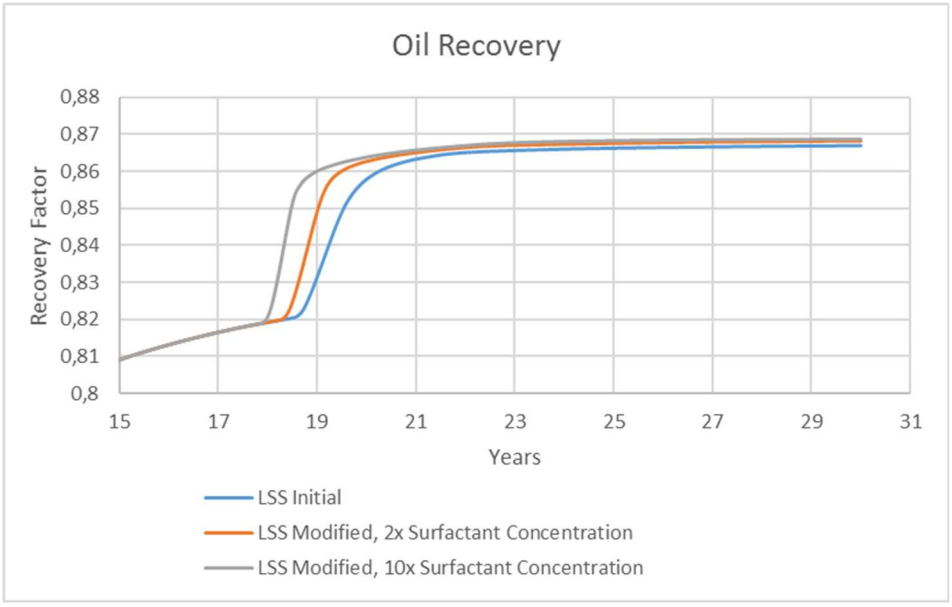

Figure 6.29: Oil recovery for the initial LSS process and two processes of LSS modified surfactant concentration – 2x and 10x concentration, altered x-axis and y-axis.

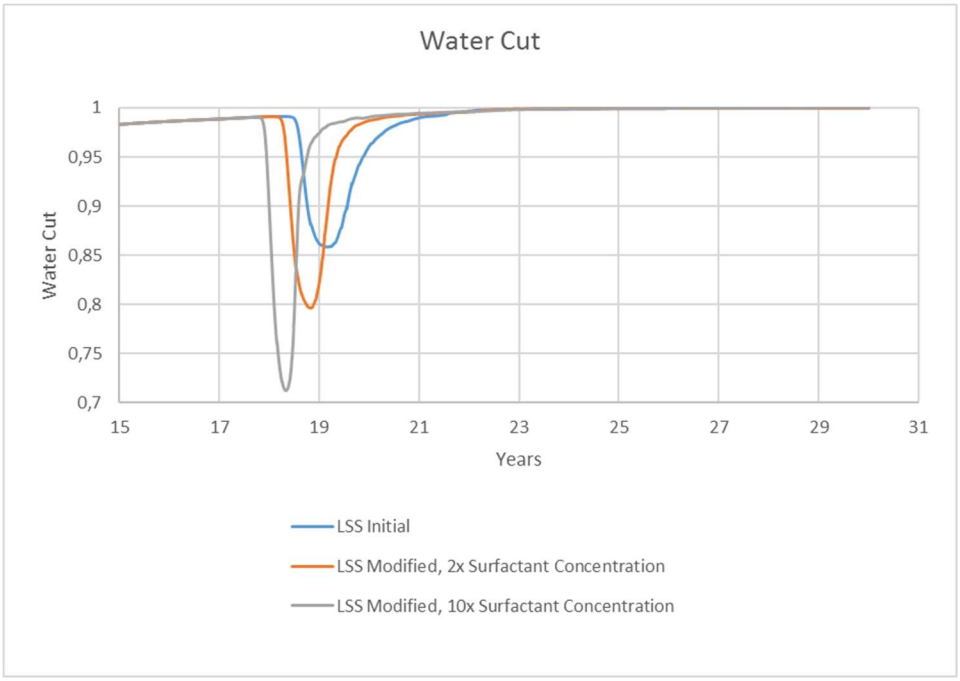

Figure 6.30: Water cut for the initial LSS process and two processes of LSS modified surfactant concentration – 2x and 10x concentration, altered x-axis and y-axis.

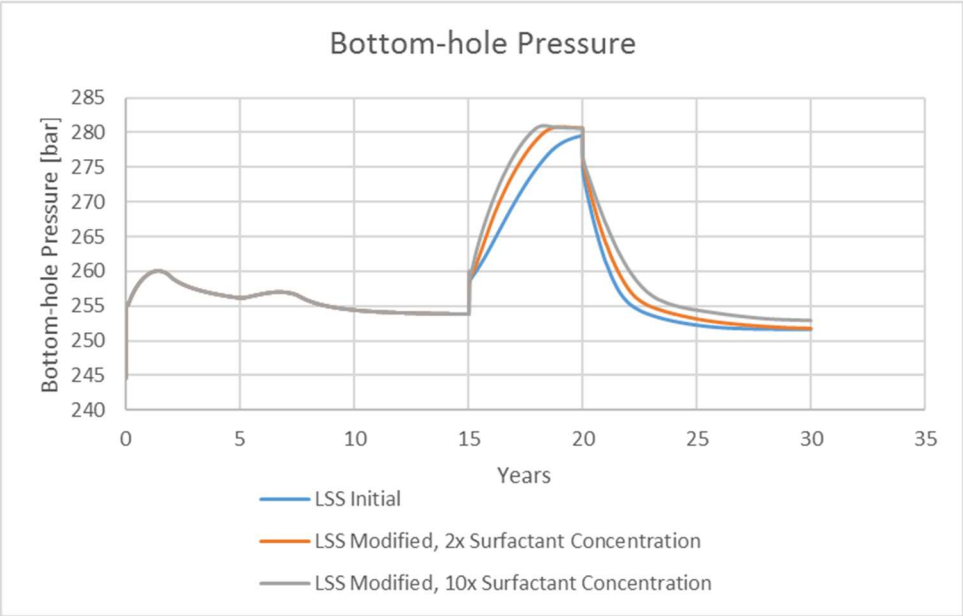

Figure 6.31: Bottom-hole pressure in injection well for the initial LSS process and two processes of LSS modified surfactant concentration – 2x and 10x concentration, altered x-axis.

6.2.6 Relative Permeability Analytical Functions

The HSW saturation range over which oil was flowing was reduced in section 6.2.2, while the LSW saturation range remained approximately unchanged, leaving a too effective LSW and a lower recovery potential for EOR chemicals. By applying the analytical Corey correlation for oil relative permeability, the LSW saturation range over which oil flows was reduced, yielding a higher recovery potential after HS-LS flooding.

$N_o(HS)$ corresponding to the modified k_{ro} in figure 6.4 was calculated to be 2.8. As previous experimental results have shown an increase in oil recovery by LS flooding, it was assumed that the Corey exponent for k_{ro} would be less during LS flooding than during HS flooding. Two simulations were run with Corey components $N_o(LS) = 1.8$ and $N_o(LS) = 2.3$ to investigate which exponents was sufficient. To further impact the fluid flow, $S_{or}(LS)$ was increased from 0.15 to 0.25.

The altered relative permeability curves are displayed in figure 6.32, with alterations done manually on k_{rw} to decrease the LS effectiveness by further affecting the mobility ratio, resulting in an improved potential for EOR chemicals.

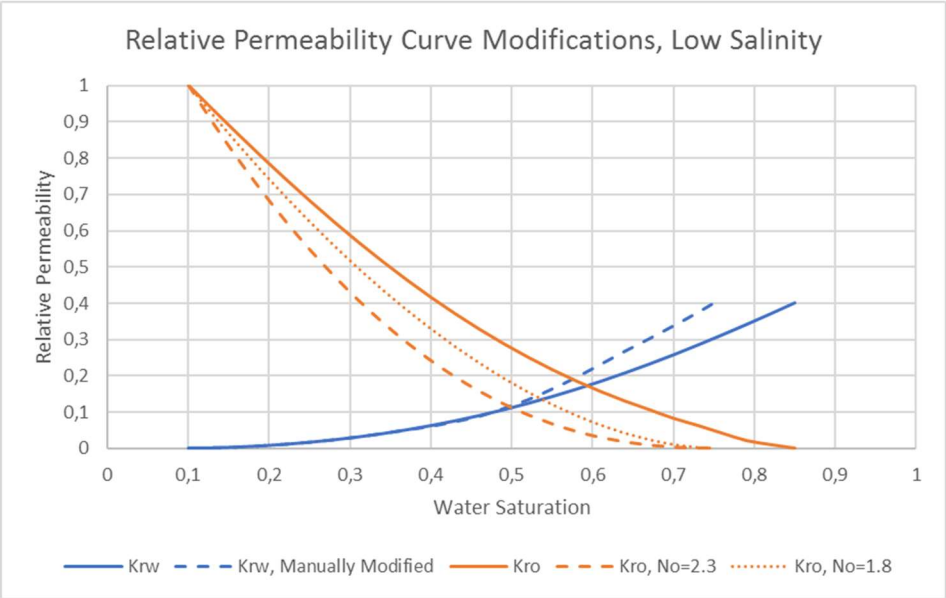

Figure 6.32: Relative permeability curves before and after manual modification and modification by Corey correlation. The solid curves are the relative permeability curves displayed in figure 6.4, "initial k_{rw}"and "modified k_{ro}".

The flooding sequence was a high salinity waterflooding over a time span of 5 years (1 PV) followed by a low salinity chase water injected for 10 years (2 PV), which is equal to the flooding sequence first described in section 6.2.1. A third simulation was run with conventional high salinity waterflooding over a total time span of 15 years (3 PV) to compare the effect of altering Corey exponents for $k_{ro}(LS)$ on oil recovery. The production results are summarized in table 6.10, with recovery factor and cumulative oil production.

Table 6.10: Production results at the last production date from HS waterflooding, HS-LS flooding with Corey correlation $N_o(LS)=1.8$ and HS-LS flooding with Corey correlation $N_o(LS)=2.3$

Case Study	Oil Recovery [%OOIP]	Oil Produced [m^3]
HS	62.90	28 139.61
HS-LS, N_o(LS)=2.3	67.77	30 315.91
HS-LS, N_o(LS)=1.8	70.06	31 339.18

An increase in oil recovery by LS injections was observed, where the HS-LS oil recoveries differed with only 2.29% of OOIP. $N_o(LS) = 2.3$ resulted in the lowest oil recovery between the two with a corresponding S_{or} of 0.29, while a slightly lower S_{or} of 0.27 was achieved for $N_o(LS) = 1.8$. Figure 6.33 displays the oil recoveries, where Corey exponent 2.3 gave a sufficient flooding potential for EOR chemicals, and was therefore a reasonable value to apply in further simulations. Corresponding figures of water cut and BHP are displayed in appendix figures D.2-D.3.

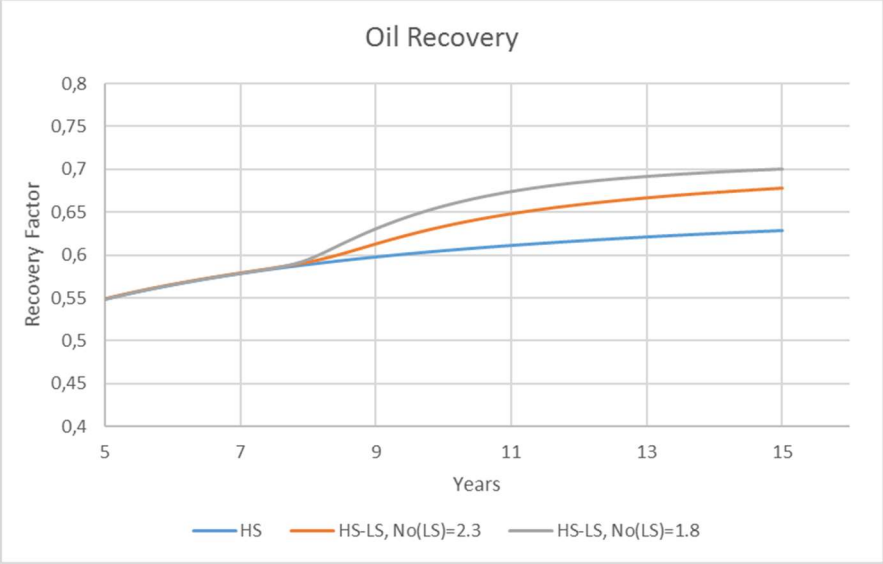

Figure 6.33: Oil recovery for HS flooding compared to the HS-LS flooding with Corey correlation N_o(LS)=1.8 and HS-LS flooding with Corey correlation N_o(LS)=2.3, altered x-axis and y-axis.

Residual Oil

The remaining oil saturations in figure 6.34-6.35 reveals a slightly more efficient sweep in the upper layers after applying Corey exponent 1.8, as there was less restriction to the flow of oil. The S_{or} remained mostly in the corners of the reservoirs, where the injection waters had not yet sweeped properly.

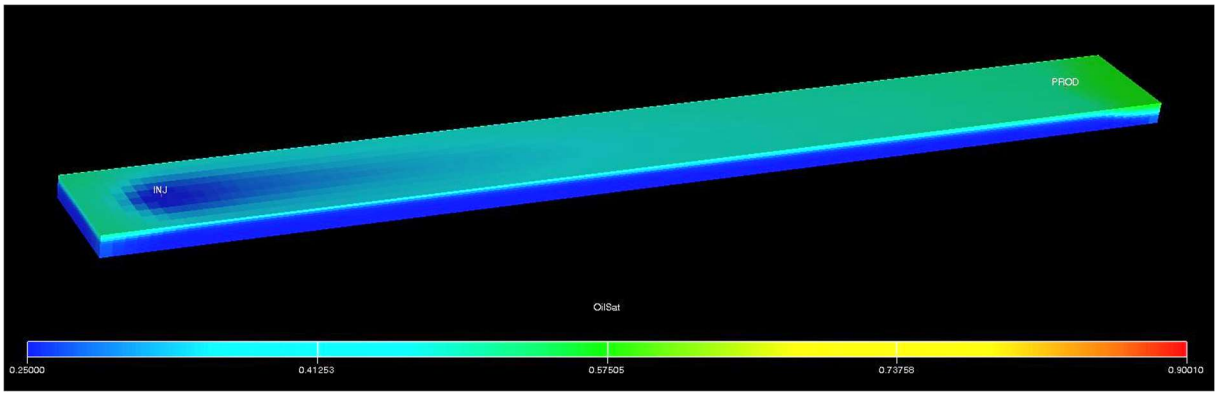

Figure 6.34: 3D illustration of the sector model: HS-LS flooding with Corey correlation N_o(LS)=2.3 at the end of production, illustrated with oil saturation scale.

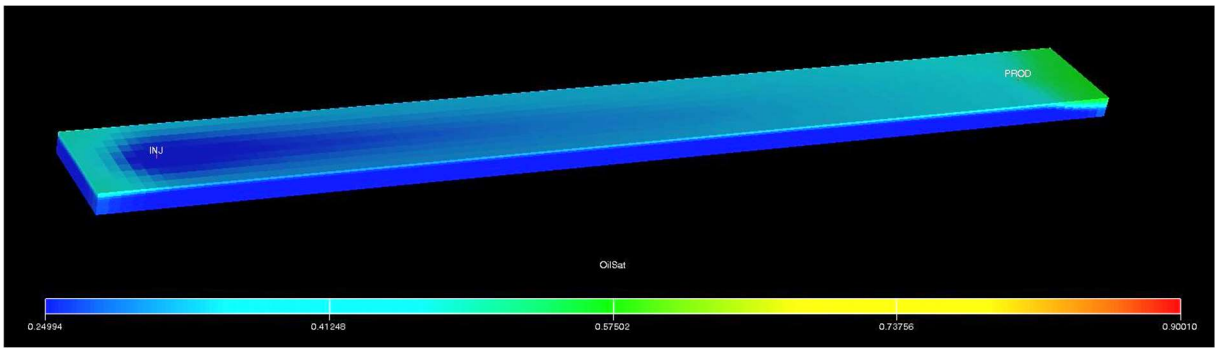

Figure 6.35: 3D illustration of the sector model: HS-LS flooding with Corey correlation N_o(LS)=1.8 at the end of production, illustrated with oil saturation scale.

6.2.7 Applying Sensitivity Study Results – LSS, LSP and LSSP Flooding

Useful insight on the sensitivity of the model to changes in input parameters have been achieved, which have led to final optimal results from sensitivity studies. These final results were applied in the sector model where the simulations were run with flooding sequences corresponding to the hybrid sequences previously listed in table 6.3. The applied results were: 1) optimal maximum adsorption and 2) Corey relative permeability analytical function, figure 6.32. The simulations were initialized with the HS-LS process described in section 6.2.6. Table 6.11 lists a summary of the production results, while figure 6.36 displays the corresponding oil recovery developments throughout flooding.

Table 6.11: Production results at the last production date from the final LSS, LSP and LSSP processes with applied results from sensitivity studies

Case Study	Oil Recovery [%OOIP]	Oil Produced [m^3]
Final LSS	77.93	34 862.92
Final LSP	71.74	32 090.84
Final LSSP	78.11	34 939.14

The LSP process resulted in an additional recovery of 2.63% of OOIP after injecting polymers, which was 2.45% higher than the LSSP process where only an additional recovery of 0.18% of OOIP was observed after polymer injection. During the latter process, surfactants were injected after LSW, allowing the surfactants to produce an additional 8.93% of OOIP after HS-LS. This resulted in a lower recovery potential for polymers in the LSSP process. The final oil recoveries of the LSS and LSSP processes terminated close in value. Corresponding figures of water cut and BHP are displayed in appendix figures D.4-D.5.

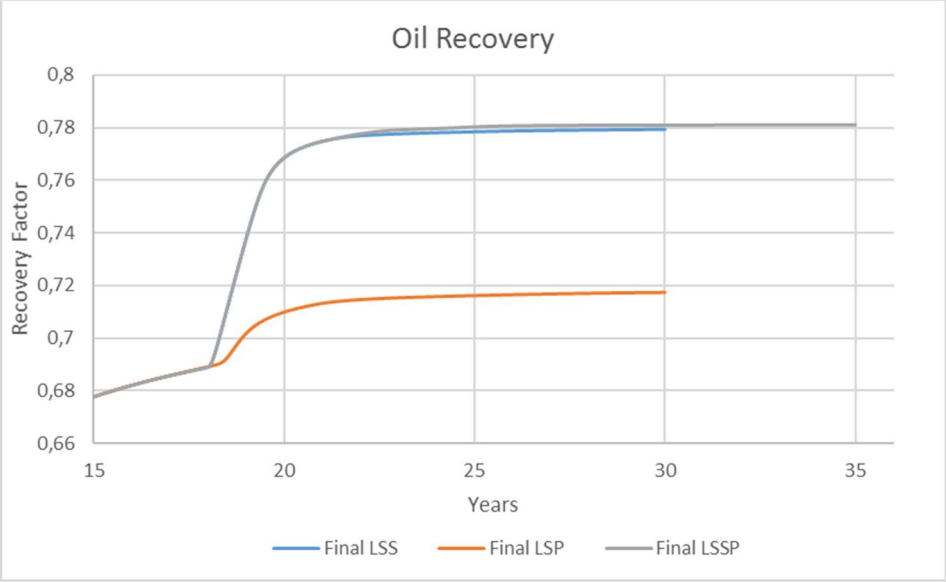

Figure 6.36: Oil recovery for the final LSS, LSP and LSSP processes in the sector model with applied results from sensitivity studies, altered x-axis and y-axis.

6.2.8 Timing of Low Salinity Surfactant/Polymer Flooding

Altering slug sizes can affect incremental oil recovery by controlling the sweepage time of injection fluids. Results from simulations can be used to determine if flooding processes are economically profitable, or if the expenses might exceed the profits. Four hybrid LSSP processes were simulated, where the slug size of each injection fluid is listed in table 6.12. The resulting cumulative oil productions and corresponding recovery factors from simulations are listed in table 6.13, in addition to water cut and BHP. Base Case Water was included to compare conventional high salinity waterflooding with the effect of flooding with EOR chemicals. The Base Case in table 6.12-6.13 corresponds to the LSSP process in section 6.2.7.

Table 6.12: Flooding sequence for conventional high salinity waterflooding and each LSSP process with varying slug size

Flooding Sequence	Base case	Case 1	Case 2	Case 3	Base Case Water
HS (years)	5	4	2	1	15
LS (years)	10	4	1	0.5	-
Surfactant (years)	5	2	1	0.5	-
Polymer (years)	5	2	1	0.5	-
LS (years)	10	10	10	10	-

Table 6.13: Production results at the last production date from conventional high salinity waterflooding and each LSSP process with varying slug size in sector model

Case Study	Recovery factor [%OOIP]	Oil Produced [m^3]	Water Cut [%]	BHP [bar]
Base Case	78.10	34 939.14	99.99	251.91
Case 1	77.23	34 549.61	99.94	252.04
Case 2	74.83	33 472.38	99.83	252.36
Case 3	72.03	32 221.81	99.50	252.85
Base Case Water	62.91	28 139.61	98.79	254.56

Oil Recoveries

An expected development of oil recovery was observed, where the length of each slug size was directly related to the amount of oil produced – longer time spans of each flooding sequence resulted in additional oil recovered. Conventional HS waterflooding resulted in the lowest recovery factor of 62.91% of OOIP, which was 15.19% lower than the Base Case with the longest time span and corresponding highest recovery factor.

Base Case and Case 1 terminated relatively close in regards to recovery factor, and varied only with 0.87% of OOIP. The total flooding time of Case 1 was 13 years shorter than the Base Case, indicating that the expenses of flooding for 35 years could have been drastically reduced by reducing the slug sizes, and still yielding an approximately equal amount of oil recovered.

Oil recovery displayed in figure 6.37 for the four LSSP processes leveled out relatively early compared to the corresponding time spans, indicating that the processes could have terminated earlier while yielding approximately the same amount of oil produced. The effect of polymers is not visible on oil recovery in figure 6.37, as the oil recovery potential for polymers was highly reduced after surfactant flooding.

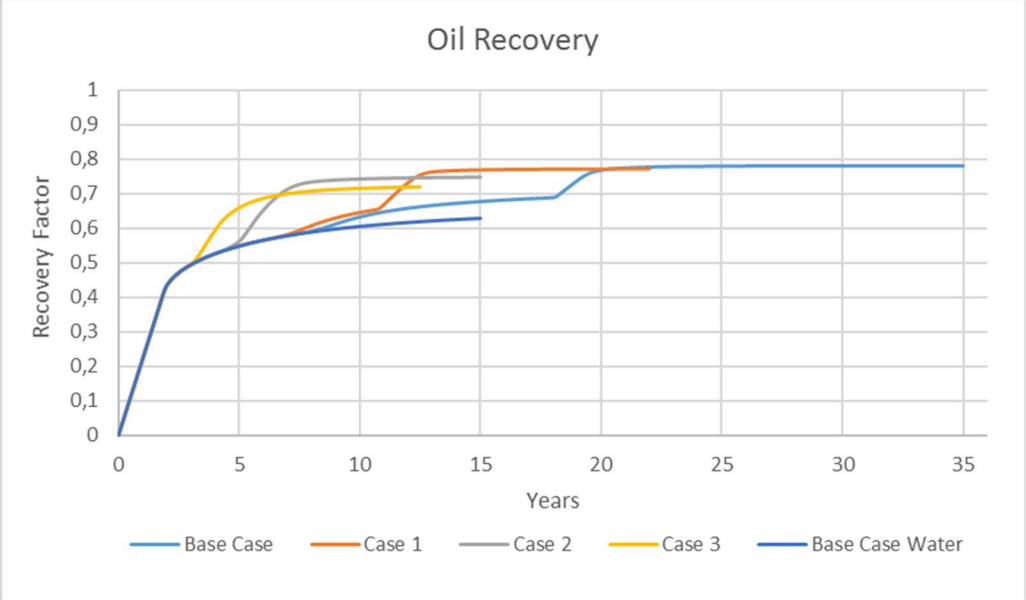

Figure 6.37: Oil recovery for conventional high salinity waterflooding and each LSSP process with varying slug size in the sector model.

Water Cuts

The effect of flooding with EOR chemicals becomes apparent in water cut for all four LSSP processes, as displayed in figure 6.38. The difference in the timing and amount of decrease in water cut were corresponding to the slug sizes. An early introduction of EOR chemicals in Case 3 resulted in an earlier and a larger decrease in water cut compared to the Base Case, as the potential for EOR chemicals was largest in the former process. The recovery potential for EOR chemicals in the Base Case was reduced by a longer HS-LS time span. The effect of LSW injection on water cut was only observed for the Base Case and Case 1.

If water cut exceeds 95%, additional flooding will often result in more expenses than profits. This becomes apparent for all four LSSP processes in both figure 6.37 and 6.38. As an example, the Base Case water cut exceeded 95% several times. 20 years of flooding resulted in a recovery of 76.76% of OOIP, where only an additional 1.34% of OOIP was achieved by flooding for additional 15 years, indicating that the flooding was not economically profitable. The oil recovery for the Base Case started leveling out after 20 years, which also indicated that an earlier termination would be sufficient.

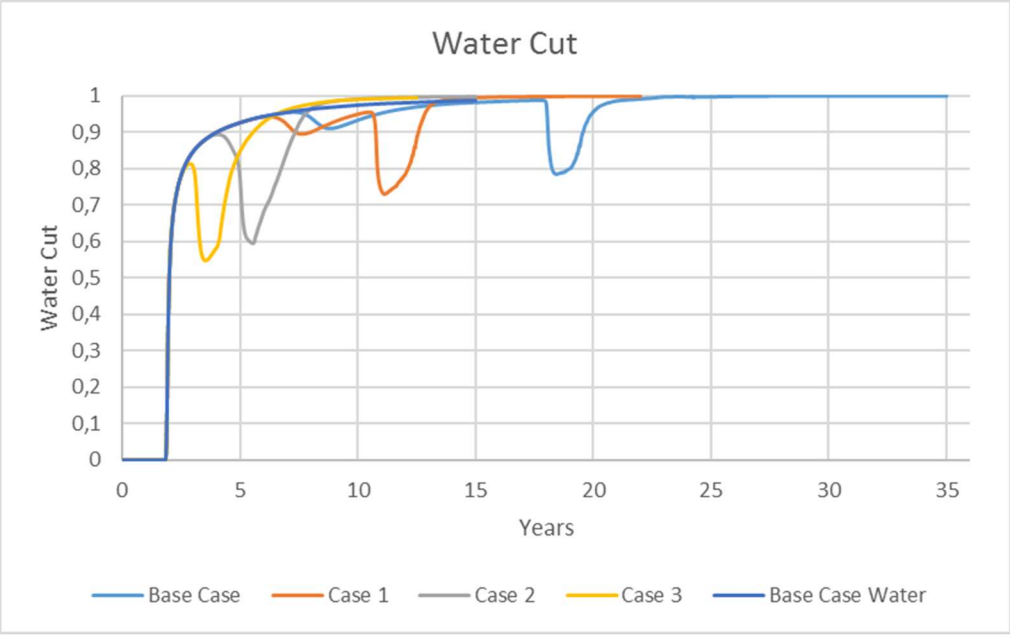

Figure 6.38: Water cut for conventional high salinity waterflooding and each LSSP process with varying slug size in the sector model.

Bottom-hole Pressures

A resulting BHP buildup for each LSSP process during injection of surfactants and polymers is observed in figure 6.39, which corresponds well with expected results. A longer time span of each slug caused a larger BHP buildup, as larger quanta of each chemical were injected.

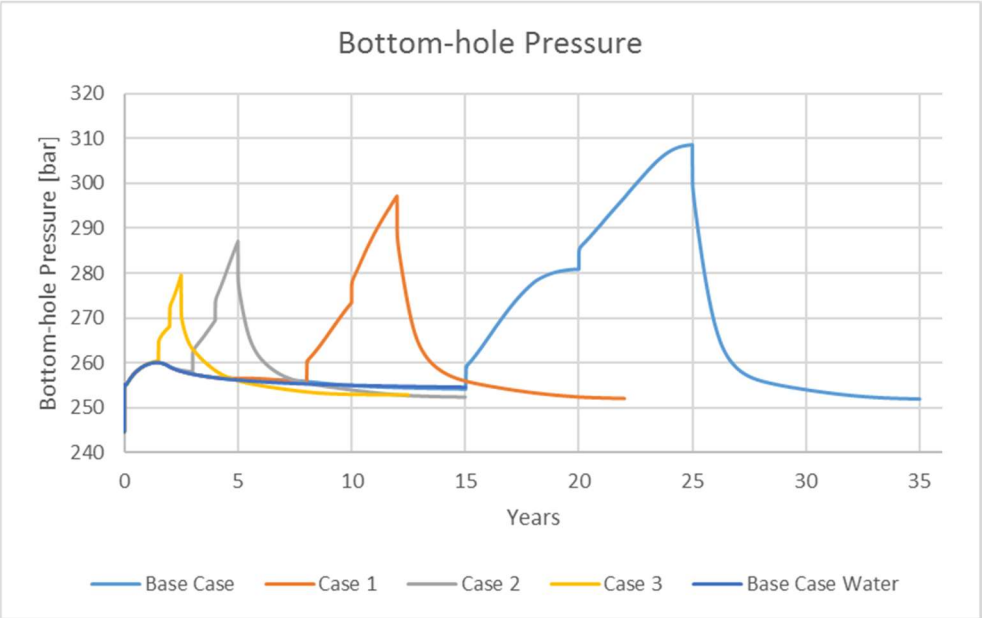

Figure 6.39: Bottom-hole pressure in injection well for conventional high salinity waterflooding and each LSSP process with varying slug size in the sector model, altered x-axis.

6.3 Results from Sensitivity Study Applied in Field Model

Flooding sequences in table 6.12 were applied in the field model along with final results from sensitivity studies listed in section 6.2.7. Both the injection rate and production rate were set to a target of 7884 rm^3/day, which corresponds to 1 PV of water injected per 5 years. Table 6.14 lists the production results at the last production date for conventional high salinity waterflooding and each LSSP process with varying slug size.

Table 6.14: Production results at the last production date from conventional high salinity waterflooding and each LSSP process with varying slug size in field model

Case Study	Recovery factor [%OOIP]	Oil Produced [m^3]	Water Cut [%]	BHP [bar]
Base Case	72.94	$25.98 \cdot 10^5$	1	256.86
Case 1	70.06	$24.95 \cdot 10^5$	99.99	257.28
Case 2	66.48	$23.68 \cdot 10^5$	99.96	257.27
Case 3	62.73	$22.34 \cdot 10^5$	99.81	257.58
Base Case Water	53.71	$19.13 \cdot 10^5$	99.74	266.90

Oil Recoveries

The oil recoveries in figure 6.40 reveal a similar trend as for the sector model with corresponding flooding sequences; a larger slug size resulted in a higher oil recovery. Otherwise, the results revealed a slightly larger difference in recovery factor between the simulated processes in the field model compared to the simulated processes in the sector model, as summarized in tables 6.13 and 6.14.

As for the sector model, the LSSP processes leveled out early after injecting EOR chemicals, which indicated that the processes could terminate earlier and still yield economically profitable results. Injecting polymers resulted in no visually observed incremental oil production for either processes in figure 6.40.

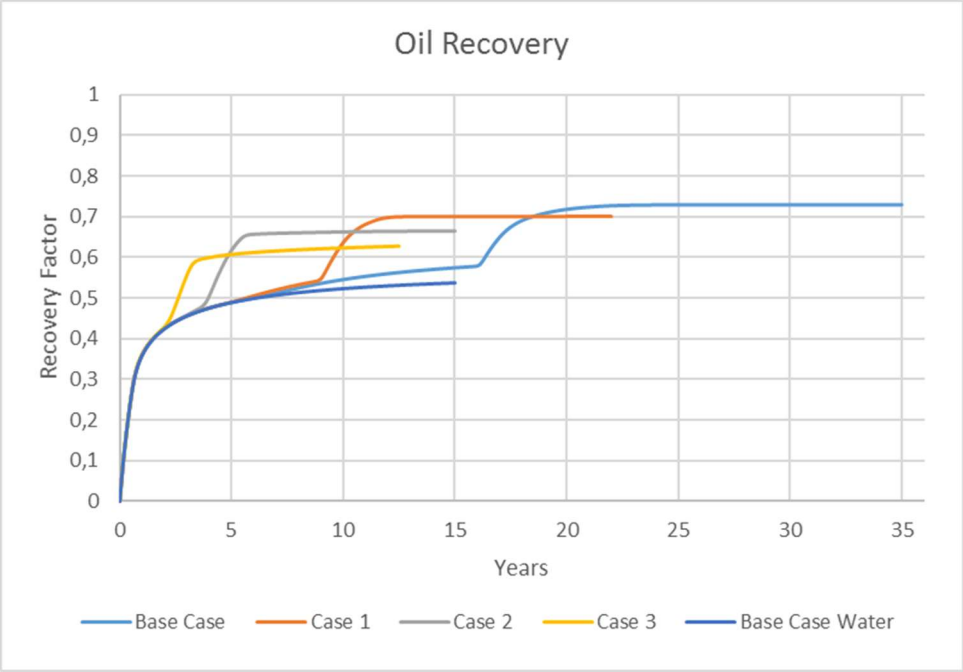

Figure 6.40: Oil recovery for conventional high salinity waterflooding and each LSSP process with varying slug size in the field model.

Water Cuts

The water cut for all five processes investigated increased quite rapidly the first 2 years of flooding. The decrease in water cut for all processes in figure 6.41 corresponded well with the observed results in oil recoveries in figure 6.40. At the initialization of the chase water slug for each LSSP process, the water cuts quickly exceeded 95%, which indicated that additional flooding after this point would not lead to a significant amount of incremental oil production, as described in section 6.2.8, and further flooding would not be profitable.

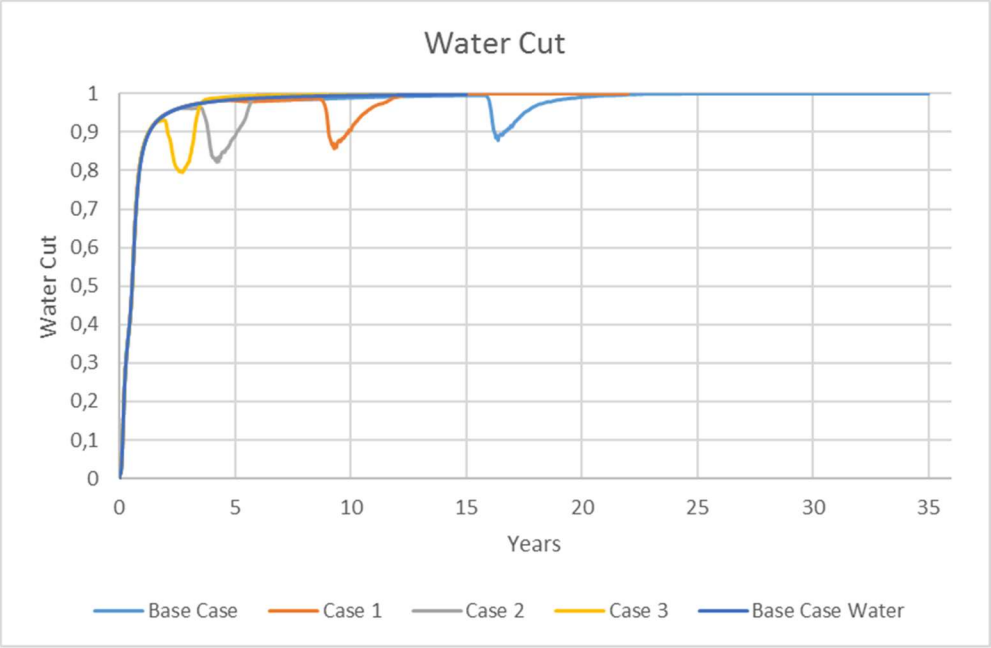

Figure 6.41: Water cut for conventional high salinity waterflooding and each LSSP process with varying slug size in the field model.

Bottom-hole Pressures

The response in BHPs corresponded well to the timing of flooding phases. Injecting EOR chemicals at a rate of 7884 rm^3/day resulted in a large and rapid BHP increase for all LSSP processes, where a BHP difference of only 8.96 bar was observed between the shortest process Case 3 and longest process Base Case. The corresponding difference in the sector model BHP was at a higher 29.06 bar. The BHPs dropped rapidly at the start of LS chase water injection.

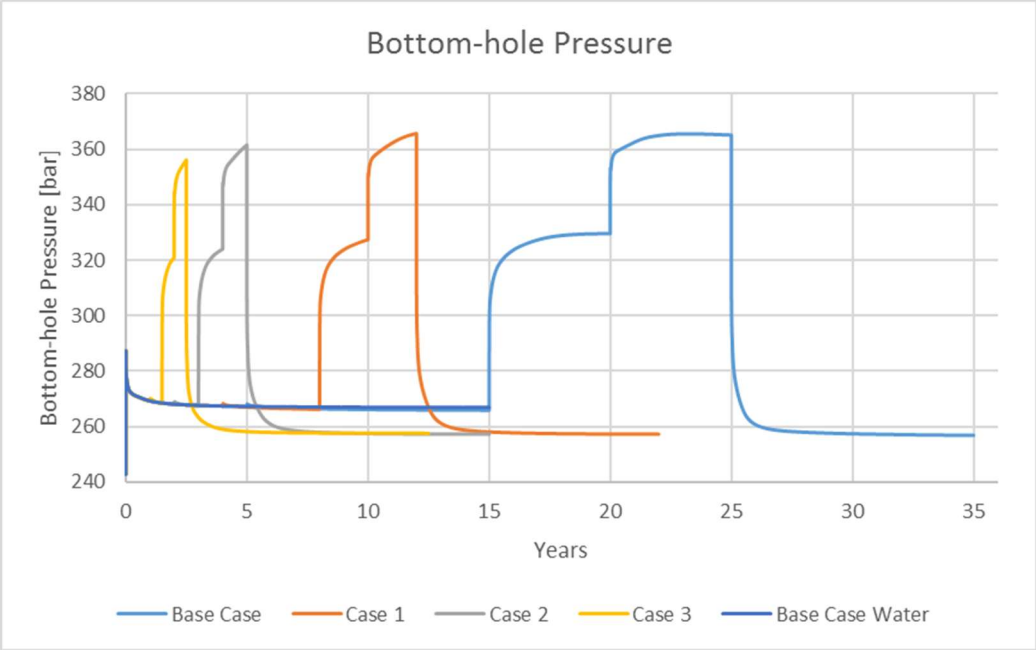

Figure 6.42: Bottom-hole pressure in injection well for conventional high salinity waterflooding and each LSSP process with varying slug size in the field model, altered x-axis.

6.4 Summary and Overall Discussion

Simulations conducted in chapter 6 have revealed sensitivity of the models to changes in input parameters through trial and error, where the main contributor to change in recovery have been the shift from HS to LS relative permeability. The low salinity option was modeled through utilizing a set of salinity dependent relative permeability curves [43].

The initial simulation run of the sector model revealed an oil recovery from flooding with LSW in secondary mode, which appeared to be only an extension of the oil recovery resulting from primary HS waterflooding. This recovery development indicated a too effective HS flooding with no following effect of LS flooding, which is contradictory to expected results from published papers. Altering relative permeability flow functions revealed a great impact on oil recovery, which by reducing the HSW saturation range over which oil was flowing led to more a realistic HS-LS flooding.

By modeling EOR chemical injection, the surfactant option allowed for a second relative permeability set to be defined, where a transition from immiscible relative permeability curves at low capillary number to miscible relative permeability curves at high capillary number was allowed [43]. The polymer option defined polymer-oil relative permeability to be treated as water-oil relative permeability. Surfactant flooding in an established LS environment combined mobilizing oil by LSW and reducing capillary pressure by surfactants to avoid re-trapping of mobilized oil, which resulted in favorable incremental oil production. Low salinity polymer injection increased the macroscopic sweep by inducing a more favorable mobility ratio, and to prevent viscous fingering, causing an accelerated oil recovery and a slight increase in incremental oil production.

Sensitivity studies on polymer input parameters 1) polymer concentration, 2) polymer adsorption and 3) polymer viscosity revealed a sector model less sensitive to polymer concentration. Increasing polymer viscosity further proved to be less effective on oil recovery than altering adsorption, as the former only substantially increased BHP. Defining a new maximum adsorption caused a slight incremental oil production while an accelerated oil production was the most apparent effect. Sensitivity study on increasing surfactant concentration revealed approximately no incremental oil production, where the concentration had most likely reached CMC, although this is only a speculation. Only an accelerated oil production was observed.

Applying an analytical function for altering relative permeability affected the LS effect further. The Corey correlation for oil was applied to lower the LSW range over which oil was flowing to further increase the potential of EOR chemicals after LS waterflooding. Results revealed a higher oil recovery by flooding with polymers in a LS established environment compared to polymer flooding after a low salinity surfactant flooding.

A water cut of 95% is a good indicator on when expenses might exceed profits, where a further increase in water cut might result in an unfavorable economic production. By applying final sensitivity study results and varying slug size during a combined LSSP flooding, results could determine when it was reasonable to terminate production in regards to costs - benefits.

7. History Matching

A core sample from the field was subjected to a compositional hybrid EOR experiment performed by the research group, where LSSP slug injections were conducted on the core. The purpose was to investigate the effect of flooding low salinity water in combination with surfactant and polymer. The amount of oil produced and measured differential pressure were further used for history matching and to estimate relative permeability curves. These relative permeability curves along with measured properties of the core sample were used to produce a core model, which reasonable simulated the historical behavior of the existing core.

This section includes a presentation of the results from history matching achieved by the research group. These results were further applied in simulations on the sector model and field model for an analytical evaluation of reservoir heterogeneity and its effect on oil recovery.

7.1 Model Verification

Several properties of the core sample were measured and applied in the core model for history matching and model verification. The core model is presented in chapter 5, while appendix A includes the core model data-file. The measured properties of the core sample are summarized in table 7.1 along with fluid properties such as oil viscosity and initial water saturation, and oil originally in place.

Table 7.1: Measured properties of the core sample, fluid properties and oil originally in place

Parameter	Value
Length [cm]	18.2
Diameter [cm]	3.7
Pore Volume [cm3]	55.6
Porosity [%]	28.4
K [mD]	862
Oil Viscosity [cP]	2.6
S_{wi}	0.24
OOIP [cm3]	42.5

The surfactant concentration and polymer concentration were 10 kg/m^3 and 1 kg/m^3, respectively, diluted in low salinity water with a salt concentration of 3.6 kg/m^3. The HSW contained a salt concentration of 36 kg/m^3. Table 7.2 summarizes the coreflood data after each injected solution. Results from the coreflooding experiment are displayed in figure 7.1, with production results and differential pressure as a function of injected PV. Water breakthrough and the time of initialization for each injected solution is marked in the figure.

Table 7.2: Coreflood data from flooding experiment after each flooding sequence

Slug	**Parameter**	**Value**
HS flood	R_f [%OOIP]	64.66
	S_{or}	0.27
LS flood	R_f [%OOIP]	66.77
	S_{or}	0.25
Surfactant flood	R_f [%OOIP]	69.34
	S_{or}	0.23
Polymer flood	R_f [%OOIP]	87.90
	S_{or}	0.09
Chase Water	Final R_f [%OOIP]	90.46
	Final S_{or}	0.07

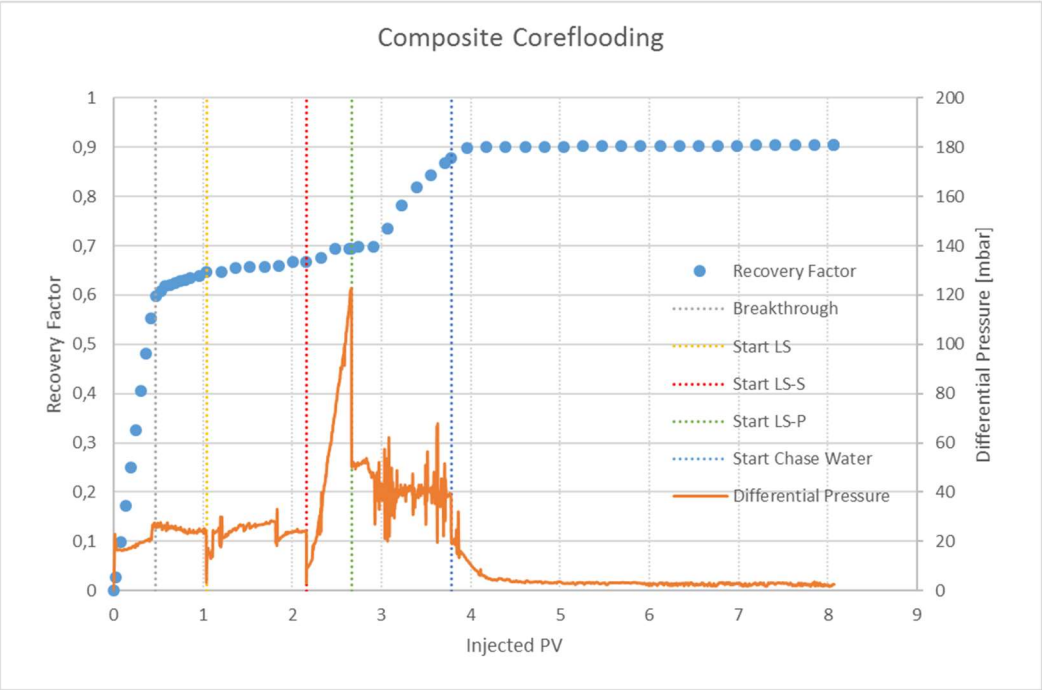

Figure 7.1: Experimental results from the coreflooding experiment, with recovery factor and differential pressure displayed. Water breakthrough and the start of each injected slug is marked.

History Matching

The relative permeability curves displayed in figure 5.4-5.5 were tuned to match the oil production and differential pressure. Through history matching and sensitivity studies, the core model was verified. The results from history matching are displayed in figure 7.2 and 7.3. The rapid increase in experimentally measured differential pressure by injecting surfactants could have been matched by increasing surfactant viscosity further in the core model. However, a further increase in viscosity would have led to an unrealistic high value and a delayed simulated differential pressure increase. It was concluded that a viscosity of 0.7 cP at maximum surfactant concentration was sufficient, and an overall good match between experimental results and simulated results were achieved in both figures.

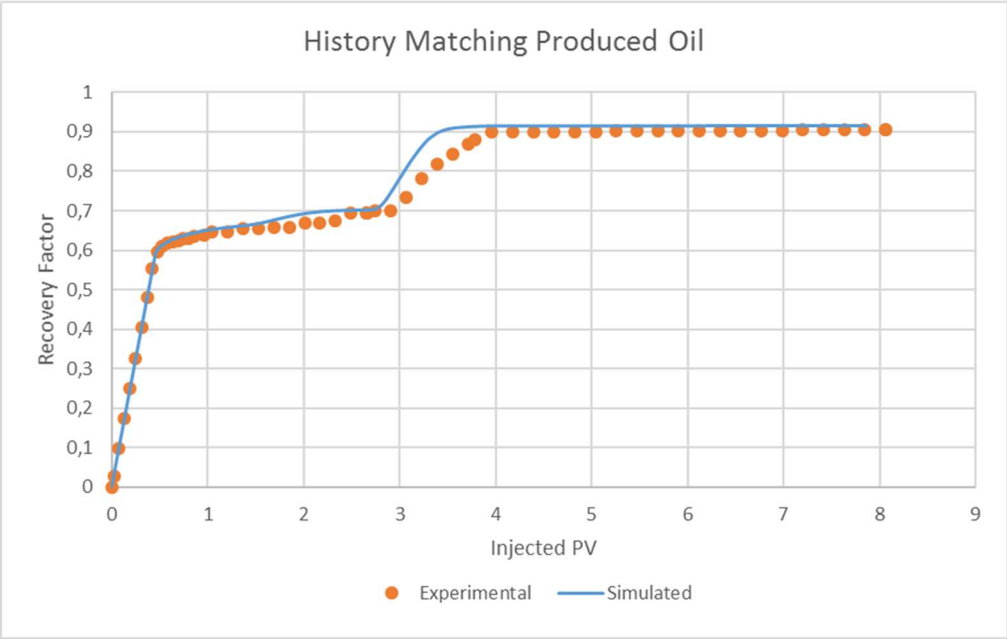

Figure 7.2: History matching of produced oil, with experimental results and simulated results from core model displayed. History matching performed by the research group.

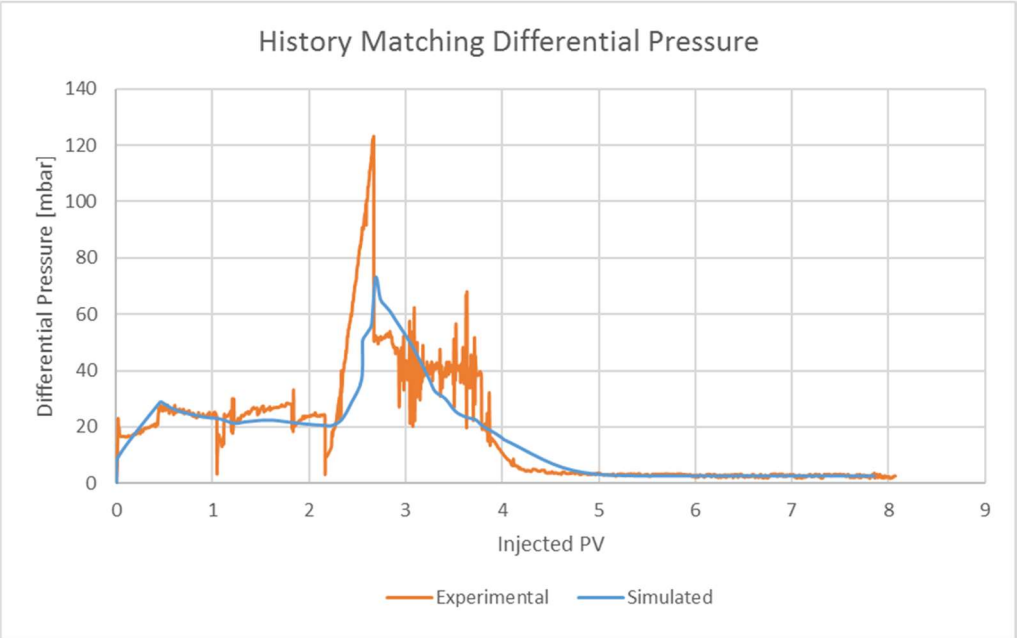

Figure 7.3: History matching of differential pressure, with experimental results and simulated results from the core model displayed. History matching performed by the research group.

7.2 Results from History Matching Applied in Sector Model and Field Model

For simulations on all three models with applied history matched results to be comparable, the volumes injected had to be proportional. Injected pore volumes applied in the models were based on the pore volumes injected during the coreflooding experiment, and are listed in table 7.3. Injection and production rates in the sector model were 34 rm^3/day, corresponding to 1 PV per 5 years. For the field model, injection and production rates were corresponding to 1 PV per 10 years, namely 3942 rm^3/day.

Table 7.3: Injected pore volumes of each slug. Slug size based on the coreflooding experiment

Slug	PV injected
HS	1
LS	1
Surfactant	0.5
Polymer	1
LS chase water	4*

*Only 1 PV of LS chase water was injected in the field model.

Gas and dissolved gas as initial phases present were removed from the generic sector model to properly match the core model. The measured porosity and absolute permeability from table 7.1 were applied, as well as fluid properties listed under the PROPS section in the core model data-file collected from appendix A. Finally, the relative permeability curves in figure 5.4-5.5 were applied, with $P_c = 0$ explained in section 4.2.1. As the field model represents established values, gas and dissolved gas were kept as initial phases, as well as corresponding PVT-tables and rock properties. Only values of adsorption, viscosity and interfacial tension for the surfactant and polymer solutions were applied, in addition to concentration of the reservoir brine and injection fluids. The relative permeability curves in figure 5.4-5.5 were applied, with initial field model P_c unaltered. The perforation alteration described in appendix section C.2 was also applied. Table 7.4 lists oil recovery in percentage of OOIP from the core model, sector model and field model after flooding with corresponding injected PV. The development of oil recoveries are displayed in figure 7.4.

Table 7.4: Oil recovery in percentage of OOIP achieved after each flooding sequence. Listed are results from core model, sector model and field model

Slug	Core Model	Sector Model	Field Model
HS waterflooding [%OOIP]	65.28	66.82	63.05
LS [%OOIP]	69.61	76.08	69.09
LSSP [%OOIP]	91.39	91.64	85.15

The total PV of the field model was calculated by ECLIPSE, which was further used in calculations of injected PV, assuming the effective PV was equal to the total PV. As ECLIPSE does not account for inactive blocks in the total PV calculation, the applied effective PV of the model was greater than the actual effective PV. This overestimated effective PV resulted in an underestimated injected PV, causing a more rapid increase in oil recovery during the start of HS waterflooding compared to the core model and sector model.

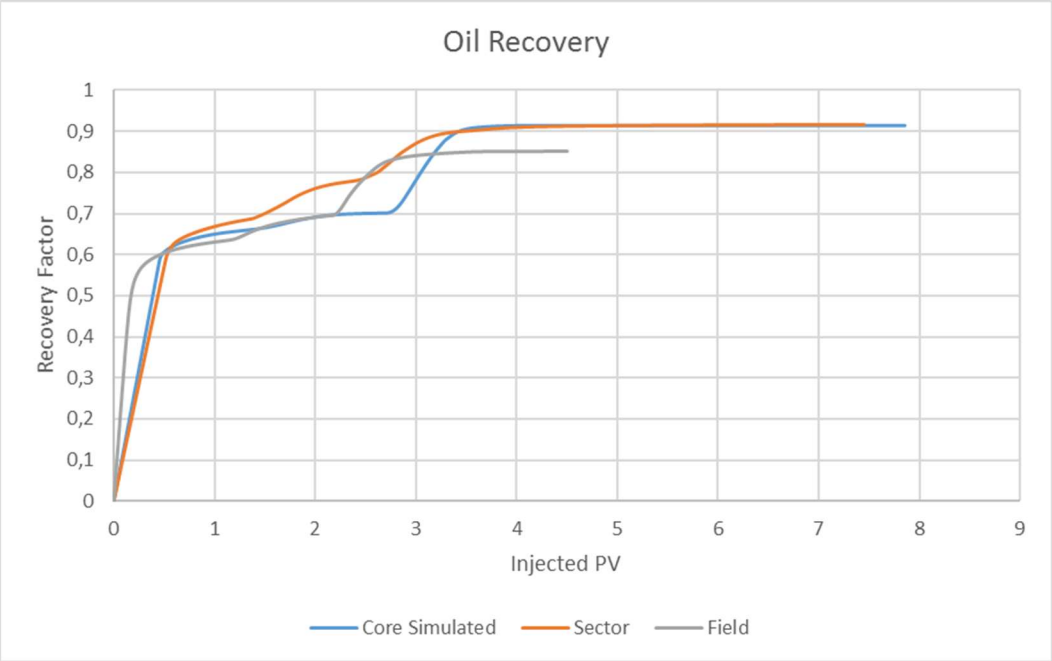

Figure 7.4: Oil recovery from core model, sector model and field model with applied results from history matching.

Flooding with LSW in the core model resulted in an additional oil recovery of 4.33%. The field model revealed similar results, with an incremental oil production after LS waterflooding of 6.04%. The two totals differed only by 0.52%, with the higher recovery achieved by the core model. The sector model resulted in the most effective LSW flooding by additional 9.26% of OOIP, where the total HS-LS recovery deviated from the core model by 6.47%. As the relative permeability curves applied during simulation in the three models were identical, the more effective LSW flooding in the sector model compared to the two other models was caused by an unknown factor.

After flooding with EOR chemicals, the core model resulted in the highest incremental oil production of additional 21.78%, while the sector model and field model resulted in similar additional oil recovered by 15.56% and 16.06% of OOIP, respectively. Despite this, the final oil recovery from the field model revealed a less effective sweep by the EOR chemicals compared to the core model and sector model, which terminated close in final recovery.

A slower mixing of the HS and LS brines injected in the field model caused a delayed established LS environment compared to the core model and sector model, causing a less efficient sweep by the LSW and EOR chemicals. Figure 7.5-7.6 display salt production rate during flooding, where 3 PV of LS waterflooding was required to establish a LS environment in the field model, while only 2 PV was sufficient in the core model and sector model.

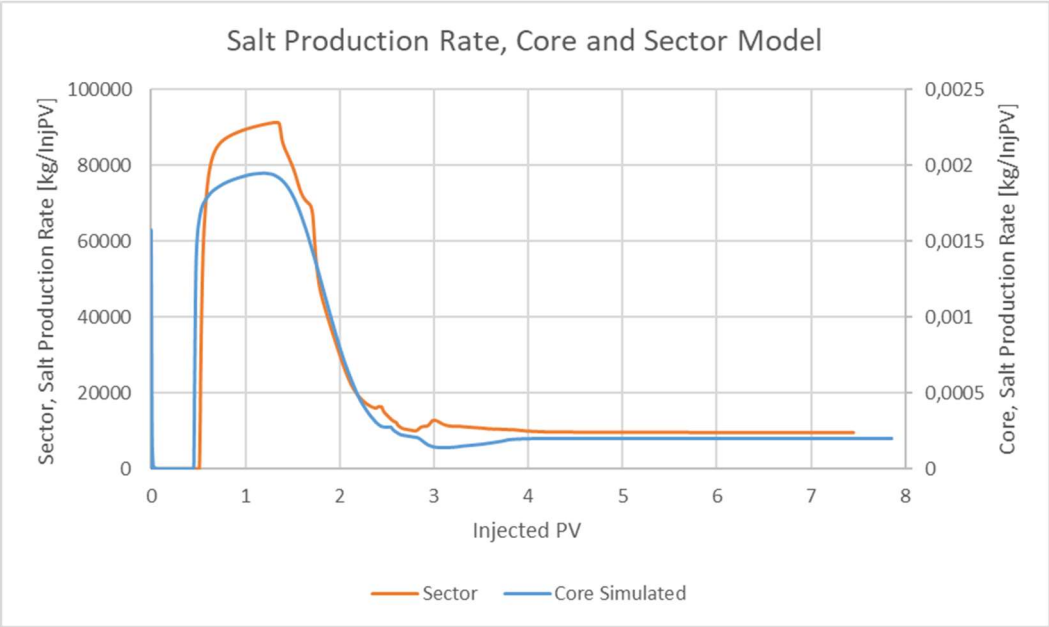

Figure 7.5: Salt production rate from simulations on the core model and sector model with applied history matching results.

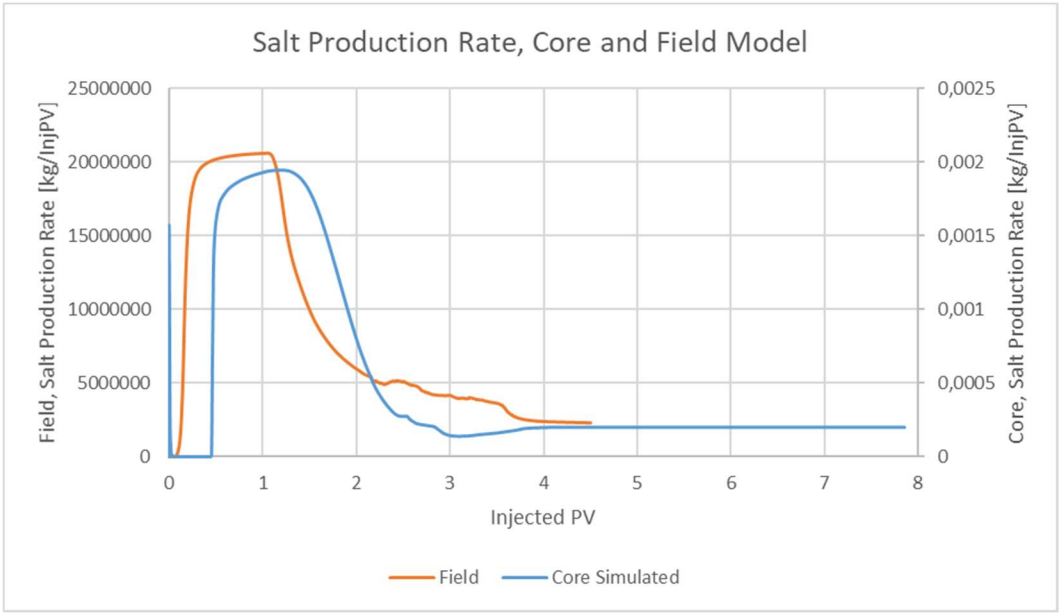

Figure 7.6: Salt production rate from simulations on the core model and field model with applied history matching results.

The final areal sweep in the field model is displayed in figures 7.7-7.9, where oil have been displaced downwards by the injection fluids. The residual oil exists as patches throughout the entire model, where the previous oil zone of layer 1-43 in K-direction in appendix section C.2 here have been extended to layer 1-75. The figures illustrate the less efficient areal sweep, which caused the lower oil recovery in the field model by slower salt mixing compared to the core model and sector model.

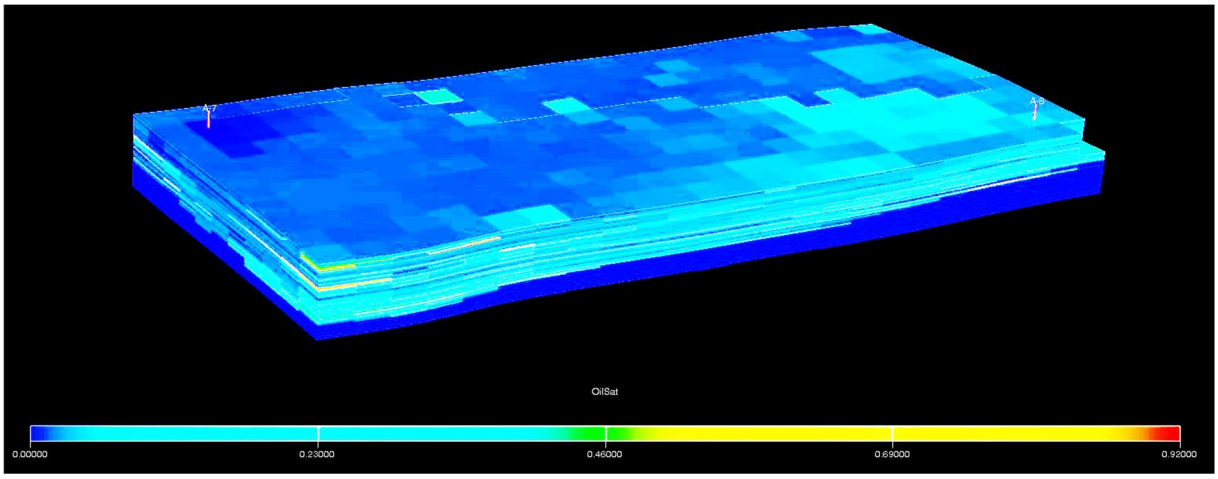

Figure 7.7: The field model at the last production date displaying a less efficient sweep by the injection fluids.

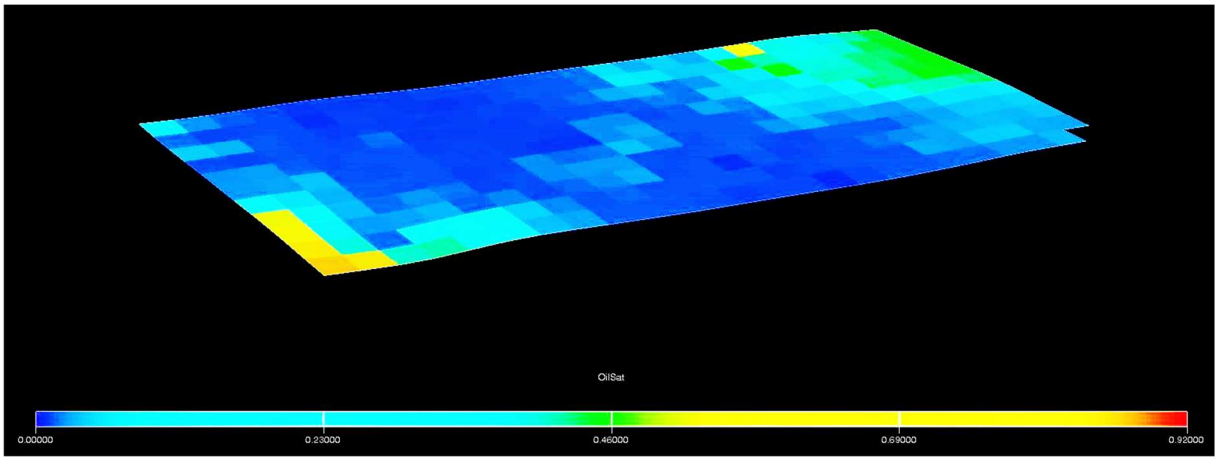

Figure 7.8: Layer 31 in K-direction of the field model at the last production date, displaying a less efficient sweep in the center of the oil zone.

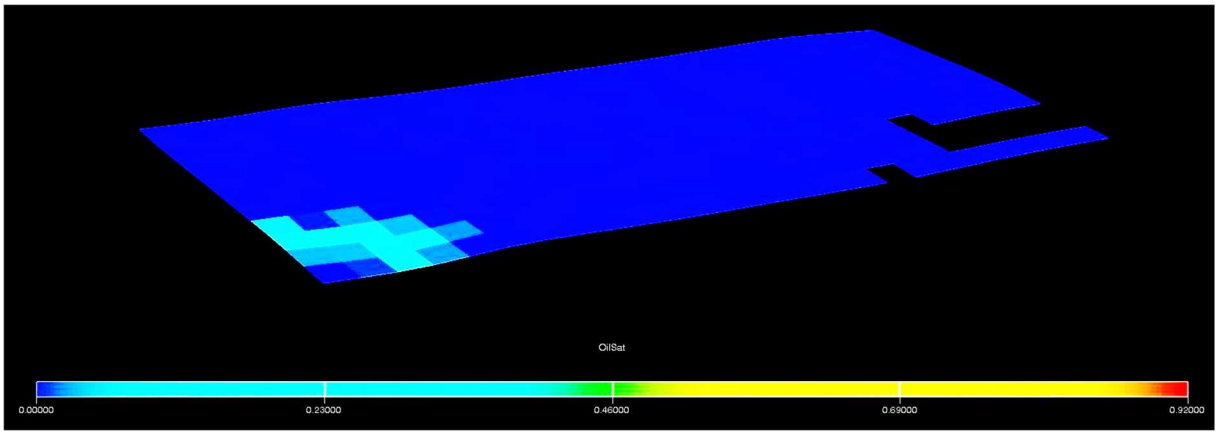

Figure 7.9: Layer 75 in K-direction of the field model at the last production date, displaying a less efficient sweep in the bottom of the oil zone.

7.3 Summary and Overall Discussion

Measured oil production and differential pressure from the composite coreflooding experiment were successfully history matched by the research group. Applying the history matching results in the sector model and field model gave insight to the performance of the models concerning fluid behavior and fluid propagation.

The models differed concerning grid and dimensions, as the field model represents a three-dimensional displacement process in a coarse grid containing inactive blocks. All blocks in the homogeneous sector model are active, where the displacement process is also three-dimensional, while the homogeneous core model represents a one-dimensional displacement process in a fine grid. The measured average porosity and permeability from the core sample were applied in the core, which resulted in a good match between simulated results and lab results. This could indicate a homogeneous core sample.

The HS effect in the field model caused a rapid increase in oil recovery compared to the core model and sector model, as the effective PV applied in calculations of injected PV was overestimated, causing an underestimated injected PV. The overall oil production in the field model revealed a less efficient areal sweep caused by a slow salt mixing and a delayed LS established environment compared to the two other models. This delayed effect might have been caused by heterogeneity in the field model, as heterogeneity affects fluid distribution and can cause a decrease in sweep efficiency [4]. A more efficient sweep was achieved in the homogeneous core and sector models, while the difference in grid could also cause a dissimilar sweep.

The sector model resulted in a more efficient sweep by LSW injection, where the governing factor behind the additional increase in recovery is unknown. The recovery by EOR chemicals were similar for the sector model and field model, while the core model resulted in around 6% higher recovery by injecting EOR chemicals.

8. Conclusions

Numerical simulation studies of hybrid EOR have been evaluated in this thesis, with emphasis placed on model sensitivity to input parameters in order to optimize the field injection strategy. Performance have been investigated through several indicators, where the three main indicators have been recovery factor, water cut and bottom-hole pressure. The findings of the simulation results have led to the following conclusions:

- The ECLIPSE Blackoil Simulator adequately modeled the low salinity surfactant/polymer processes, although underlying mechanisms of a low salinity process is more complex than only salinity dependent flow functions. Wettability, ion exchange and pH may be some of the other mechanisms behind incremental oil recovery by low salinity waterflooding. In this study, the low salinity effect is included in the relative permeability representation and shift in end-point oil saturation.
- The simple ECLIPSE surfactant model only models capillary number as a function of surfactant concentration and interpolates relative permeability functions with change in capillary number. This simple approach seems to be sufficient to describe the effect of surfactants in the hybrid processes, without need for a more detailed surfactant phase behavior.
- ECLIPSE adequately modeled the processes by interpolating salinity dependent relative permeability and capillary pressure, where polymer-oil relative permeability was treated as water-oil relative permeability. The polymer solutions were therefore modeled only as viscosity effects, where non-Newtonian behavior was omitted in this study, as the reservoir bulk rates were approximately constant.
- Polymers are needed after surfactants to improve the mobility ratio and stabilize flow after the high differential pressure observed when surfactants are injected.
- The history match of the core experiment was made with a polymer residual resistance factor (RRF=1) indicating no formation damage by the polymer injection.

9. Recommendations for Future Work

The following recommendations are proposed to improve the weaknesses in the models and test additional sensitivities:

- A third set of relative permeability functions may be defined for polymer injection to model polymer injection more accurately, and to prevent limitations regarding acceptable relative permeability curves.
- The sensitivity studies in chapter 6 were conducted prior to available lab data. A new optimization of the hybrid EOR process could be made anchored on the experimental data presented in chapter 7.
- Further studies should investigate the difference in low salinity response between the core model, sector model and field model, as this was unknown in this thesis.
- A cost-benefit analysis of the evaluated injection strategies could be beneficial by determining the cost of each slug size for furtherer improvement of the field injection strategies.

10. Bibliography

1. *Technical Potential*, chapter in *Resource Report 2017 – Fields and Discoveries*. Norwegian Petroleum Directorate, 2017. https://www.npd.no/en/facts/publications/reports/resource-report/resource-report-2017/technical-potential/
2. *World Energy Outlook 2018, Executive Summary*, Layout in France by DESK, November 2018. IEA Publications, International Energy Agency. https://webstore.iea.org/download/summary/190?fileName=English-WEO-2018-ES.pdf
3. *Resource Report 2017 – Enhanced Oil Recovery (EOR) Methods*, subchapter in *Technical Potential*, Norwegian Petroleum Directorate, 2017. https://www.npd.no/contentassets/516ed5b967e9454791c23b0412fad58f/technical-potential.pdf
4. Skarestad, M. and Skauge, A., *Reservoarteknikk II, PTEK213 – Fluid Properties and Recovery Methods.* Bergen: Universitetet i Bergen, 2012. 222 p.
5. Skauge, A., Ghorbani, Z. and Delshad, M., *Simulation of Combined Low Salinity Brine and Surfactant Flooding*. 16th European Symposium on Improved Oil Recovery, Cambridge, UK: 2011. 13 p.
6. Skauge, A., *Modelling of Hybrid EOR Processes*. 18th European Symposium on Improved Oil Recovery, Dresden, Germany: 2015. 9 p.
7. Lien, J.R., *PTEK211 - Grunnleggende Reservoarfysikk (Kjerneanalyse og logging).* Institutt for fysikk og teknologi, Universitetet i Bergen, 2004. 76 p.
8. Zolotukhin, A.B. and Ursin, J.R., *Introduction to Petroleum Reservoir Engineering*. Høyskoleforlaget, Norwegian Academic Press, 2000. 407 p.
9. Lien, J.R., *PTEK212 - Reservoarteknikk I*. Institutt for fysikk og teknologi, Universitetet i Bergen, 2015. 173 p.
10. Lake, L.W. and Society of Petroleum Engineers. *Enhanced Oil Recovery*. Richardson, Tex: Society of Petroleum Engineers, 2010. 550 p.
11. Anderson, W.G., *Wettability Literature Survey – Part 5: The Effects of Wettability on Relative Permeability.* Journal of Petroleum Technology. 1987: **39**(11). Society of Petroleum Engineers (SPE-16323-PA). 1453-1468 p.
12. Prores, *Sendra User Guide*, Sendra Windows Version 2016,2. 112 p.
13. Anderson, W.G., *Wettability Literature Survey – Part 4: Effects of Wettability on Capillary Pressure.* Journal of Petroleum Technology. 1987: **39**(10). Society of Petroleum Engineers (SPE-15271-PA). 1283-1300 p.

14. Lien, J.R., Jakobsen, M. and Skauge, A.*, PTEK100 - Introduksjon til petroleums- og prosessteknologi*. Universitetet i Bergen, 2007. 99 p.

15. Anderson, W.G., *Wettability Literature Survey – Part 2: Wettability Measurement*. Journal of Petroleum Technology. 1986: **38**(11). Society of Petroleum Engineers (SPE-13933-PA). 1246-1262 p.

16. Anderson, W.G., *Wettability Literature Survey – Part 6: The Effects of Wettability on Waterflooding*. Journal of Petroleum Technology. 1987: **39**(12). Society of Petroleum Engineers (SPE-16471-PA). 1605-1622 p.

17. Labastie, A., *Increasing Recovery Factors: A Necessity*. Journal of Petroleum Technology. 2011: **63**(08). Society of Petroleum Engineers (SPE-0811-0012-JPT) 12-13 p.

18. Jerauld, G.R., Lin, C.Y., Webb, K.J., Seccombe, J.C., *Modeling Low-Salinity Waterflooding*. SPE Reservoir Evaluation & Engineering. 2008: **11**(06). Society of Petroleum Engineers (SPE-102239-PA). 1000-1012 p.

19. Morrow, N. and Buckley, J., *Improved Oil Recovery by Low-Salinity Waterflooding*. Journal of Petroleum Technology. 2011: **63**(05). Society of Petroleum Engineers (SPE-129421-JPT). 106-112 p.

20. Katende, A. and Sagala, F., *A Critical Review of Low Salinity Water Flooding: Mechanism, Laboratory and Field Application* in *Journal of Molecular Liquids*: 2019. Volume 278. Science Direct. 627-649 p.

21. Martin, J.C., *The Effects of Clay on the Displacement of Heavy Oil by Water*. Venezuelan Annual Meeting. 1959: Society of Petroleum Engineers (SPE-1411-G). 24 p.

22. Bernard, G.G., *Effect of Floodwater Salinity on Recovery of Oil from Cores Containing Clays*. SPE California Regional Meeting. 1967: Society of Petroleum Engineers (SPE-1725-MS). 8 p.

23. Bartels, W.-B., Mahani, H., Berg, S. and Hassanizadeh, S.M., *Literature Review of Low Salinity Waterflooding from a Length and Time Scale Perspective* in *Fuel*: 2019. Volume 236. Science Direct. 338-353 p.

24. Lager, A., Webb, K.J., Black, C.J.J., Singleton, M. and Sorbie, K.S., *Low Salinity Oil Recovery – An Experimental Investigation1.* Petrophysics. 2008: **49**(01). Society of Petrophysicists and Well-Log Analysts (SPWLA-2008-v49n1a2). 28-35 p.

25. Tang, G.Q. and Morrow, N.R., *Salinity, Temperature, Oil Composition, and Oil Recovery by Waterflooding*. SPE Reservoir Engineering. 1997: **12**(04). Society of Petroleum Engineers (SPE-36680-PA). 269-276 p.

26. Tang, G.Q. and Morrow, N.R., *Influence of Brine Composition and Fines Migration on Crude Oil/Brine/Rock Interactions and Oil Recovery* in *Journal of Petroleum Science and Engineering*: 1999. Volume 24, Issues 2-4. Science Direct. 99-111 p.

27. Sharma, M.M. and Filoco, P.R., *Effect of Brine Salinity and Crude-Oil Properties on Oil Recovery and Residual Saturations*. SPE Journal. 2000: **5**(03). Society of Petroleum Engineers (SPE-65402-PA). 293-300 p.

28. Webb, K.J., Black, C.J.J. and Al-Ajeel, H., *Low Salinity Oil Recovery – Log-Inject-Log*. In *SPE/DOE Symposium on Improved Oil Recovery*, Tulsa, Oklahoma: 2004. Society of Petroleum Engineers (SPE-89379-MS). 7 p.

29. Skrettingland, K., Holt, T., Tweheyo, M.T. and Skjevrak, I., *Snorre Low-Salinity-Water Injection--Coreflooding Experiments and Single-Well Field Pilot*. SPE Reservoir Evaluation & Engineering. 2011: **14**(02). Society of Petroleum Engineers (SPE-129877-PA). 182-192 p.

30. Kiil, S. and Kontogeorgis, G.M., *Introduction to Applied Colloid and Surface Chemistry*. Chichester, UK; Hoboken, NJ: John Wiley & Sons, 2016. 367 p.

31. Kuznetsov, D., Cotteril, S., Giddins, M.A. and Blunt, M.J., *Low-Salinity Waterflood Simulation: Mechanistic and Phenomenological Models*. In *SPE Asia Pacific Enhanced Oil Recovery Conference*, Kuala Lumpur, Malaysia: 2015. Society of Petroleum Engineers (SPE-174615-MS). 19 p.

32. Alagic, E. and Skauge, A., *Combined Low Salinity Brine Injection and Surfactant Flooding in Mixed-Wet Sandstone Cores*. Energy & Fuels, 2010: **24**(06). 3551-3559 p.

33. Holmberg, K., Kronberg, B. and Lindman, B., *Surface and Interfacial Tension*. Chichester, UK: John Wiley & Sons, 2014. 481 p.

34. *Surfactants & Critical Micelle Concentration (CMC)* in *Understanding Interfaces*. https://www.dataphysics-instruments.com/knowledge/understanding-interfaces/surfactants-cmc/

35. Hirsch, M., *Surface Active Agents (Surfactants)* in Prospector, 2015. https://knowledge.ulprospector.com/3106/pc-surface-active-agents-surfactants/

36. Spildo, K., Sun, L., Djurhuus, K. and Skauge, A., *A Strategy for Low Cost, Effective Surfactant Injection* in *Journal of Petroleum Science and Engineering*: 2014. Volume 117. Science Direct. 8-14 p.

37. Shiran, B.S. and Skauge, A., *Enhanced Oil Recovery (EOR) by Combined Low Salinity/Polymer Flooding*. Energy & Fuels, 2013: **27**(03). 1223-1235 p.

38. Mohammadi, H. and Jerauld, G., *Mechanistic Modeling of the Benefit of Combining Polymer with Low Salinity Water for Enhanced Oil Recovery.* SPE Improved Oil Recovery Symposium, Tulsa, Oklahoma, USA: 2012. Society of Petroleum Engineers (SPE-153161-MS). 11 p.

39. Pettersen, Ø. and Skauge, A., *Simulation of Complex Composite EOR Processes at Lab and Field Scale*. SPE Europec featured at 78th EAGE Conference and Exhibition, Vienna, Austria: 2016. Society of Petroleum Engineers (SPE-180098-MS). 22 p.

40. Holstein, E.D., *Volume V: Reservoir Engineering and Petrophysics*; In *Petroleum Engineering Handbook*. Society of Petroleum Engineers, 2007.

41. Pettersen, Ø., *Basics of Reservoir Simulation With the Eclipse Reservoir Simulator – PTEK255 Lecture Notes*. University of Bergen, Department of Mathematics, 2006. 114 p.

42. Schlumberger, *Blackoil Reservoir Simulation – Training and Exercise Guide.* Schlumberger, 2014. 344 p.

43. Schlumberger, *ECLIPSE Industry-Reference Reservoir Simulator – Technical Description*. Schlumberger, 2016. 1076 p.

44. *ECLIPSE EOR* in Schlumberger; Software. https://www.software.slb.com/products/eclipse/eor

45. Schlumberger, *ECLIPSE Industry-Reference Reservoir Simulator – Reference Manual*. Schlumberger, 2016. 2814 p.

46. Fanchi, J.R., *Principles of Applied Reservoir Simulation*. 3rd ed. Amsterdam; Gulf Professional Pub., 2006. 511 p.

A. Appendix – Core Model ECLIPSE Data-file

This appendix includes the initial data file of the core model, which was provided by the research group. A more detailed description of the model is included in chapter 5. The red keywords indicate the start of a new section, while "--" indicates comments.

```
RUNSPEC
TITLE
'Core'
DIMENS
102  1  1 /
WATER
OIL
POLYMER
SURFACT
LOWSALT
BRINE
TRACERS
0  1  0  0  DIFF /
LAB
START
01 JAN 2019 /
UNIFOUT
TABDIMS
3  1  70  30  4  20  6*  1 /
--Table dimensions
--RelPerm 1: High Salinity
--RelPerm 2: Low Salinity
--RelPerm 3: Surfactant
WELLDIMS
2  10  1  2  6*  1 /

GRID
NOECHO
DX
0.01  100*0.182  0.01 /
DY
102*3.28 /
DZ
```

```
102*3.28 /
TOPS
102*1 /
PORO
0.999  100*0.284  0.999 /
PERMX
10000  100*862  10000 /
PERMY
10000  100*862  10000 /
PERMZ
10000  100*862  10000 /
ECHO

PROPS
SWOF
0.24   0.0          1            0
0.27   0.00001      0.9          0
0.3    0.0001       0.8          0
0.35   0.001        0.65         0
0.4    0.005        0.48         0
0.45   0.01         0.34         0
0.5    0.018        0.22         0
0.55   0.02         0.11         0
0.6    0.03         0.06         0
0.65   0.035        0.03         0
0.7    0.05         0.014        0
0.75   0.07         0.001        0
0.8    0.09         0            0
/
0.24   0.0          1.0          0
0.3    0.000012     0.989        0
0.35   0.00017      0.65         0
0.4    0.0011       0.48         0
0.45   0.005        0.34         0
0.5    0.018        0.22         0
0.55   0.02         0.11         0
0.6    0.03         0.06         0
0.65   0.035        0.03         0
0.7    0.05         0.014        0
0.75   0.07          0.001       0
0.8    0.08         0.00012      0
```

```
0.85   0.1          0.00005      0
0.90   0.2          0.00001      0
1.0    1.0          0            0
 /
0.240  0.0          1            0
0.272  1.6-06       1            0
0.297  6.5-06       0.989        0
0.322  2.0-05       0.97         0
0.347  5.4-05       0.95         0
0.372  0.00013      0.88         0
0.40   0.00027      0.83         0
0.422  0.00054      0.66         0
0.45   0.0010       0.45         0
0.472  0.0018       0.35         0
0.50   0.0031       0.25         0
0.522  0.0052       0.18         0
0.55   0.0083       0.12         0
0.572  0.013        0.09         0
0.60   0.016        0.07         0
0.622  0.017        0.05         0
0.65   0.02         0.035        0
0.70   0.03         0.028        0
0.75   0.05         0.024        0
0.80   0.08         0.02         0
0.85   0.1          0.015        0
0.9    0.2          0.012        0
0.95   0.3          0.0001       0
1.00   1.0          0            0
 /
PVTW
0.005  1.0  4.6E-5  0.5  0.0 /
TRACER
'ESF'  'WAT' /
/
DENSITY
0.87  1.1  0.0010 /
ROCK
25  0.00007 /
PVDO
1  1.01    2.6
15 1.001   2.6
```

```
25 1.0001  2.6
31 1.00    2.6/
SALTNODE
 0.0
 0.0036
 0.036 /
PLYVISCS
0.0       1
          1
          1 /
0.001     8.0
          8.0
          8.0 /
/
PLYADS
0.0       0.000
0.001     0.00003 /
/
/
PLMIXPAR
1.0 /
PLYMAX
0.001     0.0036  /
PLYROCK
0  1  2.6500  2  0.0003 /
0  1  2.6500  2  0.0003 /
0  1  2.6500  2  0.0003 /
SURFVISC
0.0  0.5
0.01  7.0 /
SURFADS
0.0      0.0
0.001    0.000001
0.002    0.00001
0.01     0.00002 /
/
/
SURFST
0.0      16
0.001    0.01
0.01     0.0005 /
```

```
SURFCAPD
-20    0
-4.25  0
-1     1
10     1 /
/
/
SURFROCK
2   2.650 /
/
/
LSALTFNC
0.003    1.0  1.0
0.0036   1.0  1.0
0.036    0.0  0.0 /
/
/

REGIONS
EQUALS
 SATNUM 1 /
 LWSLTNUM 2 /
 SURFNUM 3 /
 /

SOLUTION
PRESSURE
102*1 /
SWAT
1  100*0.24  1 /
SALT
102*0.036 /
TBLKFESF
102*0 /
RPTSOL
RESTART=1 FIP=2 /

SUMMARY
BPR
2 1 1 /
101 1 1/
```

```
 /
FWIR
FOPR
FOPT
FLPR
FLPT
FWPR
FWPT
FGPR
FGPT
FSIR
FSPR
FTIRSUR
FTPRSUR
FTADSUR
FCPR
FCIR
FCPT
FCAD
FWIR
FWIT
FWCT
FGOR
FOE
FPR
WBHP
 /
EXCEL
NEWTON
TIMESTEP
TCPU

SCHEDULE
TUNING
0.0001  5.0 /
/
30  1  100  1  25 /
RPTRST
BASIC=4 FREQ=2 /
WELSPECS
Prod   G1  102  1   1*  OIL /
```

```
Inj    G1  1    1   1*  WATER /
 /
COMPDAT
Prod  102  1   1   1   OPEN  2*  0.005  4* /
Inj   1    1   1   1   OPEN  2*  0.005  4* /
/
WCONPROD
Prod  OPEN   BHP 5*  1 /
/
WCONINJE
Inj  WATER  OPEN  RATE  5.79  1*  2 /
/
WPOLYMER
Inj   0.0   0.036 /
/
TSTEP
0.35  10*1.0 /
WPOLYMER
Inj   0.0   0.0036  /
/
TSTEP
1.35  9*1.0 /
WSURFACT
Inj  0.01 /
/
TSTEP
0.7  4*1.0 /
WPOLYMER
Inj   0.001   0.0036 /
/
WSURFACT
Inj   0 /
/
TSTEP
1.33  9*1.0/
WPOLYMER
Inj   0.0   0.0036 /
/
TSTEP
0.7  39*1.0 /
END
```

B. Appendix – Sector Model Initial ECLIPSE Data-file

This appendix includes the initial data file of the sector model. The sector model is a generic model with properties collected from the PROPS section of the field model, where the latter was provided by the research group.

A more detailed description of the sector model is included in chapter 5. Modifications on the model are described in chapter 6 and 7. The red keywords indicate the start of a new section, while "--" indicates comments.

```
RUNSPEC
TITLE
'Sector
DIMENS
10   100   10 /
DISGAS
WATER
OIL
GAS
POLYMER
SURFACT
LOWSALT
BRINE
TRACERS
0   1   0   0   DIFF /
METRIC
START
1 SEP 1993 /
UNIFOUT
TABDIMS
3   1   30   30   4   20   6*   1 /
--Table dimensions
--RelPerm 1: High Salinity
--RelPerm 2: Low Salinity
--RelPerm 3: Surfactant
WELLDIMS
2   10   2   2   6*   1 /
MESSAGES
3*   1000   2*   3*   6000 /
```

```
GRID
NOECHO
DX
10000*5 /
DY
10000*5 /
DZ
10000*1 /
TOPS
1000*1000
1000*1001
1000*1002
1000*1003
1000*1004
1000*1005
1000*1006
1000*1007
1000*1008
1000*1009 /
PORO
10000*0.25 /
PERMX
10000*200 /
PERMY
10000*200 /
PERMZ
10000*200 /
ECHO

PROPS
PPCWMAX
10  NO /
10  NO /
10  NO /
SWATINIT
10000*0.1 /
SWOF
0       0          1         2.51
0.1     0          1         2.5
0.13    0.00096    0.9216    1.9
0.16    0.00384    0.8464    1.4
```

```
0.19    0.00864    0.7744    0.9
0.22    0.01536    0.7056    0.65
0.25    0.024      0.64      0.5
0.28    0.03456    0.5776    0.4
0.31    0.04704    0.5184    0.3286
0.34    0.06144    0.4624    0.275
0.37    0.07776    0.4096    0.2333
0.4     0.096      0.36      0.2
0.43    0.11616    0.3136    0.1727
0.46    0.13824    0.2704    0.15
0.49    0.16224    0.2304    0.1308
0.52    0.18816    0.1936    0.1143
0.55    0.216      0.16      0.1
0.58    0.24576    0.1296    0.0875
0.61    0.27744    0.1024    0.0765
0.64    0.31104    0.0784    0.0667
0.67    0.34656    0.0576    0.0579
0.7     0.384      0.04      0.05
0.73    0.42336    0.0256    0.0429
0.76    0.46464    0.0144    0.0364
0.79    0.50784    0.0064    0.0304
0.82    0.55296    0.0016    0.025
0.85    0.6        0         0.02
1       1          0         0
/
0     0     1     2.51
0.1   0     1     2.5
0.13  0.00091947   0.933460362  1.9
0.16  0.003100219  0.868137696  1.4
0.19  0.006403582  0.80428786   0.9
0.22  0.010817439  0.742148331  0.65
0.25  0.016361734  0.68193573   0.5
0.28  0.023070252  0.623843893  0.4
0.31  0.03098336   0.568042501  0.3286
0.34  0.040144046  0.514676276  0.275
0.37  0.050595223  0.463864731  0.2333
0.4   0.062377567  0.415702422  0.2
0.43  0.0755276    0.370259666  0.1727
0.46  0.090075884  0.327583667  0.15
0.49  0.106045269  0.287699972  0.1308
0.52  0.123449202  0.250614209  0.1143
```

```
0.55   0.14229009   0.216314032  0.1
0.58   0.162557789  0.184771227  0.0875
0.61   0.184228234  0.155943917  0.0765
0.64   0.207262293  0.129778846  0.0667
0.67   0.231604893  0.106213723  0.0579
0.7    0.257184486  0.085179629  0.05
0.73   0.283912907  0.066603539  0.0429
0.76   0.311685676  0.050411077  0.0364
0.79   0.340382763  0.036529721  0.0304
0.82   0.369869841  0.024892966  0.025
0.85   0.4    0.015446539  0.02
1      1      0      0
/
0      0      1      2.51
0.25   0.25   0.75   0.5
0.5    0.5    0.5    0.11
0.75   0.75   0.25   0.03
1      1      0      0
/
SGOF
0       0            1            0
0.05    0            0.8          0
0.1     0.0027682    0.6277319    0
0.15    0.0110727    0.484908     0
0.2     0.0249135    0.3679649    0
0.25    0.0442907    0.2735695    0
0.3     0.0692042    0.1986183    0
0.35    0.099654     0.1402378    0
0.4     0.1356401    0.0957843    0
0.45    0.1771626    0.0628441    0
0.5     0.2242215    0.0392332    0
0.55    0.2768166    0.0229978    0
0.6     0.3349481    0.0124136    0
0.65    0.3986159    0.0059865    0
0.7     0.4678201    0.0024521    0
0.75    0.5425606    0.0007759    0
0.8     0.6228374    0.0001533    0
0.85    0.7086505    0.0000096    0
0.9     0.8          0            0
1       1            0            0
/
```

0	0.0000000	1.0000000	0
0.05	0.0000000	0.8000000	0
0.1	0.0027682	0.6277319	0
0.15	0.0110727	0.4849080	0
0.2	0.0249135	0.3679649	0
0.25	0.0442907	0.2735695	0
0.3	0.0692042	0.1986183	0
0.35	0.0996540	0.1402378	0
0.4	0.1356401	0.0957843	0
0.45	0.1771626	0.0628441	0
0.5	0.2242215	0.0392332	0
0.55	0.2768166	0.0229978	0
0.6	0.3349481	0.0124136	0
0.65	0.3986159	0.0059865	0
0.7	0.4678201	0.0024521	0
0.75	0.5425606	0.0007759	0
0.8	0.6228374	0.0001533	0
0.85	0.7086505	0.0000096	0
0.9	0.8000000	0.0000000	0
1	1.0000000	0.0000000	0
/			
0	0.0000000	1.0000000	0
0.05	0.0000000	0.8000000	0
0.1	0.0027682	0.6277319	0
0.15	0.0110727	0.4849080	0
0.2	0.0249135	0.3679649	0
0.25	0.0442907	0.2735695	0
0.3	0.0692042	0.1986183	0
0.35	0.0996540	0.1402378	0
0.4	0.1356401	0.0957843	0
0.45	0.1771626	0.0628441	0
0.5	0.2242215	0.0392332	0
0.55	0.2768166	0.0229978	0
0.6	0.3349481	0.0124136	0
0.65	0.3986159	0.0059865	0
0.7	0.4678201	0.0024521	0
0.75	0.5425606	0.0007759	0
0.8	0.6228374	0.0001533	0
0.85	0.7086505	0.0000096	0
0.9	0.8000000	0.0000000	0
1	1.0000000	0.0000000	0

```
/
PVTW
250.83   1.0368    4E-005   0.3162   0 /
PVTO
13.81     20.0000  1.1465   1.1032
30.0000   1.1442   1.1297
40.0000   1.1419   1.156
50.0000   1.1397   1.1821
60.0000   1.1376   1.2081
70.0000   1.1356   1.2338
80.0000   1.1336   1.2594
90.0000   1.1318   1.2848
100.0000  1.1299   1.31
102.8000  1.1294   1.3171
125.0000  1.1256   1.3724
150.0000  1.1215   1.4337
200.0000  1.1143   1.5533
244.5000  1.1085   1.6566
350.0000  1.0971   1.8901 /
20.57     30.0000  1.17       1.0034
40.0000   1.1675   1.0282
50.0000   1.1651   1.0529
60.0000   1.1627   1.0774
70.0000   1.1605   1.1017
80.0000   1.1583   1.1258
90.0000   1.1562   1.1499
100.0000  1.1542   1.1737
102.8000  1.1536   1.1804
125.0000  1.1494   1.2327
150.0000  1.1449   1.2909
200.0000  1.137    1.4045
244.5000  1.1307   1.5027
245.0000  1.1306   1.5038
350.0000  1.1182   1.7256 /
26.63     40.0000  1.1898      0.93208
50.0000   1.1872   0.95557
60.0000   1.1846   0.97891
70.0000   1.1822   1.0021
80.0000   1.1798   1.0252
90.0000   1.1775   1.0481
100.0000  1.1753   1.0709
```

```
102.8000  1.1747   1.0773
125.0000  1.1701   1.1273
150.0000  1.1653   1.1829
200.0000  1.1567   1.2918
244.5000  1.1499   1.3861
245.0000  1.1498   1.3872
350.0000  1.1365   1.6006 /
32.35     50.0000  1.2079      0.87449
60.0000   1.2051   0.89683
70.0000   1.2024   0.91905
80.0000   1.1999   0.94114
90.0000   1.1974   0.96311
100.0000  1.195    0.98496
102.8000  1.1943   0.99104
125.0000  1.1894   1.0391
150.0000  1.1842   1.0924
200.0000  1.1749   1.1971
244.5000  1.1677   1.288
245.0000  1.1676   1.289
350.0000  1.1534   1.4951 /
37.9      60.0000  1.225      0.82502
70.0000   1.2221   0.84632
80.0000   1.2193   0.86751
90.0000   1.2166   0.88859
100.0000  1.2141   0.90956
102.8000  1.2134   0.9154
125.0000  1.208    0.96153
150.0000  1.2024   1.0129
200.0000  1.1925   1.1136
244.5000  1.1848   1.2012
245.0000  1.1847   1.2022
350.0000  1.1696   1.4014 /
43.39     70.0000  1.2416      0.78104
80.0000   1.2386   0.80137
90.0000   1.2357   0.8216
100.0000  1.2329   0.84173
102.8000  1.2322   0.84735
125.0000  1.2264   0.89166
150.0000  1.2205   0.94101
200.0000  1.2099   1.038
244.5000  1.2017   1.1225
```

```
245.0000  1.2016   1.1234
350.0000  1.1856   1.316 /
48.87     80.0000  1.2579      0.74113
90.0000   1.2548   0.76054
100.0000  1.2519   0.77987
102.8000  1.2511   0.78525
125.0000  1.2449   0.82781
150.0000  1.2385   0.87525
200.0000  1.2273   0.96862
244.5000  1.2185   1.0501
245.0000  1.2184   1.051
350.0000  1.2015   1.237 /
54.39     90.0000  1.2742      0.70444
100.0000  1.271    0.72297
102.8000  1.2702   0.72814
125.0000  1.2636   0.76899
150.0000  1.2568   0.81456
200.0000  1.2448   0.90438
244.5000  1.2355   0.98285
245.0000  1.2354   0.98372
350.0000  1.2175   1.1634 /
59.97     100.0000 1.2905      0.67041
102.8000  1.2896   0.67537
125.0000  1.2826   0.71454
150.0000  1.2753   0.75829
200.0000  1.2625   0.84462
244.5000  1.2527   0.92015
245.0000  1.2526   0.921
350.0000  1.2336   1.0943 /
61.55     102.8000 1.2951      0.66132
125.0000  1.2879   0.70004
150.0000  1.2805   0.74327
200.0000  1.2675   0.82864
244.5000  1.2575   0.90337
245.0000  1.2574   0.9042
350.0000  1.2382   1.0758 /
71.16     120.0000 1.3256      0.62692
350.0000  1.2727   1.0179 /
87.93     150.0000 1.3745      0.56692
350.0000 1.3285    0.90692 /
143.83    250.0000  1.5375      0.36692
```

```
350.0000 1.5145    0.53692 /
194.14   340.0000  1.6842      0.18692
350.0000 1.6819    0.20392 /
/
PVDG
20.0000     0.061799      0.01276
30.0000     0.040712      0.01317
40.0000     0.030224      0.01350
50.0000     0.023962      0.01380
60.0000     0.019807      0.01410
70.0000     0.016856      0.01441
80.0000     0.014655      0.01473
90.0000     0.012955      0.01508
100.0000    0.011605      0.01546
102.8000    0.011272      0.01557
125.0000    0.009185      0.01656
150.0000    0.007634      0.01786
200.0000    0.005815      0.02078
244.5000    0.004904      0.02349
245.0000    0.004896      0.02352
350.0000    0.003792      0.02929
/
TRACER
'ESF' 'WAT' /
/
DENSITY
835.14   1037   1.33 /
ROCKOPTS
1*   1*   ROCKNUM /
ROCK
245.0000   7.5E-005 /
FILLEPS
SALTNODE
  0.0
  4.0
 40.0 /
PLYVISCS
0.0        1.0
           1.02
           1.039 /
0.7        10.0
```

```
           10.2
           10.39 /
/
PLYADS
0.0     0.000
0.4     0.0015
0.8     0.0025 /
/
/
PLMIXPAR
1.0 /
PLYMAX
0.5   4.0 /
PLYROCK
0.15   2.67   1000.0    2    0.0035 /
0.15   2.67   1000.0    2    0.0035 /
0.15   2.67   1000.0    2    0.0035 /
SURFVISC
0.0    0.3162
1.0    0.437
5.0    2.08 /
SURFADS
0.0    0.0
1.0    0.00001
2.0    0.0001
10.0   0.0002 /
/
/
SURFST
0.0    0.016
1.0    0.00001
5.0    0.000005 /
SURFCAPD
-20         0
-4.262      0
-6.21E-2    1
 10         1 /
/
/
SURFROCK
2   2500 /
```

```
/
/
LSALTFNC
  3     1.0  1.0
  4     1.0  1.0
 40.0   0.0  0.0   /
/
/

REGIONS
EQUALS
SATNUM 1 /
LWSLTNUM 2 /
SURFNUM 3 /
/

SOLUTION
EQUIL
1000   244.5   1100  0  0  0  2  0  0 /
RSVD
100    61.55
4000   61.55
/
TBLKFESF
10000*0 /
SALTVD
1000    40.0
1010    40.0 /
RPTRST
BASIC=3 FLORES FREQ=1 /
RPTSOL
RESTART=2 FIP=2 /

SUMMARY
FOPR
FOPT
FLPR
FLPT
FWPR
FWPT
FGPR
```

```
FGPT
FSIR
FSPR
FTIRSUR
FTPRSUR
FTADSUR
FCPR
FCIR
FCPT
FCAD
FWIR
FWIT
FWCT
FGOR
FOE
FPR
WBHP
/
EXCEL
NEWTON
TIMESTEP
TCPU

SCHEDULE
WELSPECS
Prod   G1    5   93  1002  OIL    1* 1*  STOP   YES /
Inj    G1    5   7   1005  WATER  1* 1*  STOP   YES /
/
COMPDAT
Prod  5  93   2      9       OPEN     1*  0.00E+00  0.15941  1*  0  1*  Z /
Inj   5  7    2      9       OPEN     1*  0.00E+00  0.15941  1*  0  1*  Z /
/
WCONPROD
Prod   OPEN    RESV   1*  1*   1*   1*  34   30    0    0    0 /
/
WCONINJE
Inj   WATER   OPEN   RESV   1*  34  500 /
 /
WPOLYMER
Inj   0.0   40.0 /
/
```

```
TUNING
0.1  10  0.01  0.01  2  0.3  0.05  1.1  1*  10 /
/
20  1  100  1   20   20 /
DATES
1 OCT 1993 /
/
TUNING
0.1  3  0.01  0.01  2  0.3  0.05  1.1  1*  10  /
/
20  1  100  1   20   20 /
DATES
1 NOV 1993 /
1 DEC 1993 /
1 JAN 1994 /
1 JUL 1994 /
1 JAN 1995 /
1 SEP 1995 /
1 JAN 1996 /
1 SEP 1996 /
1 JAN 1997 /
1 SEP 1997 /
1 JAN 1998 /
1 SEP 1998 /
/
WPOLYMER
Inj   0.0   4.0 /
/
DATES
1 OCT 1998 /
1 NOV 1998 /
1 DEC 1998 /
/
TUNING
0.1  3  0.01  0.01  2  0.3  0.05  1.1  1*  10  /
/
20  1  100  1   20   20 /
DATES
1 JAN 1999 /
1 JUL 1999 /
1 SEP 1999 /
```

```
 /
TUNING
0.1  7  0.01  0.01  2  0.3  0.05  1.1  1*  10  /
  /
20  1  100  1   20   20 /
DATES
1 NOV 1999 /
1 DEC 1999 /
1 JAN 2000 /
1 JUL 2000 /
1 JAN 2001 /
1 SEP 2001 /
1 JAN 2002 /
1 SEP 2002 /
1 JAN 2003 /
1 SEP 2003 /
1 JAN 2004 /
1 SEP 2004 /
1 JAN 2005 /
1 SEP 2005 /
1 JAN 2006 /
1 SEP 2006 /
1 JAN 2007 /
1 SEP 2007 /
1 JAN 2008 /
1 SEP 2008 /
/
END
```

C. Appendix – Adjustment of the Field Model

C.1 Distribution of Residual Oil

The initial flooding sequence was a hybrid low salinity surfactant/polymer flooding over a total time span of 29.33 years. Table C.1 lists the individual time span of each flooding sequence. The high and low salinity salt concentrations were 40 kg/m^3 and 4 kg/m^3, respectively, while the concentration of the surfactants and polymers diluted in LSW were 5 kg/m^3 and 0.5 kg/m^3, respectively.

Table C.1: Time span of each flooding sequence for the initial field model

	HS	LS	Surfactant	Polymer	LS
Slug Size (years)	5	1	3	3	17.33

Production results from the initial simulation run are listed in table C.2, with oil recovery, corresponding recovery factor, water cut and bottom-hole pressure, while figure C.1-C.2 illustrates the development of oil recovery, water cut and injection well BHP for the initial run.

Table C.2: Production results at the last production date from the initial field model

Oil Recovery [%OOIP]	Oil Produced [m^3]	Water Cut [%]	BHP [bar]
69.93	$24.91 \cdot 10^5$	89.42	206.78

The HS-LS flooding resulted in a recovery of 53.81% of OOIP. By injecting EOR chemicals, the recovery increased by 16.12% of OOIP, which corresponded to a low total recovery of 69.93% of OOIP. At the last production date, the water cut was 89.42% and still increasing. Figure C.1 also reveals a rapid increase in oil recovery at the end of the production, indicating that additional production of oil could be achieved had the flooding been prolonged. As the

water cut only reached 89.42%, it was reasonable to believe that a prolonged flooding would cause a profitable production. As there was no visual effect of the chemicals injected, this was investigated during sensitivity studies performed on the sector model where results are presented in section 6.2.

The response in BHP was an unstable development during flooding. Injection and production rates were governed by surface flow rate, which was not proportional to reservoir flow rate. This caused a deviation from voidage replacement, which explains the great change in BHP. The effect of applying RESV control mode on BHP was further investigated, where results are presented in section C.3.

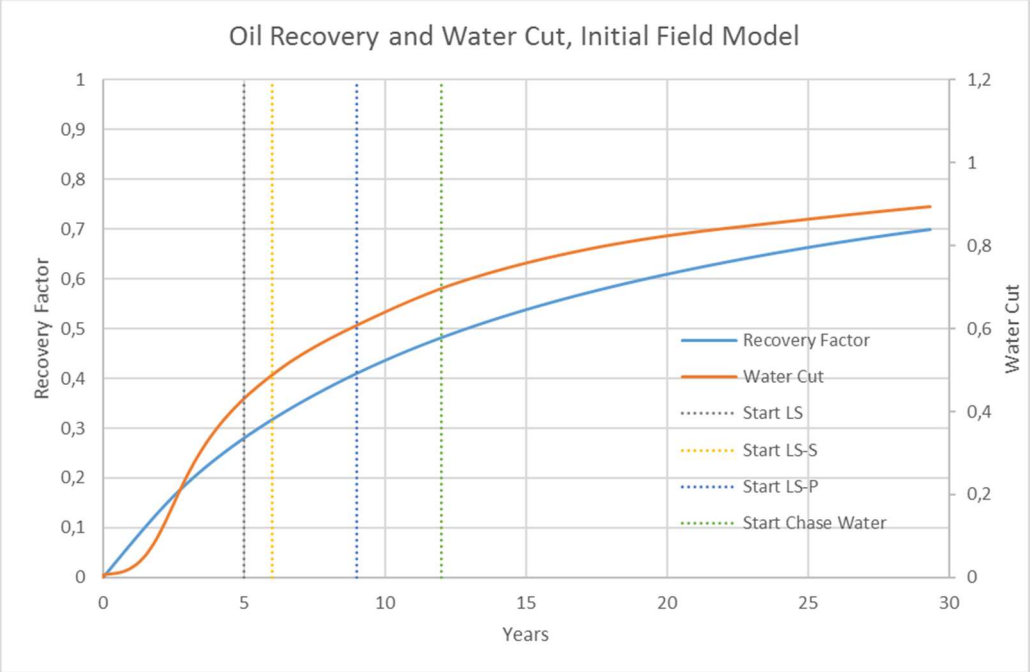

Figure C.1: Oil recovery and water cut for the initial field model LSSP process.

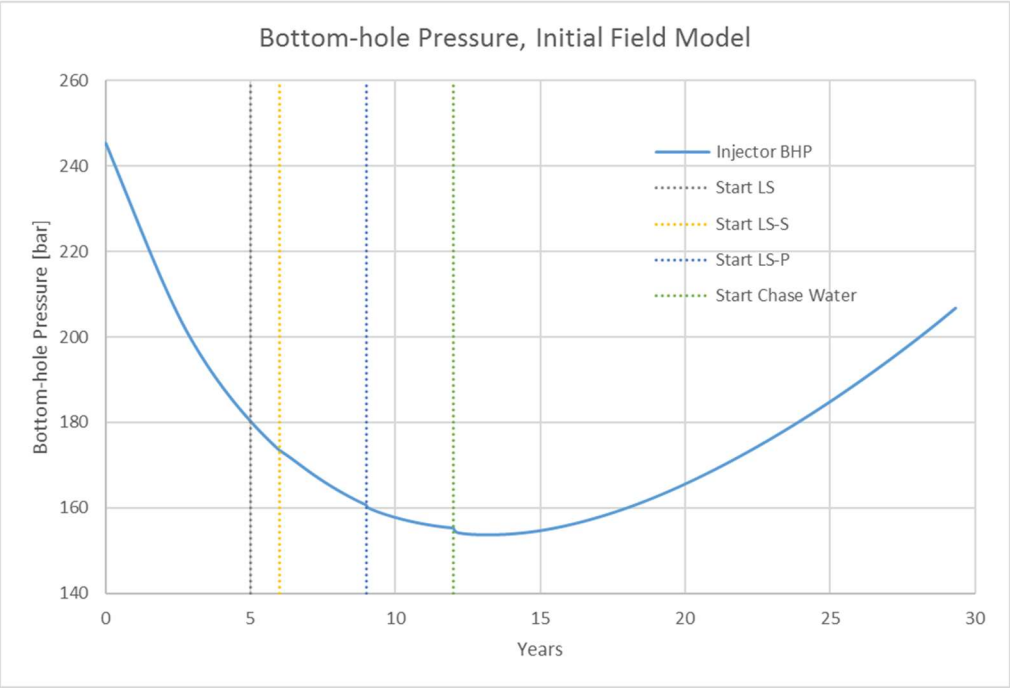

Figure C.2: Bottom-hole pressure in injection well for the initial field model LSSP process, altered x-axis.

Residual Oil

Figure C.3 visualizes oil saturation in the field model at the last production date. The figure was produced by the postprocessor FloViz, which allows for visualization of the outputs. The scale portrayed indicates oil saturation within the reservoir.

The initial oil saturation in all grid blocks from 44-90 in K-direction was zero, with all initial oil existing in the upper half of the model, where S_{oi} was 0.62. Propagation of injected fluids caused oil banking in the upper blocks, with a corresponding S_{or} of 0.19.

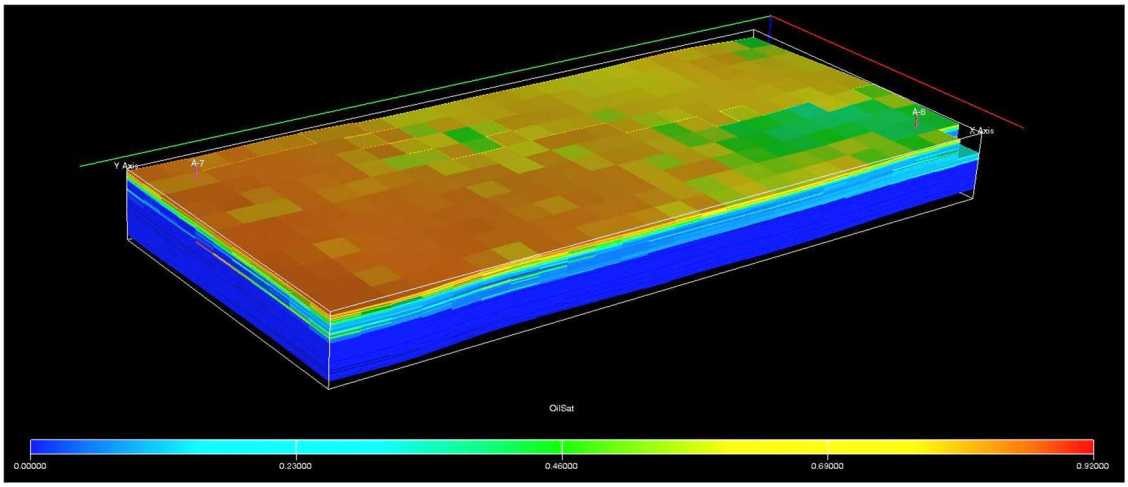

Figure C.3: 3D illustration of the initial field model LSSP process at the end of production, illustrated with oil saturation scale.

C.2 Impact of Adjusting Injection Well Perforation on Oil Recovery

The injection well was initially placed in blocks (2, 2, 29-90), which is a relatively large perforation area in the lower part of the model. The injector perforation area was decreased and raised to blocks (2, 2, 2-17). As water density is higher than oil density, water will tend to flow towards the bottom of the reservoir because of gravitational forces [4], and the macroscopic sweep around the injection well was increased by altering the perforation. Table C.3 lists the final production results, while figure C.4-C.6 display oil recovery, water cut and BHP during flooding.

Table C.3: Production results at the last production date from the initial LSSP process and LSSP process with modified perforation

Case Study	Oil Recovery [%OOIP]	Oil Produced [m^3]	Water Cut [%]	BHP [bar]
Initial LSSP	69.93	$24.91 \cdot 10^5$	89.42	206.78
Modified Perforation	77.99	$27.78 \cdot 10^5$	92.70	171.03

The impact of altering perforation area resulted in an increase in oil recovery by HS-LS injection of 63.05% of OOIP, with an additional 14.94% after EOR chemicals. The overall recovery was increased by 8.06% of OOIP after altering the perforation area, caused by a more efficient macroscopic sweep of the injection fluids. Oil recovery was still increasing at the end of production. Although altering perforation area caused a more favorable water cut and an increased recovery, the final water cut of 92.70% indicated that a prolonged flooding could have resulted in an economically favorable incremental oil production. As incremental oil production also was observed by flooding with the same injection rate applied in section C.1, the response in BHP was an enhanced BHP drop, caused by altering the injection perforation area.

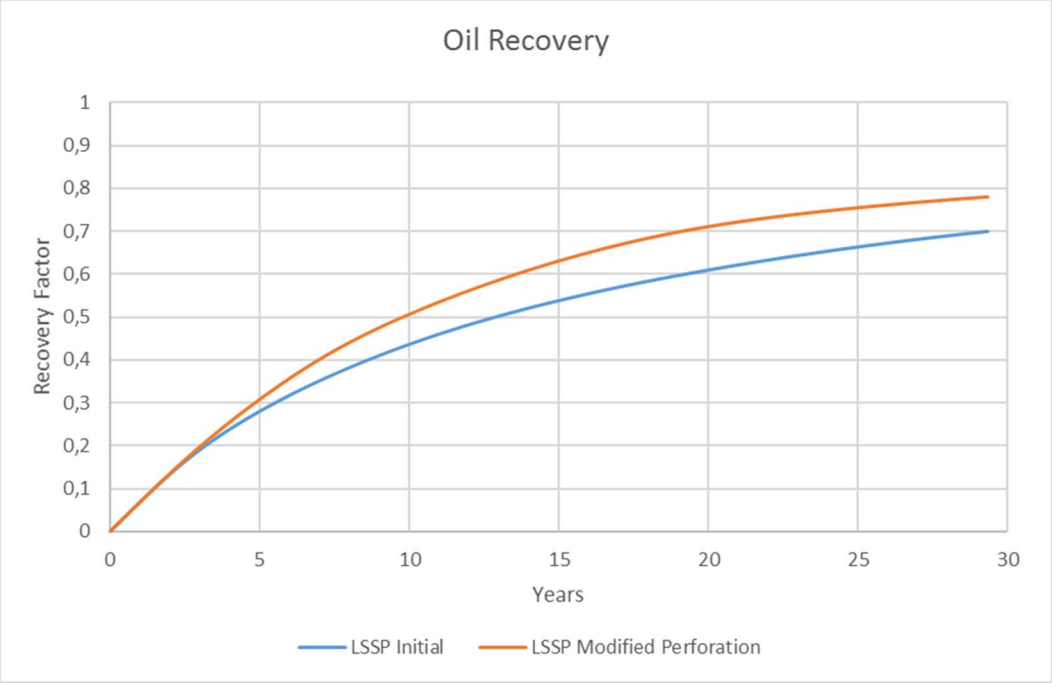

Figure C.4: Oil recovery for initial LSSP process and LSSP with modified perforation.

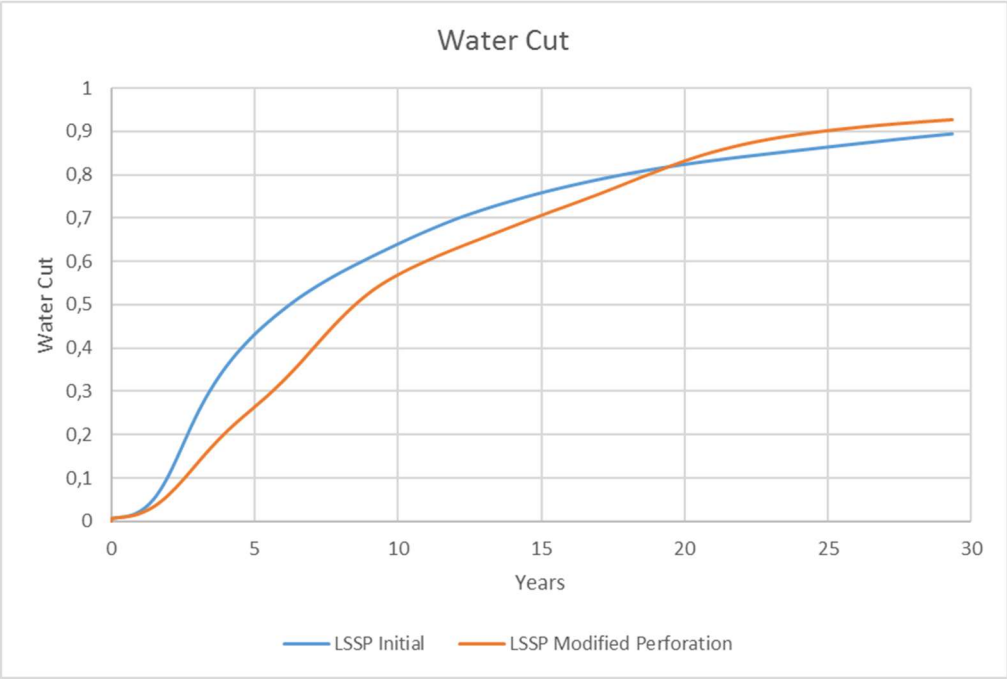

Figure C.5: Water cut for the initial LSSP process and LSSP with modified perforation.

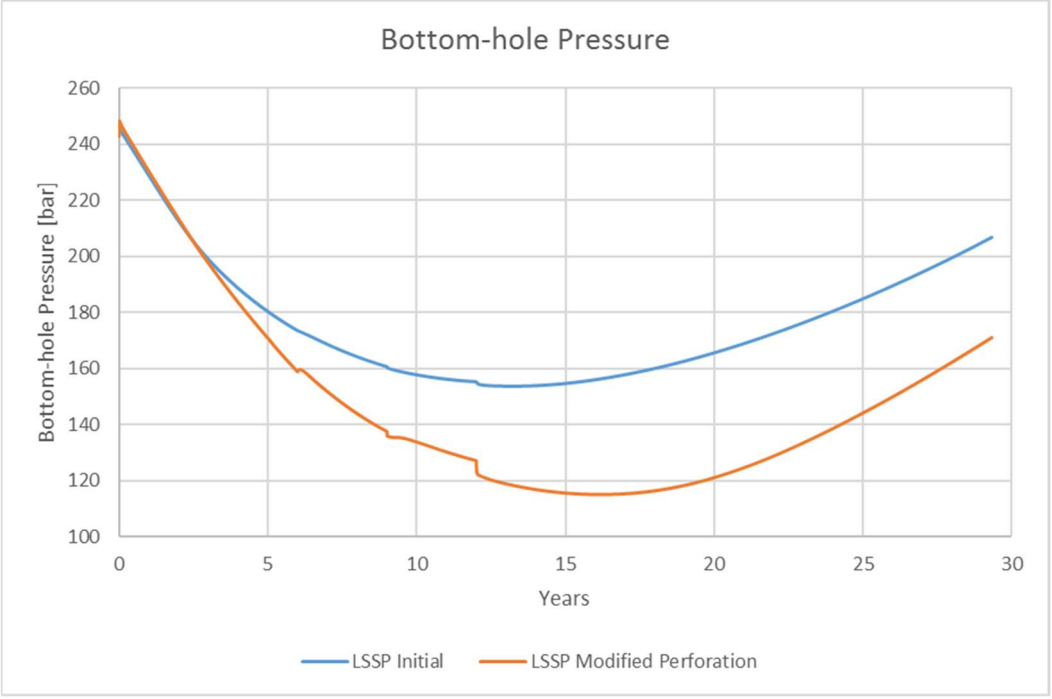

Figure C.6: Bottom-hole pressure in injection well for initial LSSP process and LSSP with modified perforation, altered x-axis.

Residual Oil

S_{or} was lowered from 0.19 to 0.14 in all upper blocks existing in K-direction 1-43, as the oil bank observed in figure C.7 was reduced. Figure C.8 reveals a more efficient sweep by the injection fluids as smaller patches of residual oil remained in the reservoir.

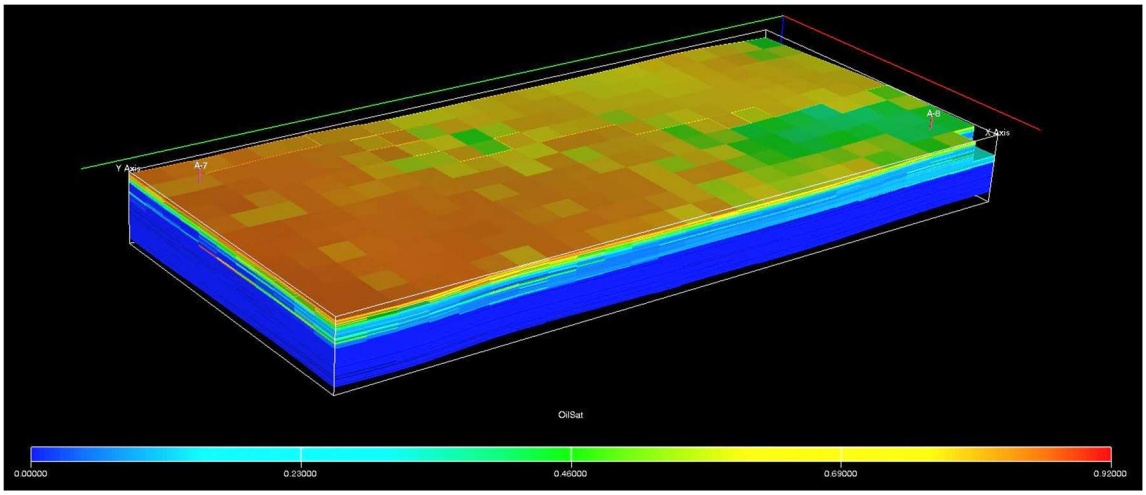

Figure C.7: 3D illustration of the initial field model at the end of production, illustrated with oil saturation scale. Figure collected from section C.1.

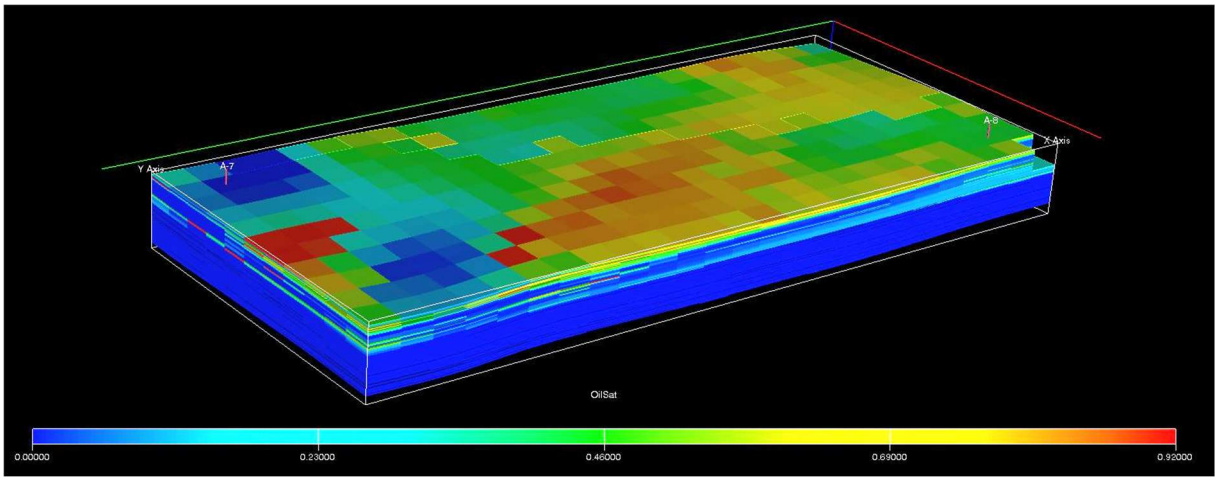

Figure C.8: 3D illustration of the field model with modified perforation at the end of production, illustrated with oil saturation scale.

C.3 Flow Governed by Reservoir Volumetric Rate

The control modes governing the fluid flow were changed from surface flow rate to reservoir fluid volume rate at a target of 718 rm^3/day for both wells to achieve an approximately constant BHP. Table C.4 lists a summary of the final production results. Figure C.9-C.11 display the development of BHP, oil recovery and liquid production rate throughout flooding.

Table C.4: Production results at the last production date from both simulation with rate control mode and simulation with reservoir fluid volume rate control mode

Case Study	Oil Recovery [%OOIP]	Oil Produced [m^3]	Water Cut [%]	BHP [bar]
Rate control mode *	77.99	$27.78 \cdot 10^5$	92.70	171.03
RESV control mode	73.26	$26.09 \cdot 10^5$	90.99	246.29

* Rate control mode corresponds to the *LSSP Modified Perforation* process previously described in section C.2.

While flow was previously governed by surface flow rate, a stable pressure could have been achieved by defining formation volume factors equal to one, namely $B_o = B_w = B_g = 1$. This assumption is not realistic, and was therefore not applied during simulations. The response in BHP by defining RESV as control mode was a more stable pressure where the only effect on pressure was type of injection fluid. The previous deviation from voidage replacement was removed, resulting in material balance throughout flooding.

Applying RESV control mode resulted in a drop in recovery factor by 4.73% of OOIP, and a lower elevation of the recovery curve displayed in figure C.10. The drop in recovery was caused by a lower production rate during the first 23 years of flooding, as displayed in figure C.11. The resulting water cut curve by modifying control mode is approximately equal to the water cut curve for *LSSP Modified Perforation* displayed in figure C.5, and is displayed in appendix figure D.6.

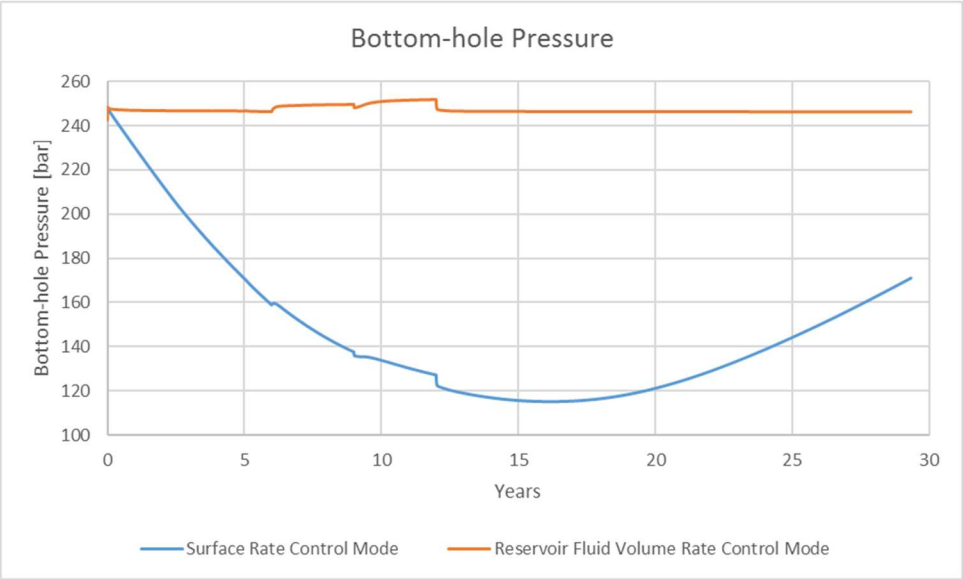

Figure C.9: Bottom-hole pressure in injection well for surface rate control mode and reservoir fluid volume rate control mode, altered x-axis.

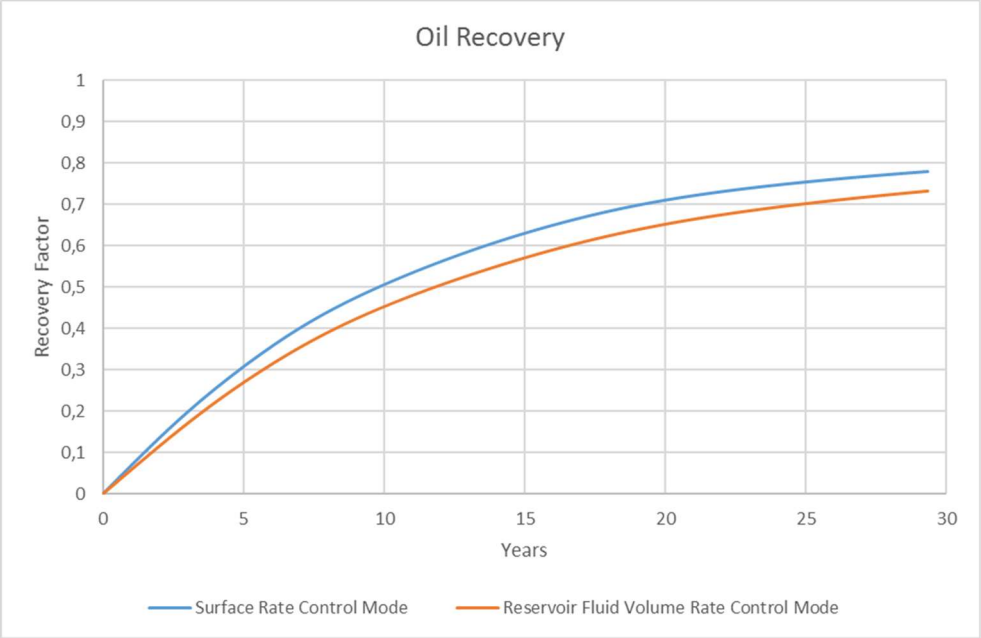

Figure C.10: Oil recovery for surface rate control mode and reservoir fluid volume rate control mode.

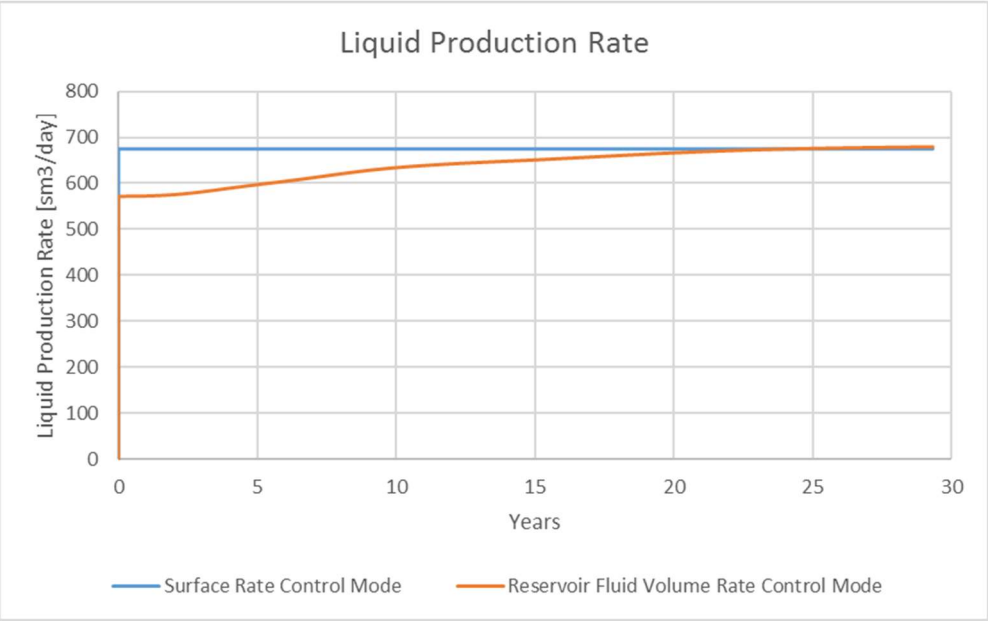

Figure C.11: Liquid surface production rate for surface rate control mode and reservoir fluid volume rate control mode.

D. Appendix – Simulated Results

D.1 Figures

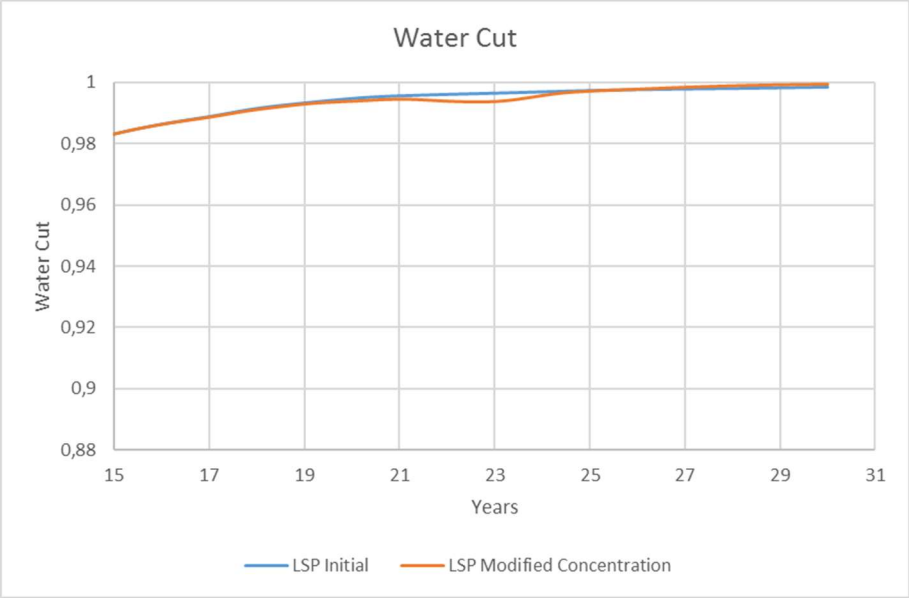

Figure D.1: Water cut for the initial LSP process and LSP with modified concentration, collected from section 6.2.4. Altered x-axis and y-axis.

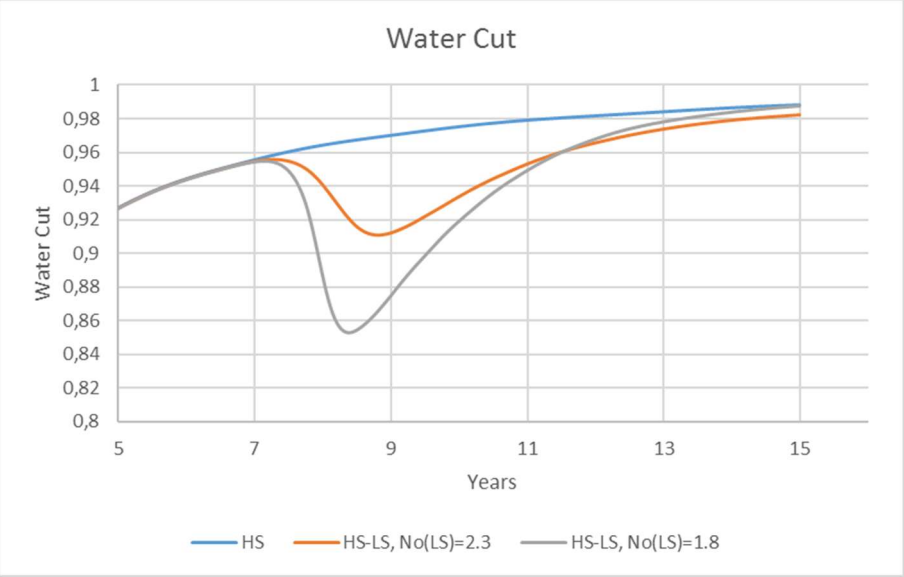

Figure D.2: Water cut for HS flooding compared to the HS-LS flooding with Corey correlation N_o(LS)=1.8 and HS-LS flooding with Corey correlation N_o(LS)=2.3, collected from section 6.2.6. Altered x-axis and y-axis.

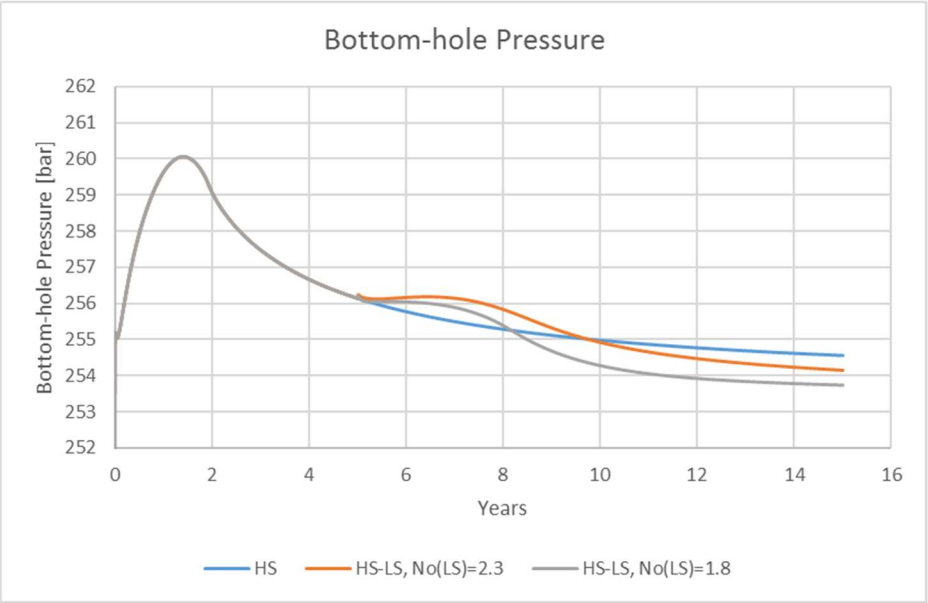

Figure D.3: Bottom-hole pressure in injection well for HS flooding compared to the HS-LS flooding with Corey correlation $N_o(LS)=1.8$ and HS-LS flooding with Corey correlation $N_o(LS)=2.3$, collected from section 6.2.6. Altered x-axis and y-axis.

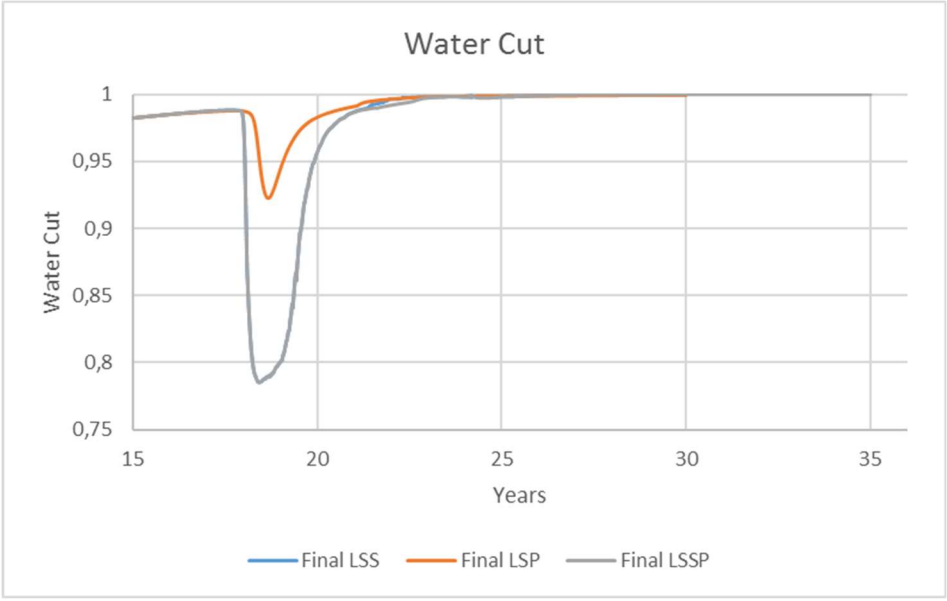

Figure D.4: Water cut for the final LSS, LSP and LSSP processes in the sector model with applied results from sensitivity studies, collected from section 6.2.7. Altered x-axis and y-axis.

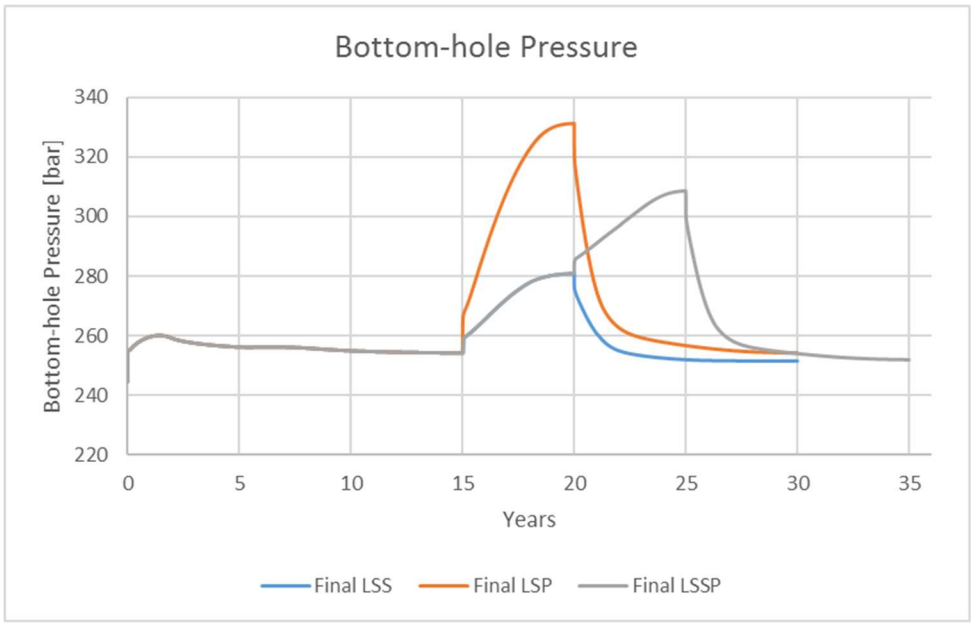

Figure D.5: Bottom-hole pressure in injection well for the final LSS, LSP and LSSP processes in the sector model with applied results from sensitivity studies, collected from section 6.2.7. Altered x-axis and y-axis.

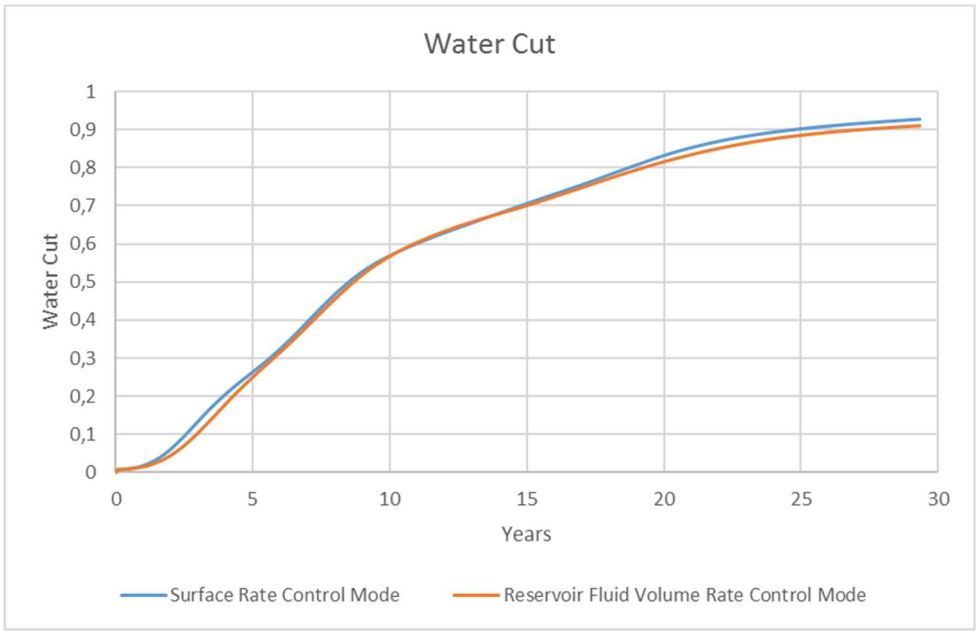

Figure D.6: Water cut for surface rate control mode and reservoir fluid volume rate control mode, collected from appendix section C.3.